Modeling the Effects of Vegetation-Erosion Coupling on Landscape Evolution

by

Daniel B. G. Collins

Submitted to the Department of Civil and Environmental Engineering
in partial fulfillment of the requirements for the degree of

Masters of Science in Civil and Environmental Engineering

at the

MASSACHUSETTS INSTITUTE OF TECHNOLOGY

June 2002

Author ....
Department of Civil and Environmental Engineering
May 10, 2002

Certified by..... .....
Rafael L. Bras
Bacardi and Stockholm Water Foundations Professor
Thesis Supervisor

Accepted by .. ..
Oral Buyukozturk
Chairman, Department Committee on Graduate Students

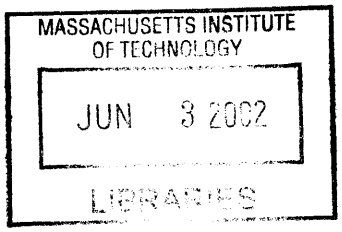

Modeling the Effects of Vegetation-Erosion Coupling on Landscape Evolution

by

Daniel B. G. Collins

Submitted to the Department of Civil and Environmental Engineering
on May 10, 2002, in partial fulfillment of the
requirements for the degree of
Masters of Science in Civil and Environmental Engineering

Abstract

From rainfall interception at the canopy to added soil cohesion within the roots, plants play a significant role in directing local geomorphic dynamics, and vice versa. The consequences at the regional scale, however, are less well known despite being the subject of conjecture spanning three centuries. In light of this, the numerical model *CHILD* is equipped with coupled vegetation-erosion dynamics, allowing for sensitivity analysis on the various aspects of vegetation behavior. The processes considered are plant growth, plant death, and the additional resistance imparted by plants against erosion. With each process is associated a single parameter, whose effects on the spatio-temporal nature of a fluvially-dominated 1.8 by 1.8 km landscape is studied.

While each parameter possessed its own geomorphic signature, some common effects were shared by all, and thus were essentially a result of the vegetation itself. Through their inhibition of erosion, plants steepened the topography and made erosive events more extreme, yet became established more widely throughout the area. As a result, erosion rates varied spatially, leading to periodic stream capture and oscillating mean elevation, erosion rates, and vegetation density, and a meta-stable biophysiography. Despite having stationary, yet stochastic, climatic forcing, and steady uplift, this oscillatory behavior arises out of the meta-stability of the vegetation-erosion coupling itself. This has implications for the nature of cut-fill cycles, and the stability and diversity of vegetation-mantled landscapes.

Thesis Supervisor: Rafael L. Bras
Title: Bacardi and Stockholm Water Foundations Professor

Acknowledgments

This work was supported by NASA Headquarters under the Earth System Science Fellowship Grant NGT5-ESS/00-0000-0085 and by the Army Research Office, both of which are greatly appreciated.

As advisor, Rafael Bras deserves the first thanks in terms of guidance and attention. Greg Tucker also provided significant help, from both sides of the Atlantic, as did geomorphology colleagues Nicole Gasparini, Jeff Niemann and Vanessa Teles. Thanks also to the other group members Frederic Chagnon, Jean Fitzmaurice, Valeri Ivanov, Scott Rybarczyk and Enrique Vivoni-Gallart. Cross-campus, and cross-continent, helpful discussions and suggestions were provided by Joe Ackerman, Ben Crosby, William Dietrich, Gary Parker, Noah Snyder and Kelin Whipple, while general academic insight and help was also imparted by numerous office mates: Anke Hildebrandt, Kirsten Findell, Megan Kogut, Rolf Reichle. Final thanks for support and motivation goes to friends John Frank, Ben Monreal, Pieter Vermeesch, Melissa Warden, and many others, and to family, Elizabeth, Roger, Simon, Eric, Joan and Richard.

from cool springs seeping
toward creeping golden shores
does the river run.

Contents

List of Figures

List of Tables

Chapter 1

Introduction

Vegetation has been long considered an important facet of geomorphic processes. Lyell (1834, p. 113) remarks

> It is well known that a cover of herbages and shrubs may protect a loose soil from being carried away by rain, or even by the ordinary action of a river, and may prevent hills of loose sand from being blown away by the wind; for the roots bind together the separate particles into a firm mass and the leaves intercept the rainwater, so that it dries up gradually, instead of flowing off in a mass and with great velocity.

Cotton (1922, p. 193) expands this theme by stating

> ... the stability of slopes depends largely on the natural vegetation. A slope may be steep and yet the soil may be so bound and protected by the vegetation, forest perhaps, that streaming is prevented and only creep permitted, ...

Disturbances of the ecological regime would consequently disrupt the geomorphic balance, as Cotton further notes:

> When the natural vegetation, whether forest or grass, is interfered with, erosion, with the formation of deep gullies, may begin on a previously graded surface. Clearing or burning the forest from [m]any steep slopes

> in New Zealand (and also in other countries) has seriously disturbed the state of balance between the rates of weathering and of removal of waste.

Lyell identifies root cohesion and diminished runoff as keys to reduced erosion. Similarly, Cotton writes of a reduction in drainage density with vegetation, and an increase following devegetation.

As geomorphic practice became more quantitative, Melton (1958) showed that drainage density decreased with humidity, which has been attributed to the stabilizing effects of vegetation (Moglen et al., 1998). This illustrates the notion of threshold-dominated morphology, in which the extent of fluvial erosion is determined by drainage area, local slope and vegetation cover (Horton, 1945; Patton and Schumm, 1975; Bull, 1979; Montgomery and Dietrich, 1988). A corollary is that sediment yield has been shown to decrease with increasing mean annual rainfall in semi-arid to humid environments, which is seen as the dominance of flourishing vegetation over the erosive potential of the wetter clime (Langbein and Schumm, 1958; Douglas 1967). Conversely, ecologists have often cited geomorphic processes as determinants of vegetation distribution and dynamics (Thom, 1967; Hupp, 1986; Burnett et al., 1998; Nichols et al., 1998; Robertson and Augspurger, 1999).

While a sizeable amount of research has been conducted on the local effects of vegetation-geomorphic interactions, little has been done to gain understanding at the landscape scale. This provides the motivation for the current thesis: to integrate local vegetation-geomorphic dynamics into a landscape evolution model, and explore the resultant effects on spatio-temporal biophysiography. Not only is this of fundamental academic value, but it may also benefit agricultural, forestry, and hazard management, as well as environmental protection.

In achieving said goal, Chapter 2 discusses the plethora of ways in which vegetation affects geomorphology, and places them in a regional context. A background to numerical landscape evolution modeling is also given, emphasizing recent efforts to incorporate vegetation effects.

Chapter 3 details the numerical model used in the study - the Channel-Hillslope Integrated Landform Development (*CHILD*) model. The chosen vegetation dynamics

to be embodied in the model are described, and the subsequent experimental method mapped out. This comprises a sensitivity analysis on the model's vegetation-related parameters.

Results of the study are presented in three parts. Firstly, Chapter 4 contains purely spatial outcomes - the static biophysiography. Chapter 5 deals solely with the spatially-averaged temporal evolution of the landscape. Lastly, Chapter 6 addresses the spatio-temporal aspects together. Qualitative and quantitative, including analytic, analyses proceed in tandem throughout the study.

The thesis in culminates in a summary of the conclusions, and suggests further avenues of research (Chapter 8).

Chapter 2

Background

Awareness that vegetation plays a role in directing landscape evolution has existed for centuries, and models of landscape evolution for decades. Coupling the two, however, has not been attempted until more recently, despite numerical modeling being an ideal testing ground for theories of vegetation-geomorphic interaction. It is this thesis' goal to further explore such new ground. Following are summaries of processes in which plants affect geomorphology and of numerical landscape evolution modeling to date, with specific emphasis on the incorporation and effects of vegetation.

2.1 Local Effects of Vegetation on Hydrology and Geomorphology

Plants modify geomorphic processes in many ways, be they hydrologic, hydraulic, or geotechnical. Presented here is an overview of these diverse effects.

2.1.1 Rainfall

Precipitation arriving at a canopy is partitioned into interception, throughfall, leaf-drip[1] and stemflow. The degree of partitioning is controlled by plant species and

[1]Distinction between uninterrupted rainfall and leaf drip is rarely made. They are often collectively termed "throughfall".

Table 2.1: Interception depths for various plant types after Coppin and Richards (1990).

Species	Storage (mm)
Big bluestem (*Andropogon gerardi*) dense stand, 0.6 m tall	2.34
Buffalo grass (*Buchloe dactyloides*) 0.3 m high, many stolons	1.65
Meadow grass (*Poa pratensis*) at maximum development	1.01
Annual ryegrass (*Lolium multiflorum*) at various growth stages	0.43-2.81
Tall wheatgrass (*Agropyron elongatum*) at various growth stages	0.25-5.08

cover, rainfall intensity and duration, antecedent conditions, and climate or seasonal factors (Aldridge and Jackson, 1968; Gregory and Walling, 1973; Wainwright et al., 2000). Intercepted rainfall may be stored briefly or be lost through evaporation or absorption to the canopy or trunk of the plant (Woo et al., 1997; Tables 2.1 & 2.2), and depends on the surface area, roughness, orientation and wettability of the leaves or bark, and wind (Lee, 1980). Raindrop size and energy are often modified by passage through the canopy, with different erosion potential, further affected by the presence of ground cover.

Rainfall's kinetic energy has been shown to both increase and decrease as a result of canopy modification. Throughfall within a New Zealand beech forest has a 50% higher total kinetic energy than that of rainfall, even after accounting for interception losses (Mosely, 1982). This results from the interception and concentration of drops by the canopy, and leads to an increase in splashed sand. Studies in the Central Andean Cordillera of Colombia (Vis, 1986) produced similar results - higher rainfall energies, greater splash volumes. Vis also showed a bimodal distribution of drop size beneath the canopy compared with a unimodal one above the canopy. Alternatively, raindrop kinetic energy per unit mass may decrease (Morgan et al., 1986; Wainwright, 2000) as a result of reduced height and disagregation. The presence of surface litter also reduces raindrop erosivity (Geddes and Dunkerley, 1999).

Table 2.2: Interception percentages for various plant types: without leaves*, during the growing season§; during low plant development¶ (after Coppin and Richards (1990) and Gregory and Walling (1973)).

Vegetation	% Interception
Northern hardwood forest	10-15, 7*
Temperate broad-leaved forest	15-25
Temperate coniferous forest	25-35
Aspen–birch	10, 4*
Spruce–spruce-fir	32
White pine	26
Hemlock	28
Red pine	29
Tropical forest	25-40
Grass	25-60
Maize	25
Cereals (wheat, oats, barley)	20-25
Corn	15.5§, 3.4¶
Oats	6.9§, 3.1¶
Clover	40§

2.1.2 Surface Storage

Not all surface water becomes surface runoff. Other than losses from infiltration and evaporation, water may be absorbed by surface litter, or ponded within microtopographic depressions. Sala and Calvo (1990) attributed differences in runoff quantities between a coniferous and deciduous forest, in part, to the abundance of litter in the latter and the associated storage of moisture. Of the treethrow pits investigated by Adams and Norton (1991), most contained some water, although Putz (1983) noted that none in the studied Panamanian treefall pits were ponded, even after a storm that delivered 10 cm of water in less than three hours — a result of the soil's high conductivity.

2.1.3 Subsurface Hydrology and Development

Below ground, plants increase permeability and infiltration capacity with their roots, vacant macropores, and increased macrosurface roughness (Whipkey, 1966; Greenway,

Table 2.3: Transpiration rates for different plants.

Vegetation	Annual Transpiration (mm)
Broadleaf woodlands	311 ± 46
Conifers	338 ± 42
Short rotation coppice	457 ± 28
Grass	353
Barley	248 ± 43
Heather	214
Bracken	165 ± 35

1987; Newman et al., 1998), thus reducing surface runoff. A four-fold increase in infiltration rate was observed on a gentle grassed slope compared with a bare slope (Nassif and Wilson, 1975), with other studies producing similar trends (e.g. Beven and Germann, 1982; Dunne et al., 1991; Woo et al., 1997). Higher conductivities have also been observed in forest than in grassland ecosystems (Burch et al., 1987; Turton et al., 1995; Ragab and Cooper, 1993). However, some evidence suggests that macropores do not unequivocally enhance subsurface flow, as reported for a coniferous forest in Britain (Rawlins et al., 1997).

Once within the soil matrix, the water is available for root uptake and photosynthesis. Transpiration rate varies among species (Table 2.3), between stages of growth, and soil and environmental conditions (Greenway, 1987). It lowers the moisture content and pore-water pressure of the soil (e.g. Brenner, 1973; Biddle, 1983), and may notably affect neighboring streamflow recession (Federer, 1973).

In addition to the structural modification of the soil (such as macropores), plants alter soil chemistry (Angers and Caron, 1998) with implications for rates of bedrock weathering (Kelly et al., 1998; Lucas, 2001). Weathering is also affected by the mechanical forces imposed by growing roots (Fitzpatrick, 1980). Soil genesis is also aided by the addition of up to 2.5 $kg/m^2/yr$ of decomposed organic matter, depending on the climatic region (Fitzpatrick, 1980).

2.1.4 Surface Runoff and Erosion

After the gross rainfall has been intercepted by the canopy, detained on the surface, or infiltrated, the remainder forms surface runoff. The distribution of rainfall among the different pathways arriving at the surface can determine how much becomes runoff, as Wainwright et al. (2000) note with nearly 80% of the concentrated stemflow in their experiments producing runoff. The timing of runoff is modified by infiltration (Nassif and Wilson, 1975), canopy effects and litter absorption (Sala and Calvo, 1990). Spatial variability in runoff production may also develop, arising from the variation of infiltration with microtopography (Dunne et al., 1991).

Channelization of flow between shrubs, less likely in grassland, reduces flow resistance (Abrahams et al., 1995). Less areal vegetation cover also leads to a drop in resistance to over land flow (Prosser and Slade, 1994; Prosser et al., 1995; Prosser and Dietrich, 1995), and channelized flow (Chow, 1959, Reid, 1989). In mountainous first order streams, woody debris are considered particularly important in channel dynamics (Smock et al., 1989; Hupp, 1999).

A combination of flow resistance and additional root cohesion are believed responsible for an elevated threshold for sediment entrainment by overland flow (Graf, 1979; Reid, 1989; Prosser and Slade, 1994; Hagberg, 1995; Prosser and Dietrich, 1995). Graf (1979) studied 67 gullies and arroyos in a montane area of Colorado's Front Range, covering a wide range of vegetation characteristics. Plotting estimates of tractive force, F, for the 10-year flood against channel biomass, B_v, showed a clear threshold between cut and uncut channels defined by a vegetation-dependent critical force of $F_c = 0.07.B_v^{2.01}$ - as biomass increases, it becomes increasingly effective in resisting erosion. More recently, critical shear stresses for different conditions have been measured. Flume experiments, fed from a 50 m^3 swimming pool, were conducted by Prosser and Slade (1994) on an unincised valley floor, to determine flow resistance and the critical shear stress for scour under natural and degraded vegetation covers (Table 2.4). Values for the critical shear stress ranged from 70 to 240 Pa. Additional values for critical shear stress under different soil and vegetation conditions are also

Table 2.4: Critical shear stress for different vegetation cover states.

Source	Description	Critical Shear Stress (Pa)
Reid (1989)	non-cohesive soil	3.6 - 7.2
	cohesive soil	3.8-51
	well-vegetated	110-200
	moderately vegetated	80-170
	poorly vegetated	15-30
Prosser and Dietrich (1995)	grassed	104-184
	clipped	20-38
Prosser and Slade (1996)	tussock grass (good)	>66
	tussock grass (moderate)	28-42
	sedge (good)	>333
	sedge (moderate)	500-530
WEPP	agricultural field[2]	0.7-7

presented in Table 2.4.

As a result of the above, erosion rates are expected to decrease with increasing vegetative cover. An empirical relation for erosion, ϵ (tons/ha), on two Californian hillside vineyards, was given by Battany and Grismer (2000) as $\epsilon = 3.9e^{-0.035 \times Cover}$. Rogers and Schumm (1991) produced a qualitatively similar result in a physical simulation, although Morgan et al.'s (1986) results showed both increasing and decreasing trends.

2.1.5 Slope Stability

Mechanisms plants employ to influence slope stability include changes in soil moisture (Greenway, 1987; Terwiller, 1990), root reinforcement (Laffan, 1979, Ziemer, 1981; Preston and Crozier, 1999; Schmidt et al., 2001), and surcharge and the transmission of wind forces to the soil (Greenway, 1987). The infinite slope equation[3] provides a

[2]Three to twelve months prior to the experiments, excess residue from the previous season's crop was removed, the sites were deep-tilled and lightly disked (Elliott et al., 1989). Deep tillage is a method of plowing, to break up compacted soil to allow root penetration. Disking is a method of soil profile inversion.

[3]The infinite slope equation is $F = \frac{c' + (\gamma z \cos^2 \beta - u) \tan \phi'}{\gamma z \sin \beta cos \beta}$, where F is the factor of safety, c' the effective cohesion, γ the unit weight of soil at natural moisture content, z the elevation, β the slope angle, u the pore-water pressure, and ϕ' is the angle of friction with respect to effective stresses (Selby, 1994).

clear example of this effect by way of pore pressure and effective cohesion. Removal of vegetation thus leads to increased landsliding potential. Landslide frequency in logged terrain on Vancouver Island, British Columbia, was nine times greater than in undisturbed forest (Jakob, 2000), with failure occurring on gentler slopes in logged areas than in natural terrain. The same factors are relevant with regards to channel bank stability (Simon et al., 1999). Logistic growth and exponential decay models have been developed to describe the changes in root strength during growth and following death (O'Loughlin, 1974; Ziemer, 1981; Sidle, 1991; Sidle, 1992).

2.1.6 Treefall

Uprooting of trees, for example from windthrow, results in small-scale variations in soil properties and microtopography, termed pits and mounds (e.g., Putz, 1995; Adams and Norton, 1991). Pit and mound coverage varies widely, accounting for up to 60% for the soil surface in areas of New York (Beatty, 1980), 39% in south-east Alaska (Bormann et al., 1995), and less than 0.1% in a site in Panama (Putz, 1983). The scarcity of treefall features in the tropics is attributed to torrential rainstorms on a litter-free soil (Putz, 1995), which erase evidence in 5-10 years, if not sooner. In temperate regions, leveling of the surface is on the order of centuries (Small, 1997; Bormann et al., 1997).

Treefall significantly disrupts pedogenesis (Admas and Norton, 1991; Beatty, 1984; Bormann et al., 1995) preventing the build-up of podzols, and allowing shade-intolerant species to live alongside shade-tolerant in a patchy environment (Admas and Norton, 1991; Putz, 1983; Beatty, 1984). Treefall also exposes soil within the root plate, ranging up to 30 m^3 (Putz, 1983), and as the slope increases, so too does mound and pit volume, with less of the soil contained within the rootplate falling back into the mound (Norman et al., 1995). Treefall is thus a source of erodible soil. However, measurements of soil removal and production rates are few.

2.2 Regional Effects of Vegetation on Hydrology and Geomorphology

Moving up to the catchment and regional scale, questions of vegetation-geomorphic interactions are often framed in the context of landuse and landuse change. Many large-scale studies of runoff and erosion have been conducted in diverse ecoregions, addressing the effects of different crops and forest types, and the consequences on introduced grazing, forestry, and fire suppression. While the scope of this thesis precludes a thorough review, a brief survey is given.

An extensive study on the effects of land use and precipitation on annual runoff and erosion was conducted in eight sites in the Mediterranean region, located in Portugal, Spain, France, Italy and Greece (Kosmas et al., 1997). The sites represented a variety of landscapes, lithologies and land uses (cereals, vines, olives, eucalyptus, and shrubland). They found the most crucial period of erosion for land planted with rain-fed cereals is from early October to late February when the soils are almost bare. Hilly areas under vines produced the greatest sediment yield, because their soils remain bare for most of the year. Olives groves, with a high density of understory vegetation and litter, produces the least erosion. Along a climatic gradient, shrubland erosion was low for both high and low annual rainfall depths and highest for intermediate depths, similar to the results of Langbein and Schumm (1958).

Pinyon-juniper woodlands in the western United States have undergone significant expansion and increase in density in the last 100 years. A number of theories have been proposed for this, including overgrazing, fire suppression, climate change, and higher carbon dioxide concentrations. Transitions from ponderosa pine (*Pinus ponderosa*), with associated herbaceous ground cover, to a woodland composed entirely of pinyon (*Pinus edulis*) and one-seed juniper (*Juniperus monosperma*) associated with a diminished understory, have led to accelerated erosion, threatening longterm stability and productivity. This threat led Wilcox et al. (1996) to study a northern New Mexico catchment that underwent such changes over the previous century. Introduction of grazing in the late 1800s with an associated reduction in fire frequency (from both

fire suppression and reduced ground fuel) allowed the pinyon-juniper population to increase. These trees have widely-spread lateral roots, allowing them to out-compete for limited water and nutrient resources. A severe drought in the 1950s killed the last of the ponderosa pine, leaving a catchment with 45% plant cover, little herbaceous vegetation, and shallow soils. Runoff accounts for less than 10% of the catchment's total water budget, consistent with other semi-arid regions. This rises to 15-25% in the summer rainy season, comprising intercanopy areas where the percentage may achieve 40%. At an erosion rate of 10,000-20,000 kg/ha/yr, Wilcox et al. estimate that the intercanopy soil will be mostly stripped within a century.

Further north, in North Fish Creek, Wisconsin, Fitzpatrick and Knox (2000) report hydrologic and geomorphic changes as a result of clear-cut logging followed by agricultural activity, after settlement in the late 1800s. These landuse changes led to a three-fold increase in flood peaks, and a five-fold increase in sediment loads, even though during the peak agricultural period in the 1920s and 1930s, more than half of the basin was reforested. Similar trends are seen New Zealand (DeRose et al., 1998), while runoff and erosion studies in Brazil (Nortcliff et al., 1990) highlight the importance of recovery of litter following clearing.

Due to landscape clearing for agriculture in Puerto Rico between 1830 and 1950, runoff increased about 50%, and sediment supply to streams by an order of magnitude (Clark and Wilcock, 2000). Widespread gullying and landsliding resulted from clearance extending into steep valley slopes. Shifting landuse in the past 50 years from agriculture to industry and residential has reduced the sediment supply, but maintained high runoff rates.

These examples serve to illustrate the regional implications of local plant-induced changes, helping to bridge the conceptual gap between local process and large-scale landscape simulation.

2.3 Geomorphic Modeling

Since their inception in the 1970s, numerical landscape evolution models have provided a testing ground for hypotheses of complex geomorphic processes, a source of new hypotheses, and more recently, tools for examining environmental issues. As distinct from the 2-dimensional (Culling, 1960; Scheidegger, 1961; Snow and Slingerland, 1987; Paola et al., 1992; Robinson and Slingerland, 1998; Roe et al., 2001), or purely hillslope- (Ahnert, 1976; Favis-Mortlock et al., 2000) or channel-based (Webb, 1995) 3-dimensional models, landscape evolution models represent the topography by a mesh of points spanning both hillslope and channel elements (Willgoose et al., 1991; Howard, 1994; Howard et al., 1994; Tucker and Slingerland, 1997; Tucker and Bras, 2000). In addition to fluvial and diffusional processes commonly modeled (Howard, 1994), the register of geomorphic processes also includes tectonics (Koons, 1989; Beaumont et al., 1992; Tucker and Slingerland, 1994; Kooi and Beaumont, 1994), weathering (Braun et al., 2001), mass wasting (Howard, 1997) and seepage erosion (Howard, 1995; Lou, 2001). Models have also been used to address climate and landuse changes (Coulthard et al., 2000; Evans and Willgoose, 2000) and vegetation dynamics (Howard, 1999; Lancaster et al., 2001). Also relevant are the works of Kirkby (1995), Mitas and Mitasova (1998), Siepel et al. (2002), and the USDA's WEPP model (Flanagan and Nearing, 1995). The pertinent features of these models will now be highlighted.

The Water Erosion Prediction Project (WEPP) was developed by the USDA to assist in soil and water conservation and environmental planning and assessment (Flanagan and Nearing, 1995). The model simulates a wide variety of processes involved in small cropland and rangeland watersheds. Plants and their residue are involved in hydrologic routing, subsurface flow and soil detachment. Plant growth is dependent on insolation, temperature and soil moisture.

Within the framework of hillslope erosion, Mitas and Mitasova (1998) illustrate a bivariate model of erosion, sediment transport, and deposition by overland flow. Of the model's parameters, only the flow roughness depended on the local vegetation

characteristics. Siepel et al. (2002) developed a rill and interrill model based on stream power. Vegetation cover had the effect of decreasing the rate of sediment re-entrainment by shielding, increasing the flow roughness (Manning's n), and absorbing energy from the flow.

Coulthard et al. (2000) constructed a cellular automaton with an adaptation of TOPMODEL (Beven and Kirkby, 1979), a hydraulic routing scheme based on Manning's equation, and a fluvial erosion and deposition algorithm based on the Einstein (1950) equation. Vegetation played a role in the flow roughness, hydrologic routing and fluvial erosion (resistant turf mat). While it was not clear whether climate change or deforestation had the greater impact on landscape evolution, it was clear that the combined effect of deforestation and climate change has a greatly disproportionate effect on erosion compared with each disturbance separately.

In assessing different mining site rehabilitation strategies, Evans and Willgoose (2000) adopt the vegetation cover approach used in the USLE and RUSLE models, applying it to Willgoose et al.'s (1991) SIBERIA model. The vegetation cover approach recognizes that plants play a role in reducing erosion, be it by reducing raindrop erosivity, increasing flow roughness, or binding soil better. Areas were either vegetated or unvegetated, giving rise to notably different estimates of capping material required to contain mine tailings for 1000 years.

Howard (1999) adapted his earlier model (Howard, 1994) to account for the inhibition of erosion by vegetation in the following manner. If the local erosion rates exceeded a critical value, E_u, vegetation is completely destroyed, lowering the threshold for erosion, τ_{cu}, to τ_{cd}, lowering the erodability from K_{tu} to K_{td}, and increasing the runoff yield, R. When the local erosion rate drops below another critical value, $E_d < E_u$, the vegetation completely re-establishes, returning the erosion threshold, erodability and runoff yield to their original values. In studying the nature of the model, the landscape was disturbed briefly, killing all vegetation. After a short time, the vegetation was allowed to regrow according to the above rules. Howard found that gullies could propagate after the disturbance had ceased, with an extent governed by the relative values of the thresholds. This was apparently the first landscape evolution

model to actively include vegetation dynamics, rather than static vegetation cover.

The most explicit landscape evolution model incorporating vegetation dynamics is that of Lancaster at al., (2001). The Channel-Hillslope Integrated Landscape Development (CHILD) model was extended to simulate the interaction between woody debris and landslides. Landslide susceptibility depends on root strength, which grows logistically, and after death, decays exponentially. Wood volume also follows a logistic growth rate, while tree height obeys a more complex empirical relation. Treefall involves an exponential random number of trees, at a rate governed by mean root strength. Fallen trees are contributed to the hillslope or riparian zone, and modify debris flow dynamics. Trees may also die from wildfires, which are exponentially distributed and kill the entire forest. The main consequence of these processes is that forest dynamics have a significant control on sediment and channel behavior.

Chapter 3

Model Description and Simulation Procedure

The numerical model used in this research is the Channel-Hillslope Integrated Landscape Development (*CHILD*) model (Lancaster, 1998; Tucker and Bras, 2000; Tucker et al., 2001a; Tucker et al., 2001b). The scope of this thesis precludes a comprehensive treatise on the model, for which the reader is directed to the above sources. Instead, a synopsis of the pertinent aspects and assumptions is presented, including the modifications required to model some of the effects of vegetation dynamics discussed in the previous chapter.

3.1 The Channel-Hillslope Integrated Landform Development Model (*CHILD*)

CHILD imitates landscape evolution by simulating discrete rainfall events, routing the runoff through an irregular mesh of points, which represent the topography, and deforming this elevation field according to the interplay of various geomorphic processes. These are, primarily, fluvial erosion and deposition, hillslope diffusion and tectonics. Meandering and aeolian deposition may also be simulated. The change in

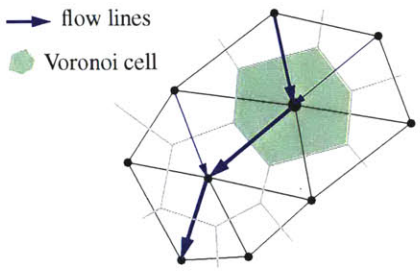

Figure 3-1: A set of nodes and their corresponding Voronoi cells. Surface discharge passes from node to node, perpendicular to cell edges.

individual node elevation with time is mathematically represented by:

$$\frac{\partial z}{\partial t} = U(x, y, t) - \nabla q_s \tag{3.1}$$

where $U(x, y, t)$ is the rate of tectonic uplift, subsidence or baselevel lowering, which may vary spatially or temporally, and ∇q_s is the rate of local sediment divergence.

The landscape is represented by a triangular irregular network (TIN) of nodes, each with an individual elevation, and confined by set boundary conditions. The configuration of nodes defines a set of Voronoi polygons about each node (Figure 3-1), through which water flows, and to which erosion and deposition is applied. The numerical procedure is based on a flexible modular framework, comprising the different processes.

3.1.1 Stochastic Rainfall

Each computational step (iteration) comprises a storm event and an interstorm period. Durations of storms and interstorms are independent exponential random variables, as is the storm intensity. The distributions have means of $\bar{T}_r$, $\bar{T}_b$ and $\bar{P}$, respectively (Eagleson, 1978):

Rainfall intensity	$f(P) = \frac{1}{\bar{P}} \exp\left(-\frac{P}{\bar{P}}\right)$	(3.2)
Storm duration	$f(T_r) = \frac{1}{\bar{T_r}} \exp\left(-\frac{T_r}{\bar{T_r}}\right)$	(3.3)
Interstorm duration	$f(T_b) = \frac{1}{\bar{T_b}} \exp\left(-\frac{T_b}{\bar{T_b}}\right)$	(3.4)

Rainfall is assumed to be uniform in space and time, a rectangular pulse.

3.1.2 Hydrology

CHILD permits the use of a number of runoff production schemes. In this study, Horton (infiltration-excess) runoff is assumed, in which the precipitation (P) less the infiltration (I_c) amounts to the depth of runoff (q) yielded by each Voronoi cell:

$$q = \begin{cases} a(P - I_c) & : \quad P > I_c \\ 0 & : \quad P \leq I_c \end{cases} \tag{3.5}$$

where a is the Voronoi cell area. This model is adopted to avoid undue complexity in a study of the vegetation-erosion coupling. Surface runoff at a point becomes the sum of the contributions of the upstream and local sources. In this way, each cell has a well-defined drainage area - the total area of Voronoi cells whose discharges flow through the element in question.

3.1.3 Hillslope Diffusion

Sediment transport processes on hillslopes, soil creep and rainsplash, are modeled as a linear diffusion process (e.g. Culling, 1960):

$$\left.\frac{\partial z}{\partial t}\right|_{creep} = k_d \nabla^2 z \tag{3.6}$$

where k_d is a diffusion transport coefficient. This in part makes up the sediment flux component of equation (3.1).

Table 3.1: Fixed model parameter values.

Parameter	Value
U	0.1 mm/yr
I_c	0 mm/hr
k_d	0.01 m/y
k_b	10^{-5} kg$^{-1.5}$m$^{1.5}$s^2
p	1.5 (detachment limited)
k_t	5 kg.m$^{-0.05}$yr$^{0.55}$
mb	0.45
ma	-0.15
nb	0.7

3.1.4 Fluvial Erosion and Transport

Fluvial erosion and sediment transport are based on an excess stream power, or excess shear stress, model (Whipple and Tucker, 1999):

$$D = \begin{cases} k_b(\tau - \tau_c)^p & : \quad \tau > \tau_c \\ 0 & : \quad \tau \leq \tau_c \end{cases} \tag{3.7}$$

$$\tau = k_t Q^{mb} A^{ma} S^{nb} \tag{3.8}$$

where D = sediment detachment or transport rate, k_b is an erodibility parameter, τ is the applied local shear stress, τ_c is the critical shear stress, a threshold for sediment entrainment, p is a parameter that depends on the mode of sediment transport, k_t is a hydraulic roughness coefficient, Q is the volumetric discharge, A is the drainage area, and mb, ma and nb are empirical coefficients. Herein, D is equated to the fluvial erosion, ϵ. Values for the coefficients used are in Table 3.1.

For the purposes of this work, the entire catchment is considered detachment-limited, akin to a number of other studies (Seidl and Dietrich, 1992; Anderson, 1994; Howard et al., 1994; Tucker and Slingerland, 1994, 1996, 1997; Moglen and Bras, 1995). This is somewhat justified by the cap-rock effect cohesive vegetation plays in protecting the soil. Since water is routed instantaneously throughout the basin, only the rainfall intensity is responsible for the occurrence of erosion; rainfall duration affects the volume eroded.

3.2 Dynamic Vegetation Modeling

As described in Chapter 2, there is a multitude of ways in which vegetation affects landscape evolution, by either changing the hydrologic characteristics of the basin, of by modifying the propensity for different erosive processes to occur. To begin modeling these effects on a basin to regional scale it is useful to identify a single way in which plants affect geomorphology. For this to be dynamic, there must also be models of plant growth and death.

3.2.1 Plant Growth

The only resource plants compete for is space. The fewer the plants in a region, the greater the local growth rate, but as the density increases, growth rate decreases such that local vegetation density never exceeds unity. Different species may grow at different rates, although only one type of vegetation may be simulated at a time. This describes the following mathematical relation:

$$\frac{dV}{dt} = \frac{1}{T_v}(1 - V), \tag{3.9}$$

where V is the local (per Voronoi cell) fractional vegetation density, and T_v is a growth timescale of the vegetation. This is preferred over the logistic form for two reasons. It has one less parameter, which makes modeling and a sensitivity analysis easier. Also, since plants are always presumed to be close at hand, growth rate is not limited by the ability to colonize, allowing growth rate at low vegetation densities to be high, assyptotically approaching zero as V approaches unity. Since the interstorm duration is generally much larger than that of storms, for the sake of numerical efficiency, simulated plant growth only occurs between storms.

T_v represents the time taken for a plant to grow to a stage where it can noticeably limit erosion. This is distinct from the time until maturity or average height. In gully rehabilitation efforts in Colorado, three years has been considered the length of uninterrupted time required for plants to establish to a point where they can

withstand large erosion events (Kulbeth, pers. comm.). The vegetation in question is blue gramma (*Bouteloua gracilis*), a tufted perennial grass. The shortest reasonable timescale for plant growth is perhaps 1 year, while slow-growing trees may only start to inhibit erosion after 10 years. A range of experimental values is thus: $T_v(yrs) \in \{1, 2, 3, 5, 10\}$, differing among species.

3.2.2 Plant Death

As this thesis focuses on the geomorphic properties of plants, less attention has been given to the manner of plant death. While in nature plants die as a result of a variety of stresses (eg. fire, herbivory, resource limitation), here it is assumed that plant density is merely reduced if its substrate is eroded:

$$\frac{dV}{dt} = \begin{cases} -K_v V(\tau - \tau_c) & : \quad \tau > \tau_c \\ 0 & : \quad \tau \leq \tau_c \end{cases} \tag{3.10}$$

in which K_v is a species-dependent vegetation erodibility parameter. Since erosion only occurs during storms, so does vegetation destruction.

No fluvial process has been studied that directly causes the death and removal of vegetation. Mass wasting processes clearly do so, but they are not being modeled here. It is reasonable to presume, however, that if erosion rates were great enough, plants may be undermined (Figure 3-2), but the rarity of such cases suggests natural plant mortality occurs before this can take place. Removal of the soil mantle above basement rock would also destroy vegetation, but this is again a special case. Instead, it is presumed that a variety of processes, associated with erosion, cause vegetation loss. Equation 3.10 is thus entirely qualitative, and so K_v is the parameter about which the least is known. For this reason, the initial stage of the study simulated landscapes with expected values of the different parameters in an attempt to identify the range of values of K_v that yielded realistic landforms. The criterion for an acceptable value was a satisfactory slope for a given drainage area; the value of K_v obtained was 1 $\text{Pa}^{-1}\text{yr}^{-1}$. To study the effect of this parameter on the landscape, it

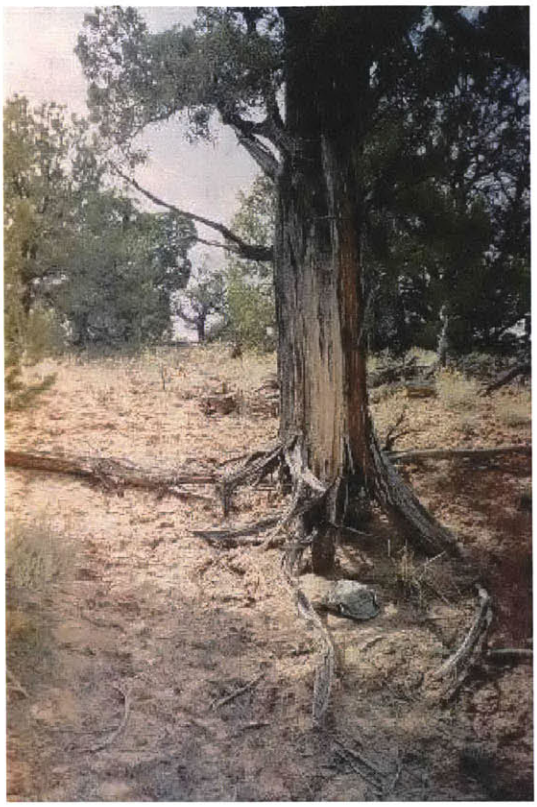

Figure 3-2: A pinyon pine (near Canyonlands, Utah) being undermined by the erosion of soil from within its root bowl.

was varied an order of magnitude on either side: $K_v(Pa^{-1}yr^{-1}) \in \{0.1, 0.5, 1, 5, 10\}$.

3.2.3 Erosion Reduction by Plants

It is clear that vegetation will modify many of the process models covered in chapter 2 (e.g. interception, infiltration, runoff duration, diffusion, and fluvial erodibility). However, for this preliminary work only changes to the critical shear stress, τ_c, will be considered. This is chosen as it is an obvious extension to *CHILD*'s fluvial erosion and transport models, and because a variety of values have already been experimentally obtained (Table 2.4). The effective critical shear stress thus becomes the sum of resistances imparted by the soil's cohesion ($\tau_{c,s}$) and the addition due to the protective

Table 3.2: The 14 simulations with their set of vegetation parameter values.

Simulation	Vegetation Modeled	$\tau_{c,v}$ (Pa)	T_v (Yr)	K_v ($Pa^{-1}Yr^{-1}$)
Bare	No			
Basic	Yes	80	3	1
Tau1	Yes	20	3	1
Tau2	Yes	50	3	1
Tau4	Yes	130	3	1
Tau5	Yes	180	3	1
Tv1	Yes	80	1	1
Tv2	Yes	80	2	1
Tv4	Yes	80	5	1
Tv5	Yes	80	10	1
Kv1	Yes	80	3	0.1
Kv2	Yes	80	3	0.5
Kv4	Yes	80	3	5
Kv5	Yes	80	3	10

vegetation ($\tau_{c,v}$), factored by local vegetation density,

$$\tau_c = \tau_{c,s} + V\tau_{c,v}. \tag{3.11}$$

The critical shear stress due to the soil alone is assumed constant, while that due to plants is dynamic and species-dependent. This permits spatially- and temporally-variable critical shear stresses, rather than constant as normally modeled, giving another degree of freedom to the excess shear stress.

From the table of values for $\tau_{c,v}$, a range of total critical shear stresses of 20-200 Pa appear to represent the gamut of vegetation states from bare ground to a secure, resistant vegetative cover. Taking a mean value to be 100 Pa, and the contribution from soil alone to be 20 Pa, the mean contribution from plants is about 80 Pa. A range of useful values, to cover a wide range of plant conditions or species, is therefore: $\tau_{c,v}(Pa) \in \{20, 50, 80, 130, 180\}$.

3.3 Simulation Procedure

With a fully described model in hand, it remains for the model to be explored. Testing and validation, while important, are not considered within the scope of the current research. Instead, numerical simulations of landscape evolution will be performed, in which each aspect of the model is varied to ascertain its effect on the nature of the landscape.

The initial topography for each simulation was a 1.8 by 1.8 km planar wedge, inclined at 11^o (Figure 3-3). Drainage is only permitted across the lowest edge. The node spacing was 60 m, sufficiently smaller than a regular hillslope length so that hillslope processes would remain important. The 1.8 km domain size would allow a number of distinct basins. Simulations, thus started, are left to evolve until some long-term equilibrium condition is reached. This was a qualitative decision based on the mean elevation time-series over a suitably long simulation time. After each simulation had reached qualitative equilibrium, the mean elevation and mean vegetation density were recorded at a frequency of 0.1 years. During this time, the complete spatial description of the landscape was recorded every 50,000 years. This was not done more frequently for reasons of simulation speed and computer storage.

There are 14 simulations in total, covering 14 sets of parameter values. Since essentially two questions are being asked, two controls are developed. One case does not incorporate the effects of vegetation, and is designated *Bare*. The other incorporates median values of each vegetation parameter, allowing a base for sensitivity analyses, and is denoted *Mean*. For each of the three parameters, four additional simulations were run, with the parameters and nomenclature as in Table 3.2. Particular sets of simulations are collectively named as follows:

- Control Comparison: *Bare* and *Mean* .
- Tau Simulations: *Tau1* , *Tau2* , *Mean* , *Tau4* and *Tau5* .
- Tv Simulations: *Tv1* , *Tv2* , *Mean* , *Tv4* and *Tv5* .
- Kv Simulations: *Kv1* , *Kv2* , *Mean* , *Kv4* and *Kv5* .

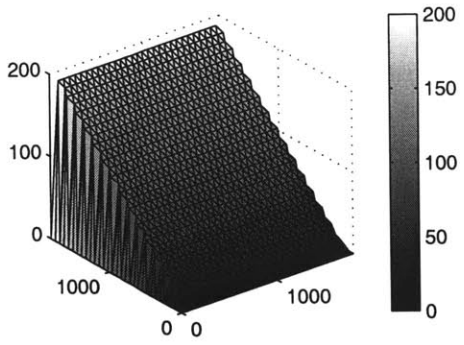

Figure 3-3: Initial topography. Planar 1.8 by 1.8 km slope inclined at 11^o, draining only through the lower edge. Voronoi cell spacing $\sim$ 60 m.

After the simulations are completed, effective area-averaged erosion is calculated from the elevation time-series. This is done by taking differences is successive heights and adjusting for the constant uplift. In this way, both fluvial and diffusional processes are subsumed into one metric, but it is assumed the fluvial erosion is the dominant component. Sediment eroded fluvially is not monitored *per se*.

Chapter 4

Spatial Biophysiographic Study

4.1 Topography and Biogeography

The most salient feature of a landscape depends on one's point of view. To a geomorphologist, it is the topography; to an ecologist, the biogeography. It is well accepted in both geomorphology and ecology that particular forms are generally expressions of particular processes (Tucker and Bras, 1998; Shugart, 1998). Thus it is the role of this section to illustrate visually and statistically the effects vegetation dynamics have on topographic and biogeographic indices.

4.1.1 Bare and Vegetated Comparison

Plants clearly tend to make the topography higher (Figure 4-1). The mean elevation and slope increase from 24.2 m and 0.08 m/m, respectively, for the unvegetated case, to 35.0 m and 0.13 m/m in the case of average vegetation parameters (Figure 4-7). The presence of vegetation increases the critical shear stress that must be overcome before erosion is initiated. For a given drainage area and long-term erosion rate, this means a vegetated cell will be steeper than a bare cell, under the same long-term erosion rate. Derived from equations 3.7, 3.8 and 3.11, the increased mean steepness is approximated by

$$S_{vegetated} = \left(S_{bare}^{n} + \frac{V \tau_{c,v}}{k_t A^m} \right)^{\frac{1}{n}}, \tag{4.1}$$

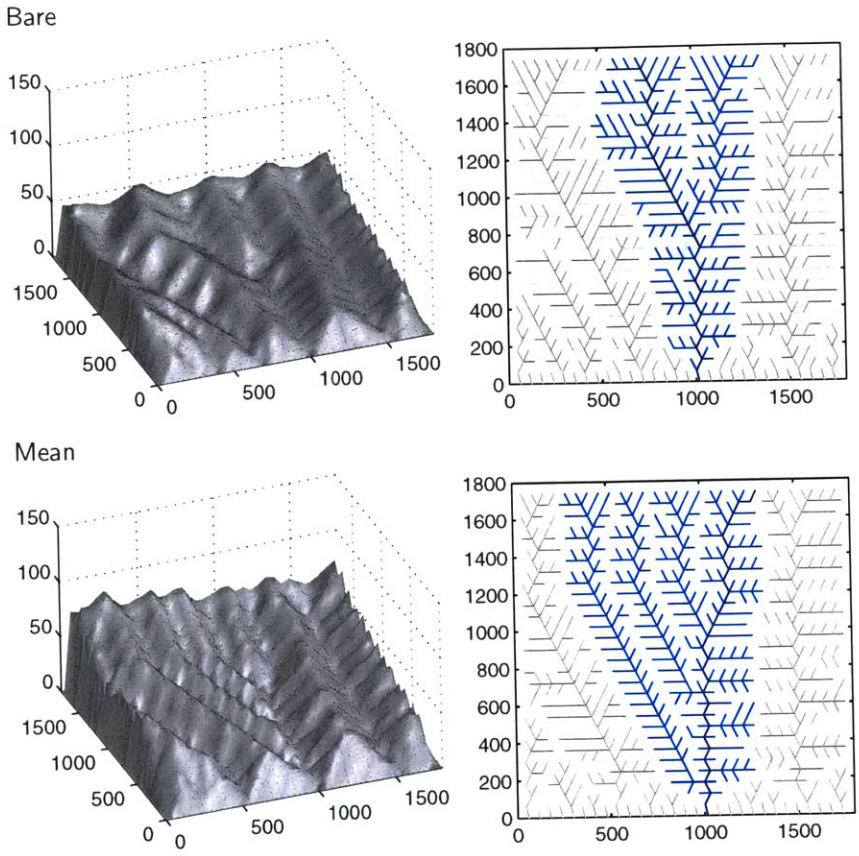

Figure 4-1: Topography of the *Bare* and *Mean* simulations after 500,000 years of equilibrium simulation (left). Their drainage networks are represented on the right (light blue represents the largest basin; dark blue the main channel).

where $S_{vegetated}$ and S_{bare} are the vegetated and bare slopes, respectively. The greater the drainage area, the less pronounced this difference, while the opposite is true for the vegetative critical shear stress.

4.1.2 Plant Resistance ($\tau_{c,v}$) Sensitivity

Increasing the additional critical shear stress due to plants is accompanied by a parallel increase in topographic indices (elevation and slope) (Figure 4-2), as expected from the previous results. Furthermore, this trend appears smooth and monotonic, suggesting no particular threshold of vegetation importance exists with respect to changes in topographic expression — any increase in erosion resistance by different plant species will be met by an increase in topographic indices.

As for the vegetation distribution, there is a striking bimodality of plant densities — cells tend to be either well-vegetated or poorly-vegetated (Figure 4-2). Bands of dense vegetation occupy ridge-lines, and are absent from the channels. A smooth, monotonic trend of the extension of well-vegetated cells with increasing erosion resistance is also apparent.

Figure 4-5 shows the distributions for the five *Tau* simulations. Increasing $\tau_{c,v}$ depresses the peak in the elevation distribution, increasing the range. This is the same for local slopes, although these are more skewed to the right. If there is a well-vegetated mode, it occurs at full cover; the poorly-vegetated mean is more variable. These observations are given more credence in Figure 4-7. The mean and variance of both elevation and slope increase, and at ever-increasing rates over the given range. While the elevation's skewness peaks for central values of $\tau_{c,v}$, the slope's clearly increases. The mean vegetation density increases, as a result of a change of poorly- to well-vegetated cells.

Higher $\tau_{c,v}$ causes gains in vegetation density to be more likely retained. Spanning over many storms, this tends to make cells well-vegetated for longer periods. The compound effect of continual uplift over this time is to significantly steepen the vegetated topography, so that when erosion does occur, and the protective plant cover is finally stripped, slopes find themselves over-steepened and will rapidly erode. This erosion will be difficult to stem, until slopes lessen significantly, so that erosion too is largely uninterrupted. To maintain equilibrium, rapid erosion must be more brief than sluggish erosive events, giving more time for re-vegetation to occur. With all slopes able to become steeper, the vegetation front extends further downstream, thus steeper landscape is also more densely vegetated.

4.1.3 Plant Growth Time-scale (T_v) Sensitivity

Increasing the time-scale of regrowth, equivalent to reducing the growth rate, has the opposite effect from increasing erosion resistance — topographic indices decrease (Figure 4-3). Mean vegetation density does the same. A similar smooth, monotonic response is again apparent in both trends.

Increasing T_v has the opposite effect from $\tau_{c,v}$ with respect to elevation and slope histograms - they become less variable - while clear peaks in the distribution are still present (Figures 4-6 and 4-8). Cells with lower vegetation density become more common and less vegetated as the time-scale of regrowth increases.

Faster growing plants recover sooner after being eroded, reducing the number of storms with an intensity great enough to cause erosion. This leads to increased slopes and more widespread vegetation. Growth rate, however, does not effect susceptibility to erosion for a given vegetation density, so the long periods of sustained uplift possible for high $\tau_{c,v}$ are not possible for low T_v, thus it is the stochastic storms that dominate the evolution rather than uplift. Plants with high T_v recover so slowly as to make the landscape essentially barren — very few cells are able to maintain a high vegetation density for long, reducing the potential for continual uplift, and thus reducing possible slopes. Again, shallower slopes, which erode less rapidly, must do so for a longer time, further suppressing vegetation establishment.

4.1.4 Plant Erodibility (K_v) Sensitivity

As plant erodibility increases, or as plants become more easily destroyed by soil loss, the topographic indices tend towards those of the unvegetated case – they decrease (Figure 4-4). Once again, this transition is smooth and monotonic, and once again, the steeper landscape is more densely vegetated.

With growth rate constant, an increasing erodibility means the surface will be less vegetated, as more vegetation is destroyed when erosion occurs. As the plants' propensity to die from the loss of soil increases, their persistence decreases, and so does their ability to re-establish. Slopes are thus less able to remain steep and vegetated.

In a similar fashion to $\tau_{c,v}$ and T_v, increasing K_v leads to a reduction in the mean and variability of elevation and slope variability (Figure 4-6). The *Kv1* simulation is the only case in which vegetation densities do not follow a clear bimodal distribution, although peaks are still present (at around 0.4, 0.5 and 0.8). For the set of simulations as a whole, increasing K_v reduces the density of the poorly-vegetated cells and increases their frequency, paralleling topographic trends. Resilient plants with low

K_v make it harder for a series of storms to erode a region, and in so doing, smooth out the evolution of the landscape, preventing stark contrasts in net uplift and erosion durations. Vegetation states are consequently more evenly distributed.

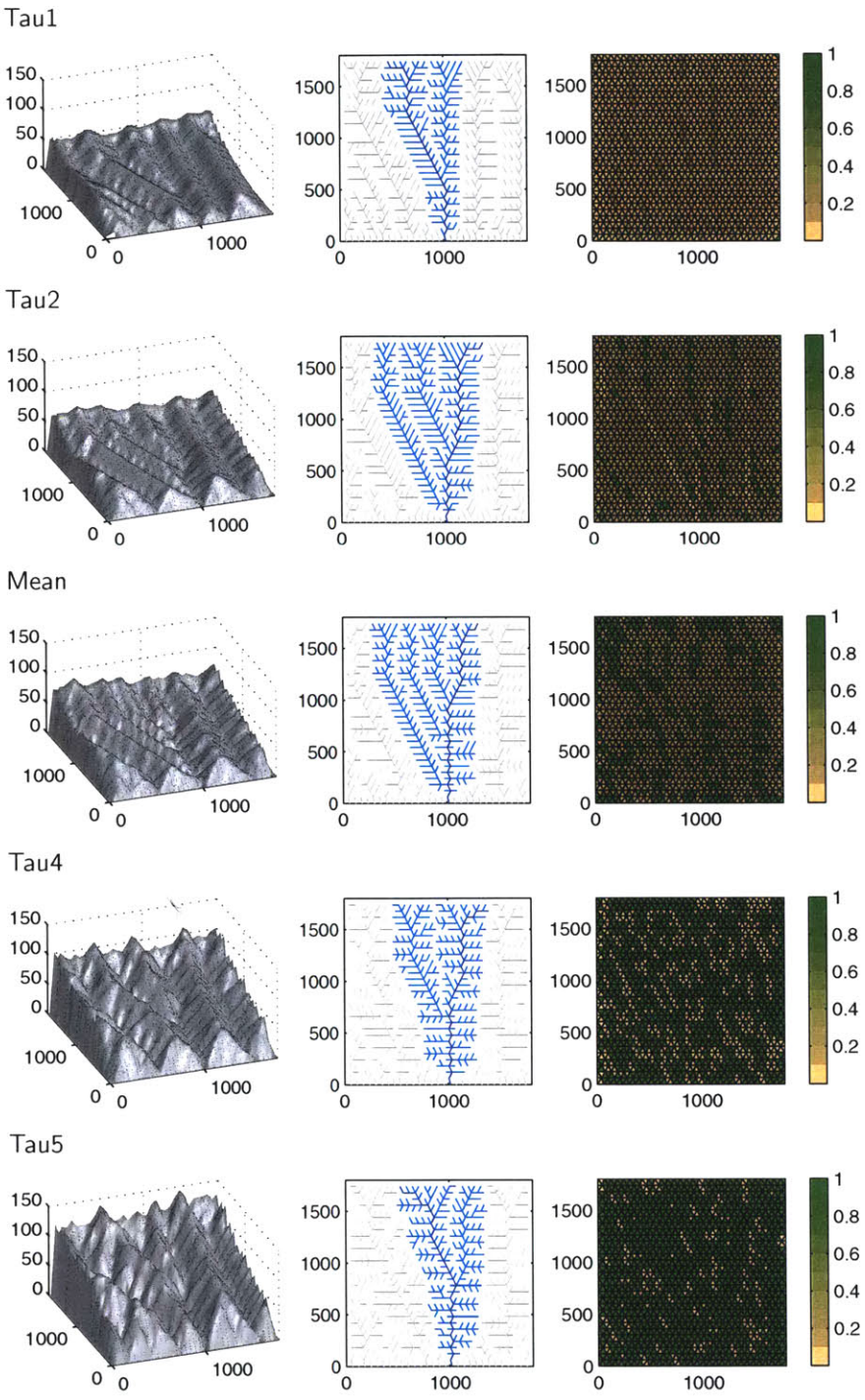

Figure 4-2: Topography (left column), channel network (center column), and vegetation distribution (right column) for the suite of $\tau_{c,v}$ simulations. $\tau_{c,v}$ increases down the page. For the channel network, light blue is the largest basin; dark blue is its main channel.

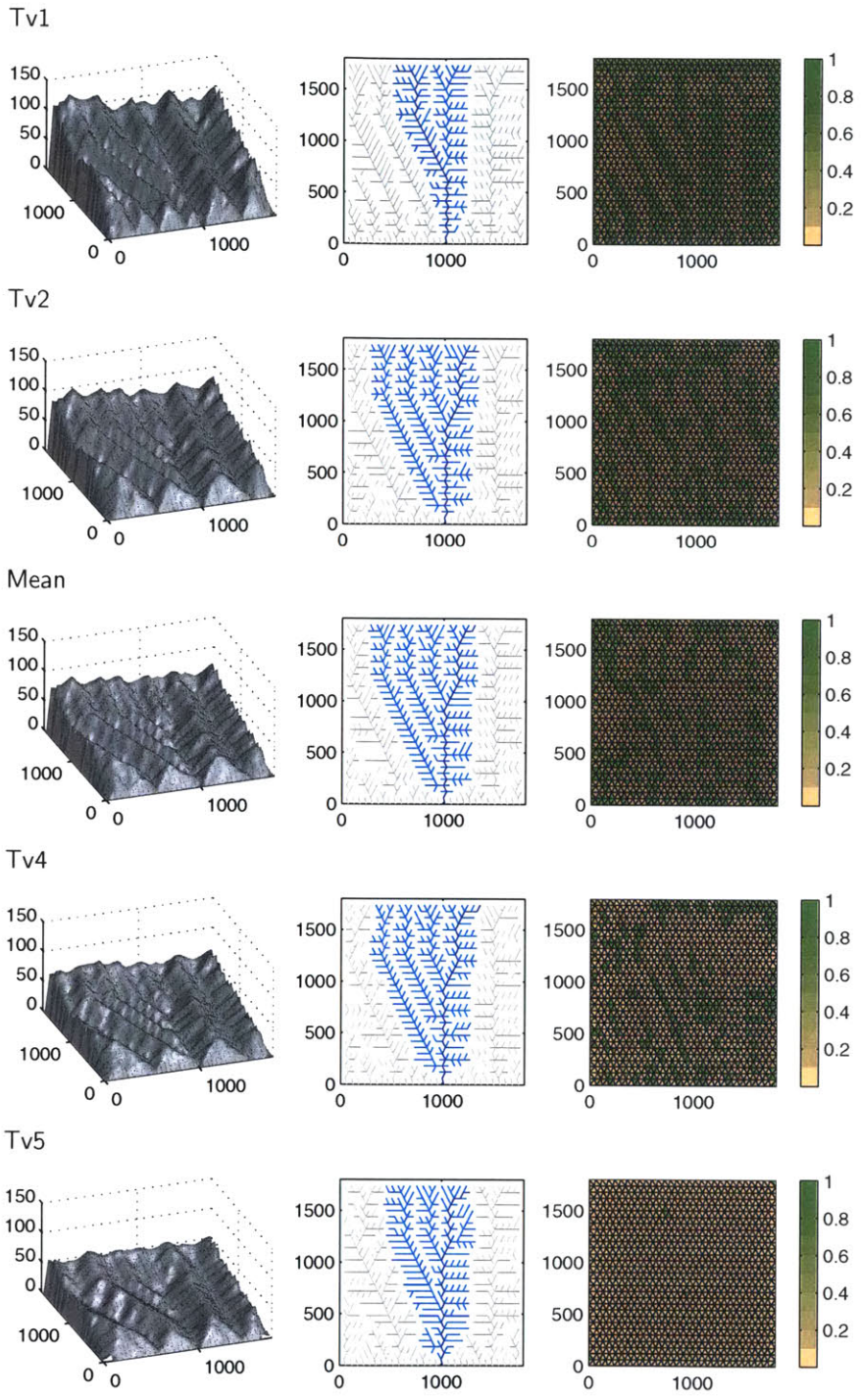

Figure 4-3: Topography (left column), channel network (center column), and vegetation distribution (right column) for the suite of T_v simulations. T_v increases down the page. For the channel network, light blue is the largest basin; dark blue is its main channel.

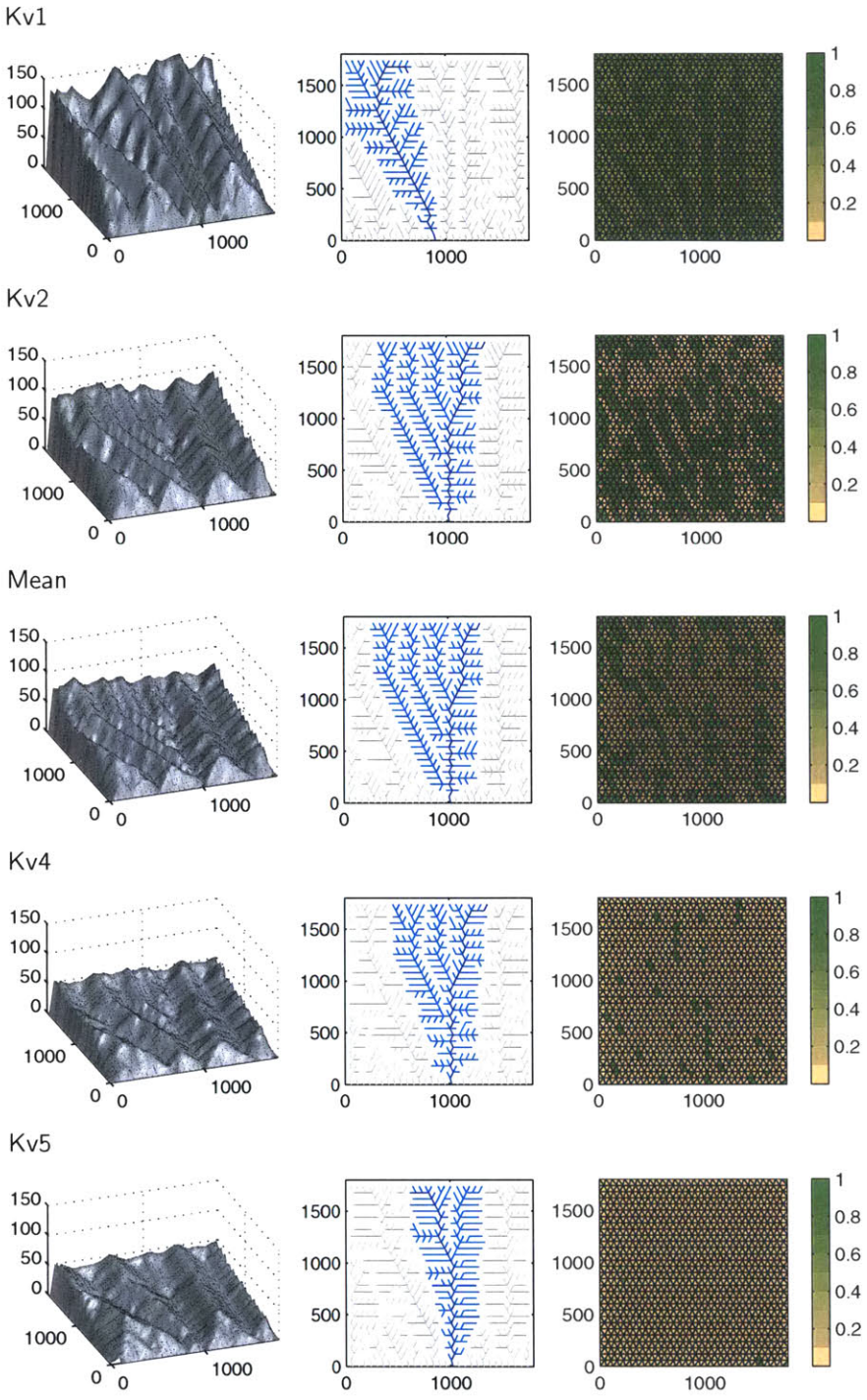

Figure 4-4: Topography (left column), channel network (center column), and vegetation distribution (right column) for the suite of K_v simulations. K_v increases down the page. For the channel network, light blue is the largest basin; dark blue is its main channel.

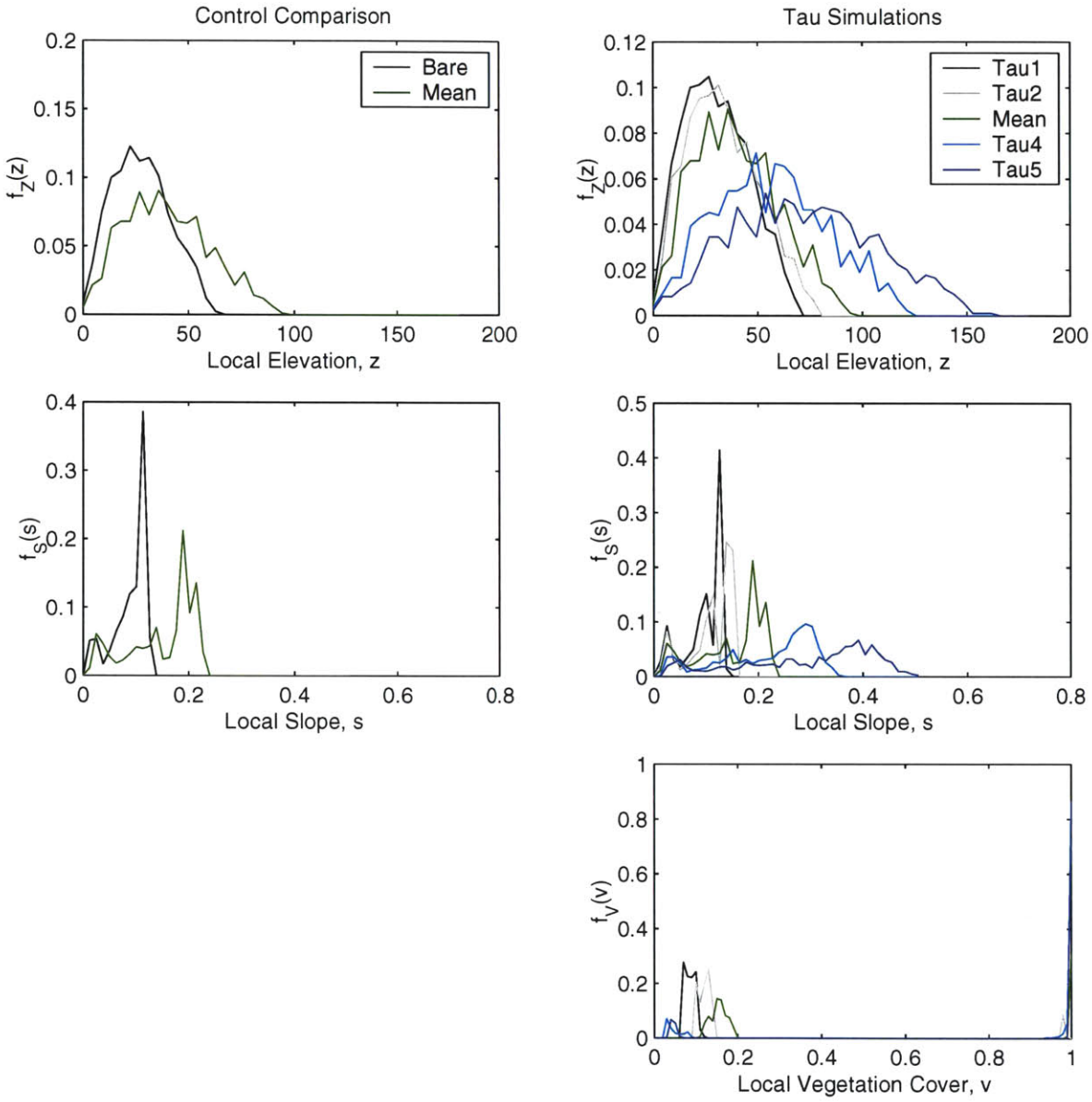

Figure 4-5: PDFs of elevation (z), slope (s) and vegetation density (v) for the *Bare* and *Mean* simulations (left), and *Tau* simulations (right).

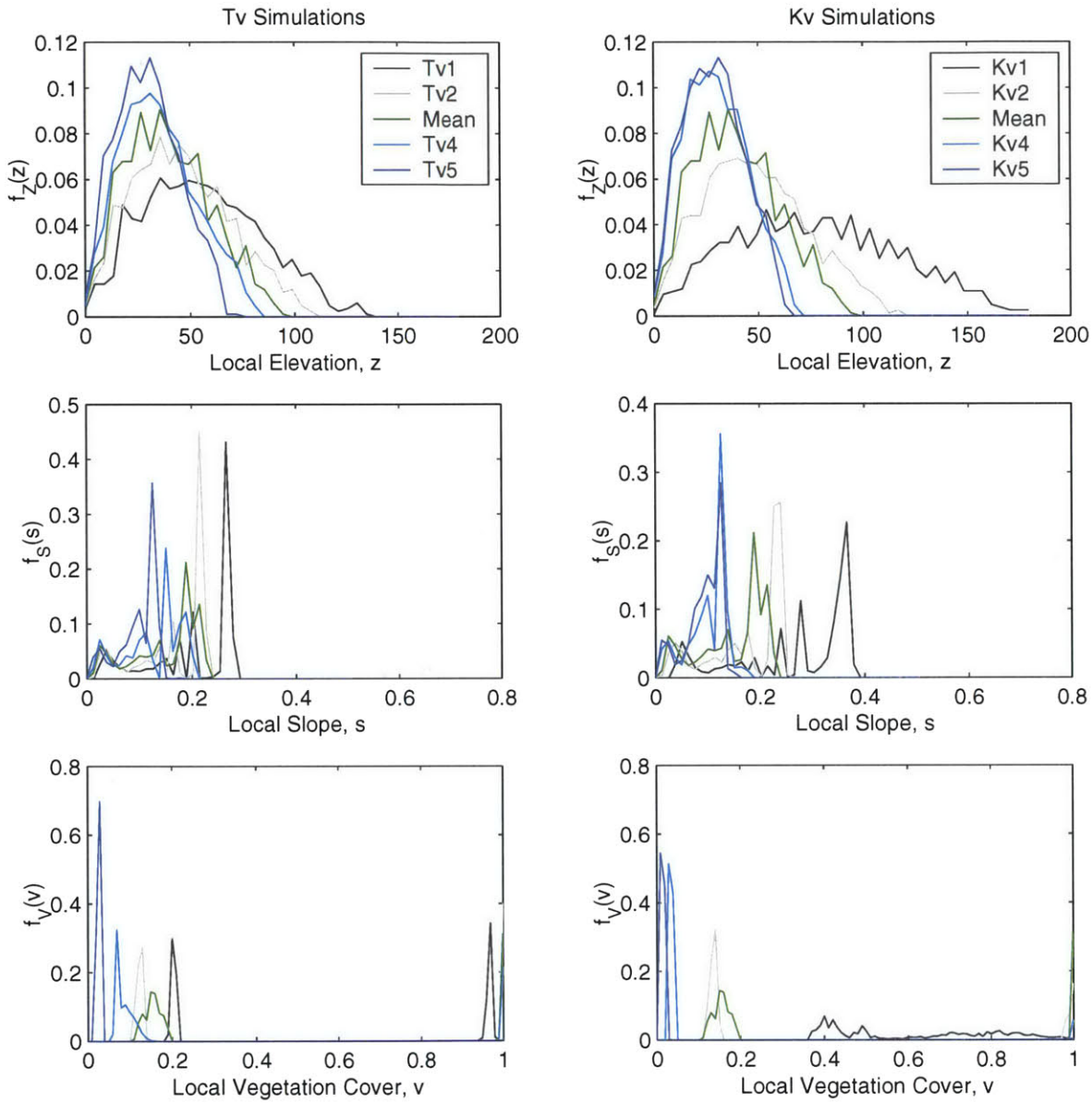

Figure 4-6: PDFs of elevation (z), slope (s) and vegetation density (v) for the suite of T_v (left) and K_v (right) simulations.

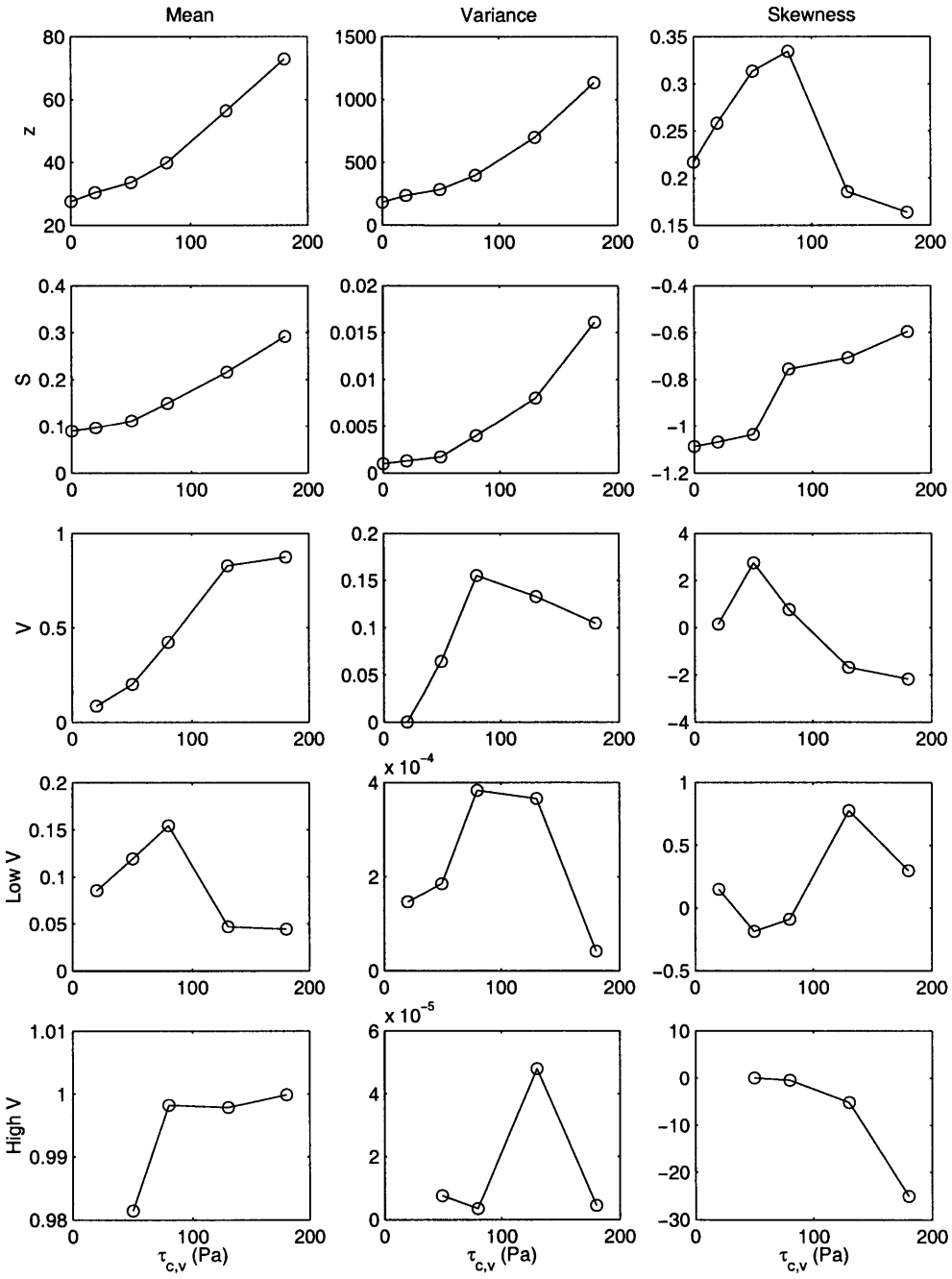

Figure 4-7: Trends in topographic and biogeographic statistics as $\tau_{c,v}$ increases.

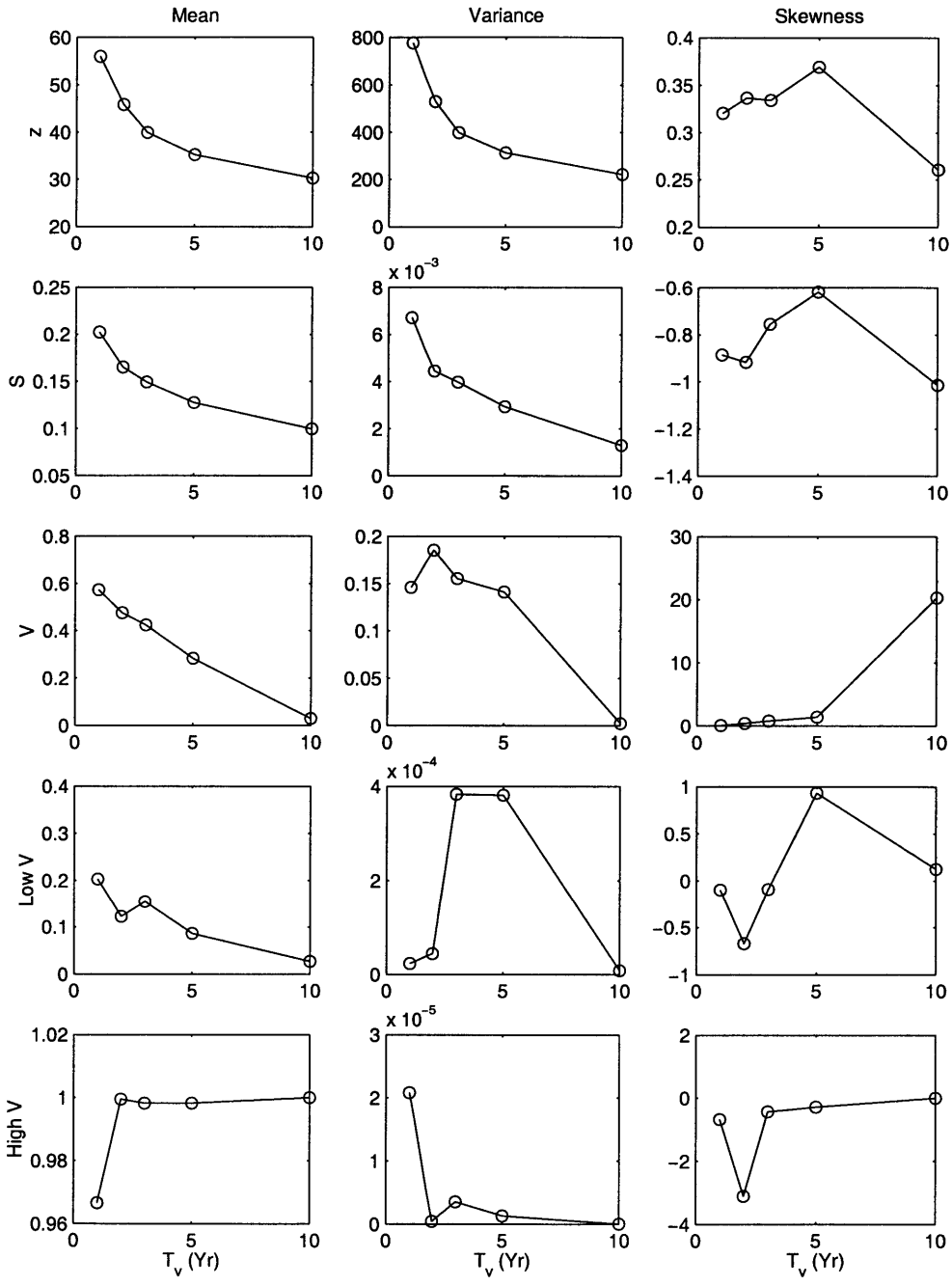

Figure 4-8: Trends in topographic and biogeographic statistics as T_v increases.

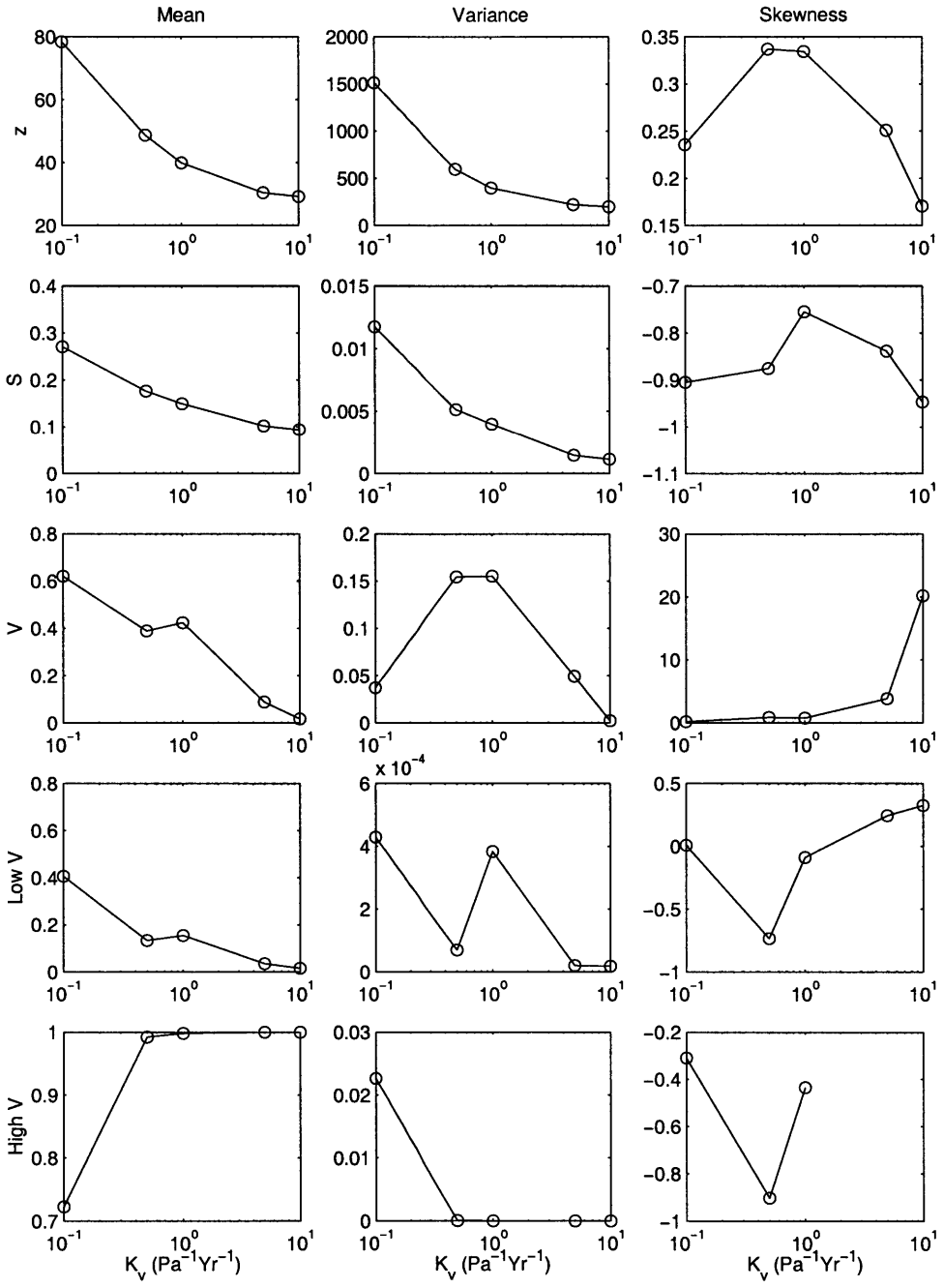

Figure 4-9: Trends in topographic and biogeographic statistics as K_v increases.

4.2 State Variable Relationships

4.2.1 Slope-Area

The slope-area (S-A) relationship is a common diagnostic measure of an evolving landscape and of landscape evolution models (Willgoose et al., 1991; Ijjasz-Vasquez and Bras, 1995), despite its universal utility being questioned of late (Schorghofer and Rothman, 2001). Even before discussing the effects of vegetation, however, one fact is glaringly obvious - the entire domain of each simulation is dominated by fluvial erosion (Figure 4-10). This is evidenced by the straight line in log-log space. A slope reversal for low drainage areas would indicate the relative importance of more diffusive processes. Its absence, which means that hillslopes are less than 60 m long (smaller than a voronoi cell) indicates that the diffusion coefficient, k_d, chosen for the simulations is too low.

The slope of the line is governed by the nature of the fluvial erosion process, which is constant for each simulation. The intercept, however, is a measure of the erosivity of the landscape under the prevailing environmental conditions. With variations only in vegetation properties, increases in the intercept result from increases in $\tau_{c,v}$ and decreases in both T_v and K_v. This corresponds directly to the increases in slope reported previously.

4.2.2 Vegetation-Slope-Area

With the addition of vegetation to area and slope as state variables, it is logical to look at the vegetation-area-slope (V-S-A) relationship (Figure 4-13). While patterns are less clear than for S-A, vegetation cover is no doubt sensitive to slope, and vice versa. Each band of like-colored points, in V-S space, represent similar drainage areas. As A decreases, S increases, and so too does the density of the poorly-vegetated cells, making a more continuous range of V values more likely at higher S. For any given drainage area, vegetation density decreases as the slope increases. This trend is concave-up for low V and concave-down for high V. The nature of the V-

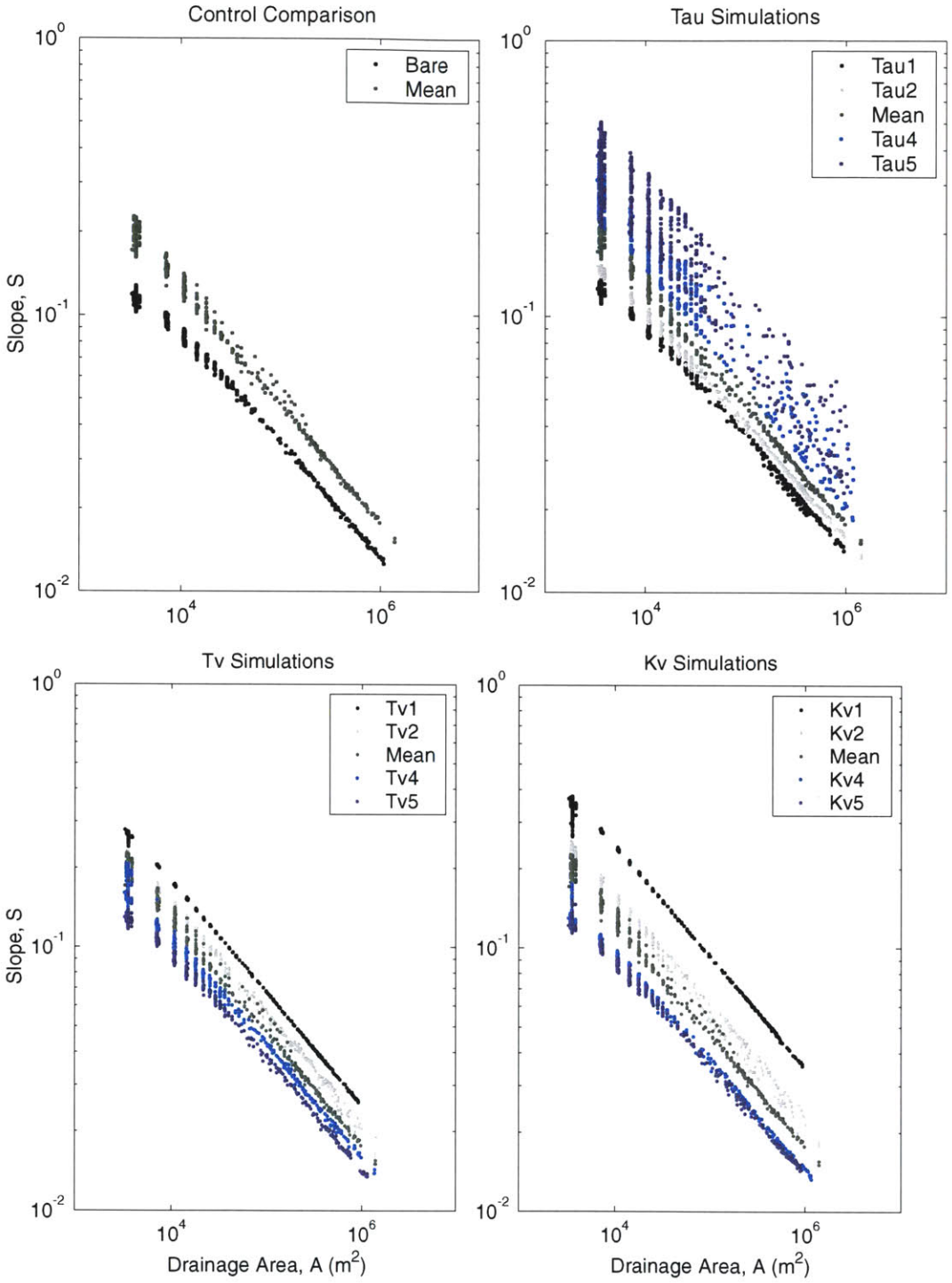

Figure 4-10: Slope-area relations for the four sets of simulations. As the fluvial process is unchanged, slopes of the lines (in log-log space) are identical. The intercept, however, is a measure of the landscape's erodibility, which depends on the vegetation parameters. The absence of a line segment with positive gradient indicates diffusion is negligible.

S-A relationship clearly depends on the vegetation parameters, however the cause is subject to conjecture. What would be illuminating is determining how, if at all, node states move through V-S-A space as the landscape evolves, so hypotheses for the patterns will be attempted in Chapter 6: Dynamic Biophysiography.

4.3 Analysis of Biogeographic Bimodality

Figures 4-5 and 4-6 show clear bimodality of vegetation states for at least 12 of the 13 simulations. In an attempt to explain why, consider the three vegetation equations (3.9, 3.10, and 3.11).

For a cell to maintain a constant vegetation density, at least for a time-scale much longer than storm and interstorm periods, (3.9) and (3.10) may be combined to become

$$\frac{\partial V}{\partial t} = \frac{1}{T_v}(1-V)\frac{\bar{T}_r}{\bar{T}_r+\bar{T}_b} - K_v V(\tau-\tau_{c,v})\frac{\bar{T}_b}{\bar{T}_r+\bar{T}_b} = 0, \tag{4.2}$$

in which the storm and interstorm durations are approximated by their mean duration.

Substituting in (3.11) and solving for τ, one gets an estimate of the mean applied shear stress required to maintain a constant vegetation density locally (Figure 4-14),

$$\tau = \frac{1-V}{T_v K_v V}\frac{\bar{T}_b}{\bar{T}_b} + \tau_{c,s} + V\tau_{c,v}. \tag{4.3}$$

Cells whose states (τ and V) plot above the line in Figure 4-14 will tend to erode and devegetate, while cells whose states plot below the line will tend to revegetate. The sharp rise to the left is due to the high growth potential for low vegetation density (a result of the mono-parametric growth equation). The rise on the right is due to the increasing difficulty for runoff to erode an increasingly armored surface. The minimum density is denoted V_*.

For a landscape to be in equilibrium, there must be some long-term mean applied shear stress that is greater than V_* (depicted by the horizontal green and red line).

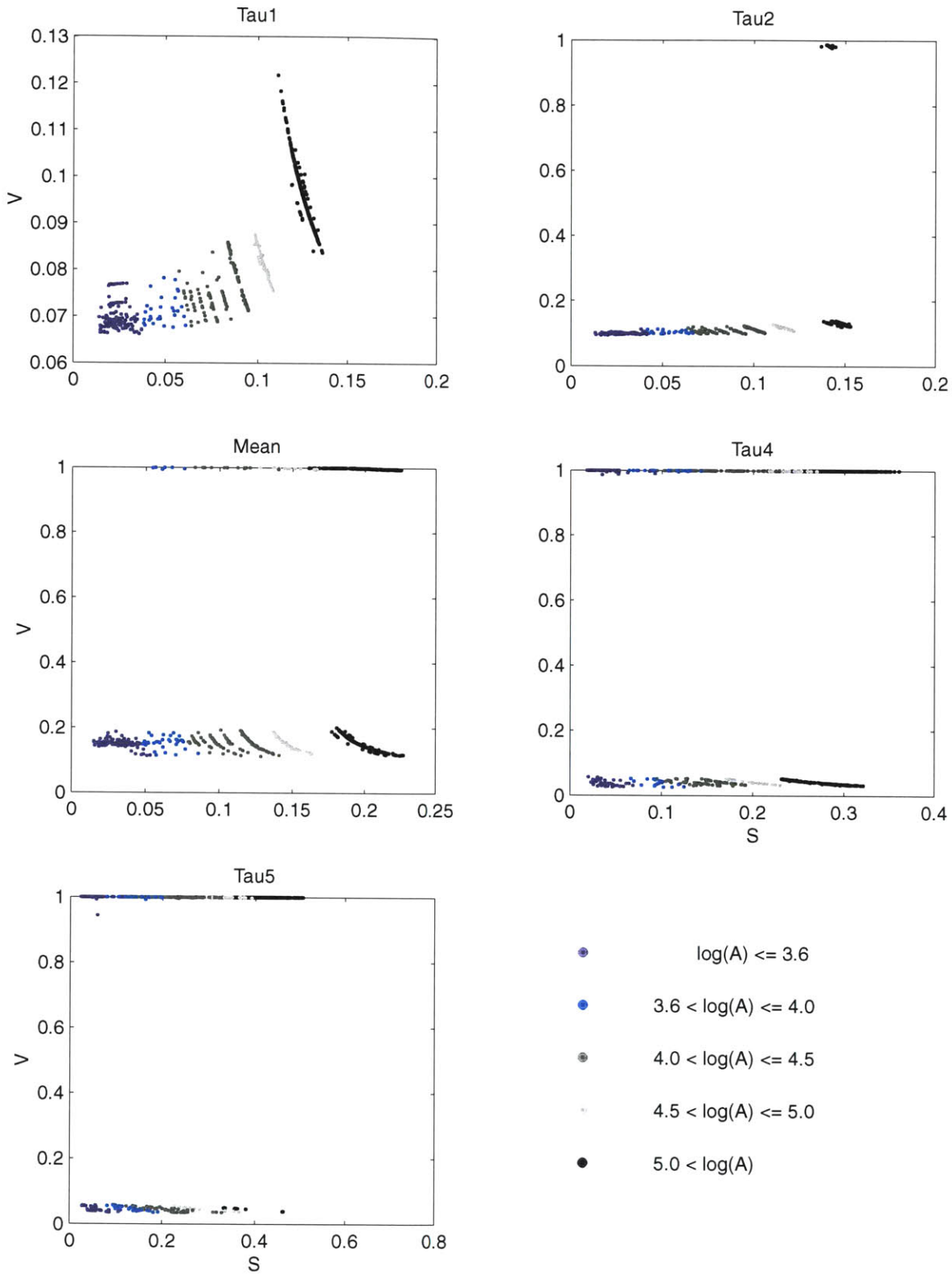

Figure 4-11: Vegetation-slope-area relations for the Tau simulations. The distinct bands of like-colored points represent similar drainage areas.

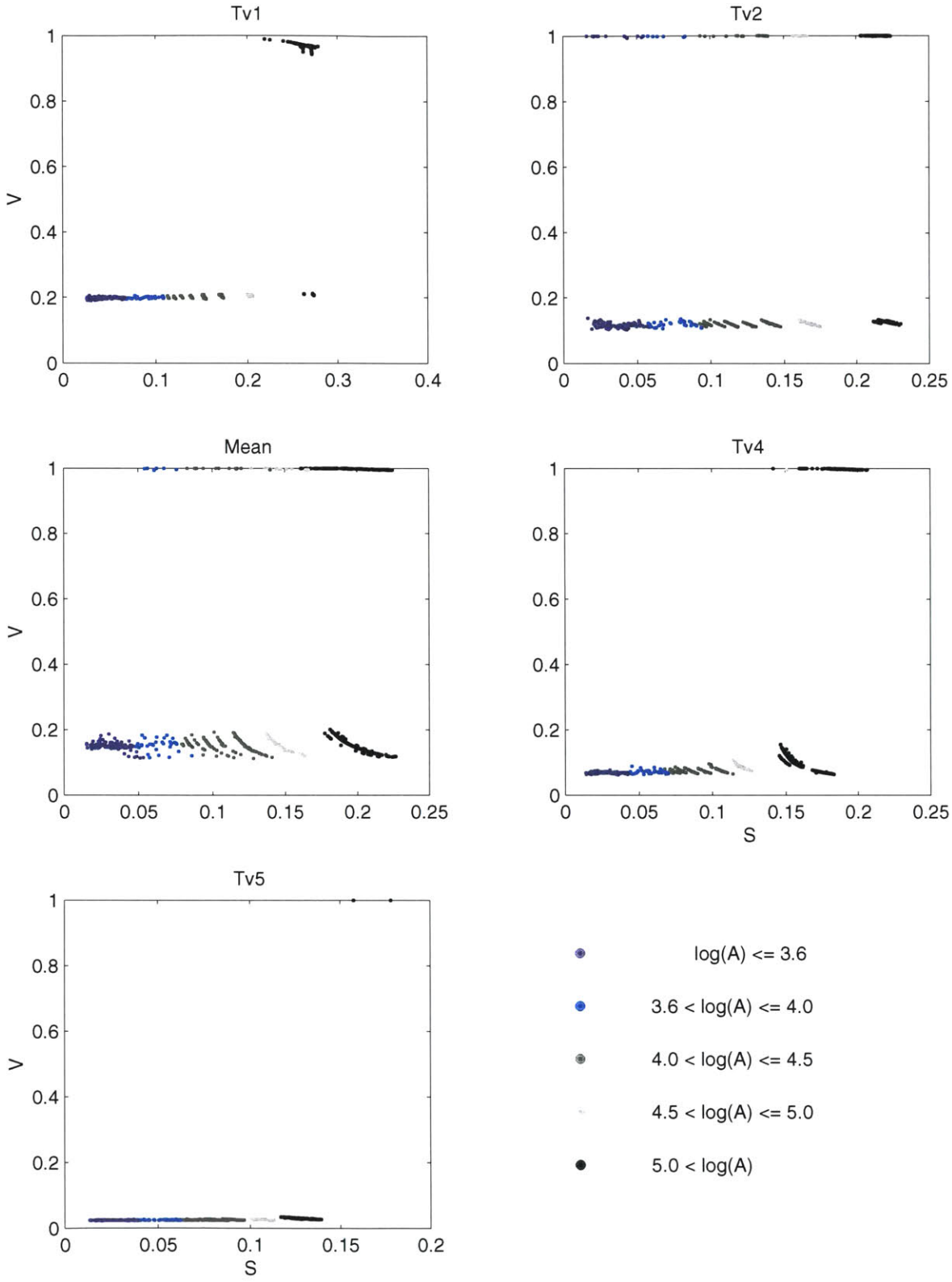

Figure 4-12: Vegetation-slope-area relations for the Tv simulations. The distinct bands of like-colored points represent similar drainage areas.

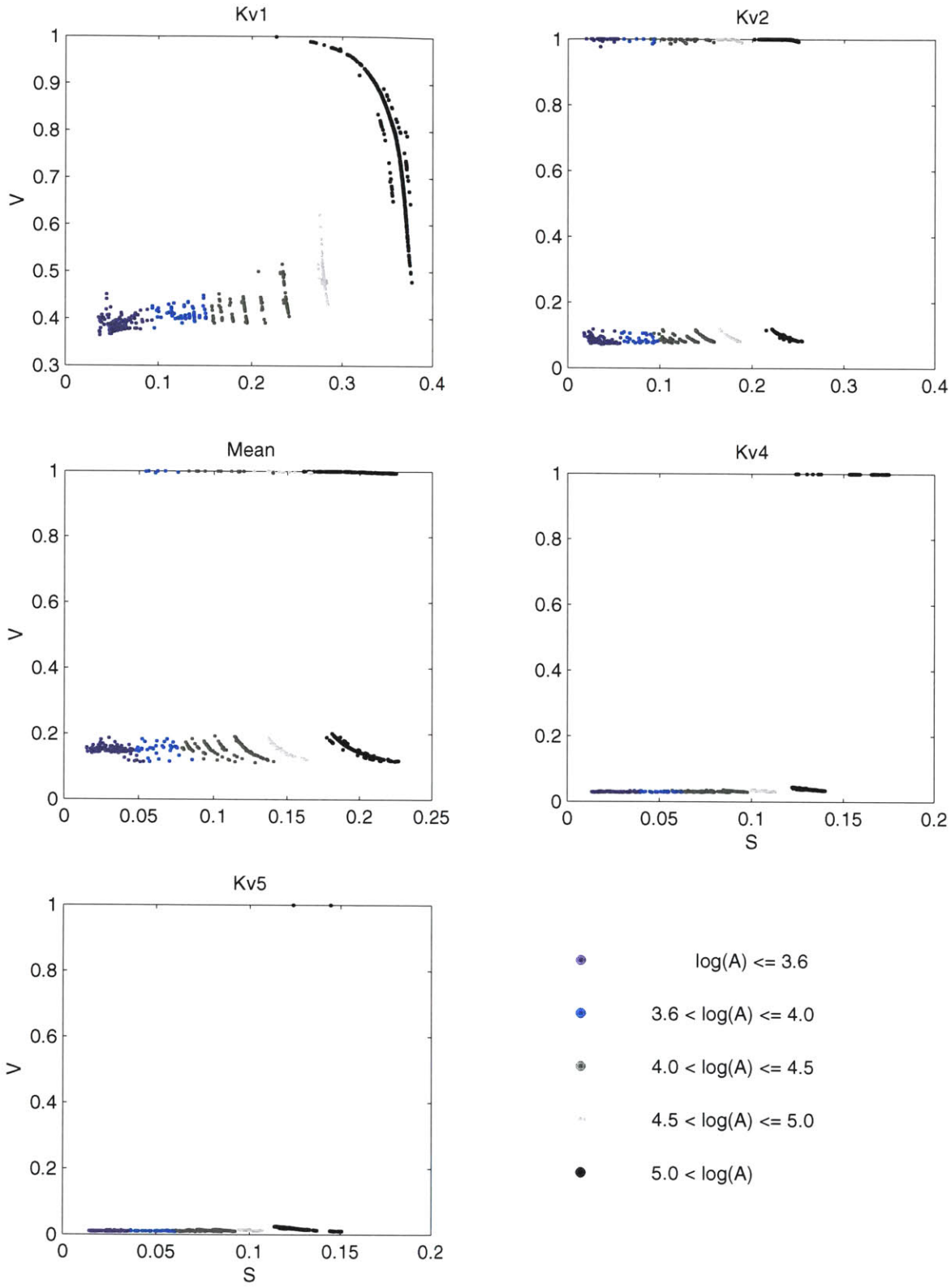

Figure 4-13: Vegetation-slope-area relations for the Kv simulations. The distinct bands of like-colored points represent similar drainage areas.

Otherwise there would be 100% vegetation cover and no erosion, which is unstable. Conversely, since for some simulations vegetation densities are observed around unity, this long-term mean shear stress must be below the value of τ_* at 100% V ($\tau = \tau_{c,s} + \tau_{c,v}$). This naturally breaks the τ-V space into three distinct domains:

1. cells have a high growth potential and will tend to re-vegetate, with little erosion;
2. cells will tend to erode, reducing the vegetation cover;
3. cells are resistant to erosion, and will consequently tend to become fully vegetated.

This leads to two distinct attracting states:

i. low vegetation density (V_*);

ii. complete vegetation cover ($V = 1$).

The minimum occurs at

$$(V_*, \tau_*) = \left(\sqrt{\frac{\bar{T}_b}{\bar{T}_b} \frac{1}{T_v K v \tau_{c,v}}}, \tau_{c,s} + 2\sqrt{\frac{\bar{T}_b}{\bar{T}_r} \frac{\tau_{c,v}}{T_v K_v}} - \frac{\bar{T}_b}{\bar{T}_r} \frac{1}{T_v K_v} \right). \tag{4.4}$$

The values of V_* are strikingly similar to the values of the lower mode mean for the different simulations (Table 4.1). Variations about this value, and also about unity, are expected as cells will change their state occasionally, and hence they must be at some intermediate value for some duration of time. A value of $V_* = 0.34$ for *Kv1* suggests the cutoff between low and high vegetation states is around 0.45, which results in a sparse vegetation mean of $\bar{V}_{low} = 0.41$. The disparity between the observed and estimated values for *Tau1*, however, suggests that the analytic solution is over-simplified. Equation 4.4 predicts ever higher V_* with decreasing $\tau_{c,v}$, which is a result of the right arm of the τ-V curve being flattened, producing a minimum more sensitive to changes in vegetation density. Hence, any analytic point has less significance given the variability of the states.

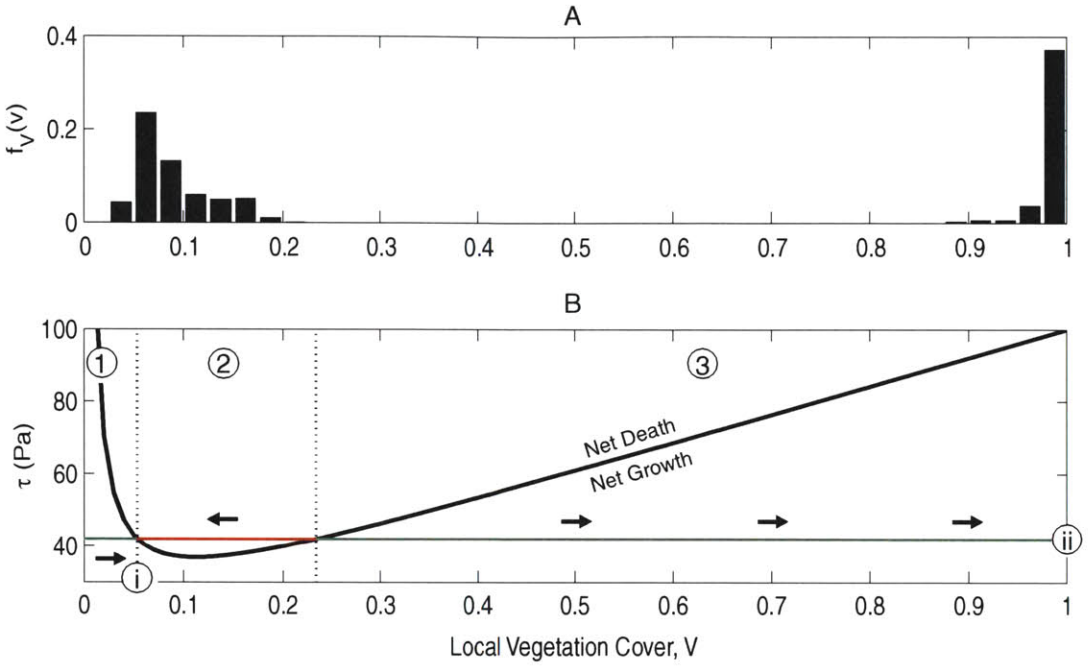

Figure 4-14: A. Histograms of local plant density generally exhibit bimodality, as in the *Mean* simulation. **B**. Comparison with equation (4.3) shows the low mode mean value occurs near the minimum of the τ-V curve.

Table 4.1: The low vegetation mode mean ($\bar{V}_{low}$) and its analytic estimate (V_*).

Simulation	$\bar{V}_{low}$	V_*
Basic	0.15	0.11
Tau1	0.09	0.22
Tau2	0.12	0.14
Tau4	0.05	0.09
Tau5	0.04	0.07
Tv1	0.20	0.19
Tv2	0.12	0.13
Tv4	0.09	0.08
Tv5	0.03	0.06
Kv1	0.41	0.34
Kv2	0.13	0.15
Kv4	0.04	0.05
Kv5	0.02	0.03

4.4 Summary

With only a static snapshot of the effects of vegetation dynamics on landscape evolution, much has been learned:

1. An increase in relative vegetative importance may be considered a consequence of higher $\tau_{c,v}$, and lower T_V and K_v. This is apparent in that the reverse effects tend towards the bare simulation;

2. Higher vegetation importance gives rise to higher mean elevation, slope and vegetation density;

3. Appropriate vegetation parameters allow slopes to increase, and increasing slopes which allow vegetation to spread;

4. Low K_v smoothes out landscape evolution;

5. Low T_v decouples proximal erosion events;

6. Local vegetation density is bimodal — well-vegetated cells ($V \sim 1$) occupy the less frequently eroding, steeper regions (hillslopes); poorly-vegetated cells occupy more gentle yet more frequently eroding regions (channels);

7. The value of the lower vegetation density mode differs between simulations and may be approximated analytically;

8. The $S - A$ relationship shows diffusion is relatively unimportant, and that vegetation properties notably affect landscape erodibility;

9. The additional state variable V leads to a non-trivial V-S-A relationship for which a satisfactory explanation is lacking.

Chapter 5

Lumped Temporal Analysis

Landscapes are not static, immutable entities. While long term equilibrium states may exist under constant prevailing environmental conditions, shorter time-scales may demonstrate a more vibrant story. Stochastic, yet stationary, storm events will inevitably lead to variable erosion rates, creating a dynamic elevation field. With the coupling of vegetation dynamics to erosion, temporal changes in plant distribution are also expected. What is harder to anticipate is whether the biophysiography (in this case elevation, erosion rates and vegetation density) will exhibit anything more than just the high frequency behavior imposed by the stochastic storms. To address this, time series of spatial mean elevation, z, erosion rate, ϵ, and vegetation density, V, are analyzed — visually and statistically.

5.1 Time-Series

The instantaneous areal averages of mean elevation and vegetation cover of all nodes are recorded at intervals of 0.1 years. The erosion rate over a period of time, Δt, is calculated as the uplift rate, U, less the rate of change of elevation,

$$\epsilon = U - \frac{z_{t+\Delta t} - z_t}{\Delta t}. \tag{5.1}$$

This makes no distinction between fluvial erosion and diffusion and is thus termed "erosion" largely for convenience. While diffusional elevation lowering is active, the resultant deposition is not. Mass is thus not conserved, potentially leading to negative values of ϵ, although in light of the fluvial dominance, this is a negligible effect.

Recording data every 0.1 years for 500,000 years gives 5,000,001 elevation and vegetation data points (which includes both the start and finish). The erosion data have one fewer. Such an abundance of data makes it infeasible to present the complete time-series clearly. Instead, the 500,000 year series is presented at the centennial scale (every 1,000th data point). Successively smaller windows of 20,000, 1,000 and 80 years are magnified at increasing resolutions of 10, 1 and 0.1 years, decomposing large-scale features into small. The distribution of elevation, erosion and vegetation are compared among like simulations, and statistics of the complete array of the 0.1-year and 100-year resolution data are also presented. The 100-year statistics are included essentially for comparisons of erosion rate skewness at the two scales. Each simulation will now be discussed separately, highlighting important observations and concepts as they appear.

5.1.1 *Bare*

Erosion rates of the *Bare* simulation fluctuate stochastically about their mean of 10^{-4} m/yr (Figures 5-2 and 5-3). They show no sign of persistence at any resolution, and so elevation resembles a random walk with no characteristic time-scale — as the resolution increases and the window decreases, the time series appears the same. Erosion skewness becomes increasingly positive at finer resolutions, and elevation fluctuations are low — of $\mathcal{O}(0.02$ m). Landscape evolution is thus driven by the independent, random storm events yielding a pattern-less temporal fingerprint.

5.1.2 *Mean*

In stark contrast to *Bare*, elevation variation of the *Mean* simulation (Figures 5-4 and 5-5) is of $\mathcal{O}(1$ m) and is clearly not a random walk — the windows do not resemble one

another. Erosion and vegetation cover are clearly negatively correlated at the large-scale, and together show persistence at two scales — the shorter meta-stable states of $\mathcal{O}$(1,000 years), and longer spells of consistent net uplift or net erosion of $\mathcal{O}$(10,000 years). Net uplift is defined as the result of erosion rates that are on average below the long-term equilibrium rate of 0.1 mm/yr (the steady uplift rate). Net erosion is the effect of erosion rates exceeding this rate. Neither the meta-stable states nor the periods of consistent net uplift or erosion are of constant duration, and so the three time series are aperiodic. The meta-stable states are medium frequency stationary periods superposed with high frequency oscillations (Figure 5-1). Changes between the meta-stable states are rapid, $\mathcal{O}$(1-10 years), and comprise the steps of the low frequency oscillations. The high frequency variability appears negatively correlated with the magnitude of the meta-stable vegetation density. The concave-up decays in erosion rate at the centennial scale (diminishing $|\frac{\partial \epsilon}{\partial t}|$ as ϵ decreases) suggest the data are positively skewed, although the measured statistic is made negative by the large, sharp reduction at 250,000 years time. Positively skewed erosion rates, in which excursions above the mean are greater than below, would imply that the time-scale of net erosion is longer than that of net uplift - the smaller excursions must last longer in order to maintain equilibrium. Similarly, negative skewness would be associated with a shorter net uplift time-scale, while zero would imply the two time-scales to be equivalent. Including vegetation dynamics into the landscape evolution model clearly alters the temporal trajectory of the physiography. While stochastic storms, and uplift, are still driving the system, their effects are modulated by the biogeomorphic coupling. The sensitivity of this effect is subsequently explored with independent variations of each vegetation parameter.

5.1.3 *Tau1*

The *Tau1* time series (Figures 5-6, 5-7 and 5-33) are much like those for *Bare*. Erosion variation is low, rapid and stationary, as is vegetation cover. Elevation changes show no characteristic time-scale, as each window looks alike, but mean elevation is slightly greater. The marginal increase in potential critical shear stress, with $\tau_{c,v}$ of 20 Pa, has

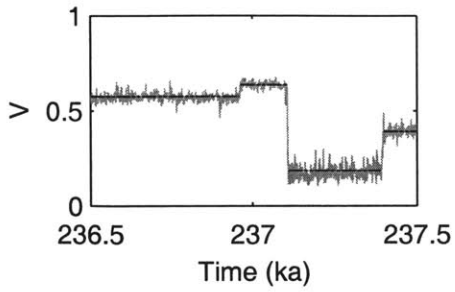

Figure 5-1: 1000-yr vegetation density time-series depicting meta-stable states (dark line), superposed with high frequency fluctuations (pale line). Changes between meta-stable states are short-lived.

little effect on the landscape. While the centennial scale behavior differs dramatically from *Mean*, the distribution of erosion rates at the 0.1 year resolution are identical. Thus, an effect of $\tau_{c,v}$ is not to alter the time-scales of individual erosion events, but to induce persistence in erosion (and vegetation changes) that are then transmitted to the topography

5.1.4 *Tau2*

Behavior of *Tau2* is intermediate between *Mean* and *Tau1*. Elevation changes are on $\mathcal{O}$(0.1 m) and appear to oscillate with a period of $\mathcal{O}$(30,000 years) (Figures 5-8, 5-9 and 5-33). Erosion and vegetation are dominated by high frequency fluctuations, with brief, periodic drops in magnitude, driven by step-changes between meta-stable states, whose magnitudes correlate with the variability. Again, vegetation and erosion are negatively correlated, as is seen for every simulation. The negatively skewed erosion rates at the 100-year scale indicate the time-scale of net uplift is shorter than that of erosion. *Tau2* differs from *Bare* and *Tau1* by possessing a large-scale temporal pattern along with *Mean*, but differs from the latter in two ways — the patterns are periodic and the erosion rates at larger time-scales are negatively skewed.

5.1.5 *Tau4*

Tau4 appears qualitatively similar to the *Mean* simulation, albeit with higher elevation and vegetation density averages (Figures 5-10, 5-11 and 5-33). The series are aperiodic, with positively skewed erosion rates at all scales indicating a shorter net erosion time-scale than for net uplift. Persistent meta-stable states exist as before, superposed with high frequency fluctuations, while elevation variation is of $\mathcal{O}$(2 m).

5.1.6 *Tau5*

Precisely the same description applies for *Tau5* as for *Tau4*, with even higher elevation and vegetation means, and a lower elevation range of $\mathcal{O}$(1.5 m) (Figures 5-12, 5-13 and 5-33). This suggests that the nature of the large-scale fluctuations, either absent, periodic or aperiodic, is not random. For low $\tau_{c,v}$ values there are no large-scale fluctuations, for low-intermediate values oscillations are periodic, and for intermediate-high values oscillations are aperiodic. Not only does $\tau_{c,v}$ determine the mean biophysiography, but also its temporal character.

5.1.7 *Tv1*

The uniqueness of the *Tv1* time series is that erosion and vegetation exhibit large, high frequency fluctuations at all scales, rather than just the finer ones (Figures 5-14, 5-15 and 5-34). On closer inspection, these resolve to become short-lived, meta-stable states of $\mathcal{O}$(10-100 years), separated by large step-changes lasting of $\mathcal{O}$(1-5 years). Consequently, persistence longer than about 1000 years is suppressed, and the range of elevations is low, of $\mathcal{O}$(0.2 m). A further difference from previous simulations is that the distribution of 0.1-year erosion rates diverges from that of the *Mean* simulation to some extent, as do all *Tv* cases, in contrast to the *Tau* simulations. The time-scale of vegetation growth must affect that of active erosion. The differential recovery of plants following erosion leads to a different proportion of storm intensities that are able to cause erosion. The negative relation between erosion and vegetation holds as before, as does that of variability and meta-stable mean. T_v thus differs from $\tau_{c,v}$ by

affecting the temporal behavior of erosion events as well as the medium- and long-term evolution, and in so doing, the fast-growing *Tv1* extinguishes the potential for long-term persistence.

5.1.8 *Tv2*

The large, frequent step-changes between meta-stable states have become more sparse in the *Tv2* simulation (Figures 5-16, 5-17 and 5-34). Erosion is positively skewed for all resolutions, the large-scale fluctuations are aperiodic, and elevation variation is of $\mathcal{O}(0.5$ m). The minimal increase in T_v, from 1 to 2 yr^{-1}, allows long-term persistence to establish by seemingly slowing the temporal evolution seen in *Tv1*.

5.1.9 *Tv4*

The large variations in erosion and vegetation have become subdued in *Tv4* (Figures 5-18, 5-19 and 5-34). The erosion's skewness is close to zero at the centennial resolution, indicating net uplift and erosion have similar time-scales, and as their rates are also similar, so too are the extrema in elevation. There is medium- and long-term persistence in the time series, resulting in periodic changes in elevation of $\mathcal{O}(0.5$ m). This is akin to *Tau2* , albeit with a much larger period, of $\mathcal{O}(150{,}000$ years).

5.1.10 *Tv5*

Fluctuations in elevation, erosion and vegetation have diminished further in *Tv5* (Figures 5-20, 5-21 and 5-34). Long-term persistence still pervades, despite the evidence of meta-stable states being subtle. Again, skewness for the centennial scale erosion rates is approximately zero, since the meta-stable changes are on the order of the high frequency variations. The periodicity of the large-scale fluctuations can not be known for certain, but is perhaps of $\mathcal{O}(400{,}000$ years), if not aperiodic. The elevation range is of $\mathcal{O}(0.2$ m). Changing the time-scale of plant growth has a clear effect on the time-scale of net erosion and uplift, and thus the long-term fluctuations - the slower vegetation recovers, the longer the oscillations. Furthermore, as T_v increases

above 3 years, coarse erosion skewness is positive and the fluctuations periodic, just as observed for *Tau2*.

5.1.11 *Kv1*

None of the time series for *Kv1* show signs of persistence, but neither does the elevation signal lack a characteristic time-scale — the 0.1 year resolution is notably smoother than at larger scales (Figures 5-22, 5-23 and 5-35). At the centennial scale erosion variability is high, as is that of vegetation. Elevation varies on $\mathcal{O}(0.2\text{ m})$, but the high frequency component is relatively much greater than in other simulations. Erosion and vegetation variability nonetheless follow vegetation magnitude, and the erosion rate histograms once again differ as K_v varies, albeit marginally. Vegetation erodibility has the effect of altering the time-scale of individual erosion events, by changing the temporal susceptibility of the landscape to rainfall, and strongly changes mean elevation and vegetation values. What is different from other simulations is that these are not paralleled by significant changes in the large-scale temporal regime. Resilient vegetation therefore prevents longterm persistence from developing, doing so presumably by damping and decoupling the effects of erosion.

5.1.12 *Kv2*

The *Kv2* time-series appear similar to *Mean*, *Tau4* and *Tau5*, although the time-scale of large fluctuations is shorter while still aperiodic (Figures 5-24, 5-25 and 5-35. Erosion is positively skewed, and exhibits meta-stable state changes along with vegetation density. There is therefore a transition between K_v of 0.1 and 0.5 $\text{Pa}^{-1}\text{Yr}^{-1}$ at which long-term persistence is enabled. Erosion events may make a significant dent in the topography following the increase in vegetation erodibility.

5.1.13 *Kv4*

The variability of erosion rate and vegetation cover is much reduced for the *Kv4* simulation (Figures 5-26, 5-27 and 5-35). The meta-stable durations are longer and fewer.

Erosion rates are negatively skewed at low resolution, and the elevations convincingly periodic of $\mathcal{O}$(150,000 yrs), akin to *Tau2*, *Tv4* and *Tv5*. Another transition therefore occurs between K_v of 1 and 5 $\mathrm{Pa}^{-1}\mathrm{Yr}^{-1}$, changing the nature of the oscillations from aperiodic to periodic.

5.1.14 *Kv5*

Compared to *Kv4*, at the centennial scale, the *Kv5* erosion and vegetation variability is further diminished, erosion skewness is approximately zero, and the periodicity is $\mathcal{O}$(200,000 yrs). Elevation variations are of $\mathcal{O}$(0.1 m), and meta-stable states are even longer lived. It is thus fair to conclude that if centennial-scale erosion rates are non-positively skewed, or net uplift time-scale is no longer than that of net erosion, then what large-scale fluctuations a simulation will exhibit will be periodic. This periodicity arises from the uniformity of uplift, which controls the steepening of slopes, and therefore the time-scale with which the landscape destabilizes. Conversely, if net erosion has the shorter time-scale, it is the stochastic storm events which dominate landscape stability, leading to aperiodic large-scale oscillations.

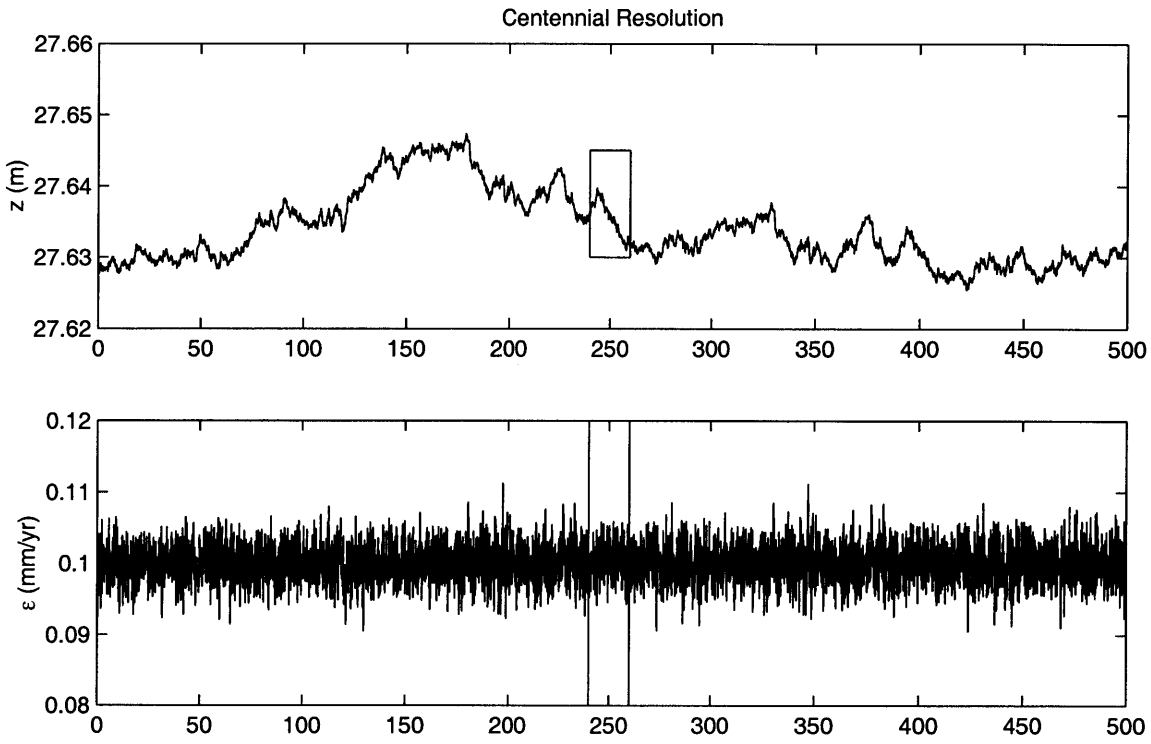

Figure 5-2: *Bare*: 500,000-year time-series of mean elevation and erosion rate at 100-year resolution. The bounded region is magnified in figure (5.3) at a decadal resolution.

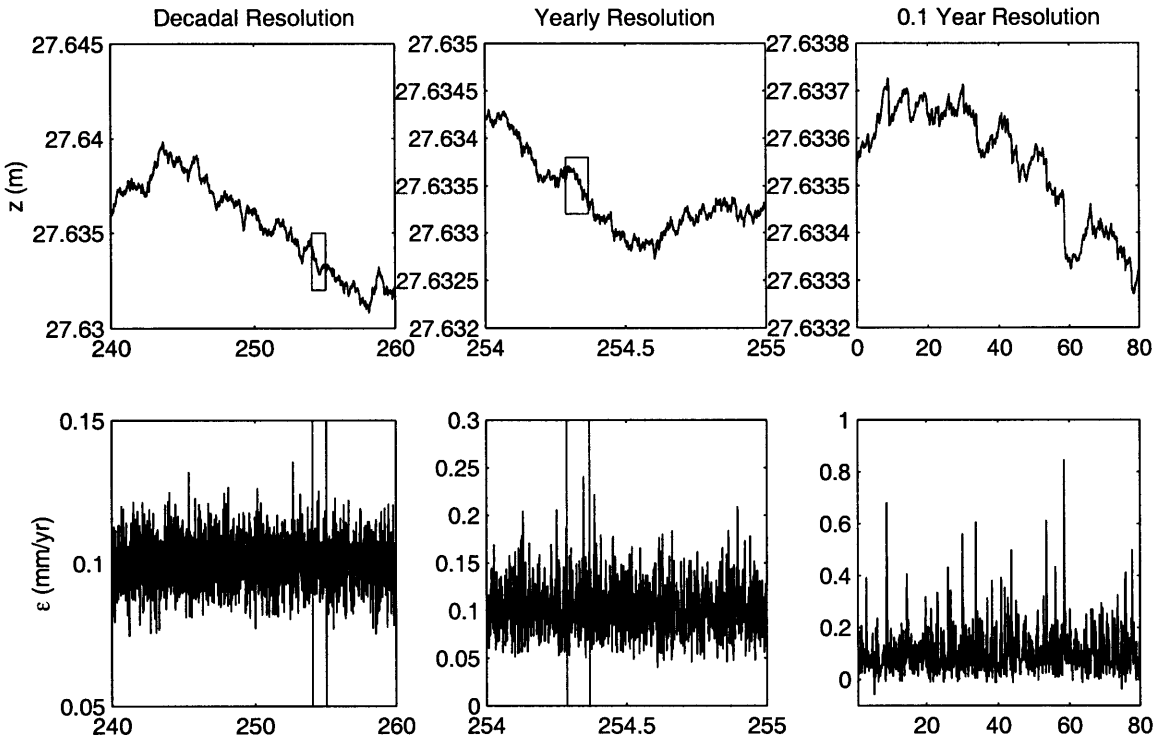

Figure 5-3: *Bare*: Ever-smaller windows of the 500,000-year time-series at increasing temporal resolutions of 10, 1 and 0.1 years (from left to right). Bounded regions are magnified in plots immediately to the right.

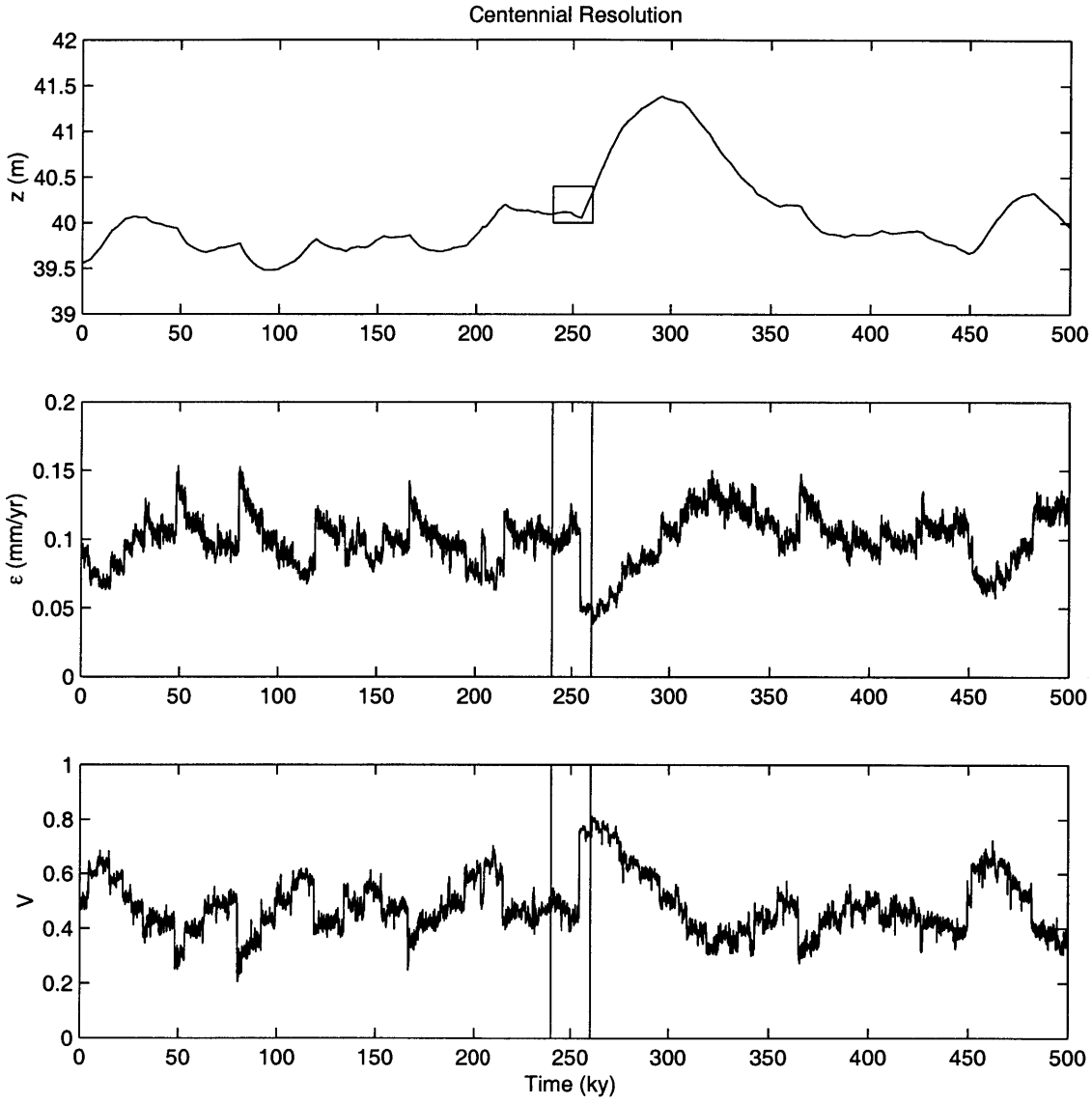

Figure 5-4: *Mean*: 500,000-year time-series of mean elevation, erosion rate and vegetation density at 100-year resolution.

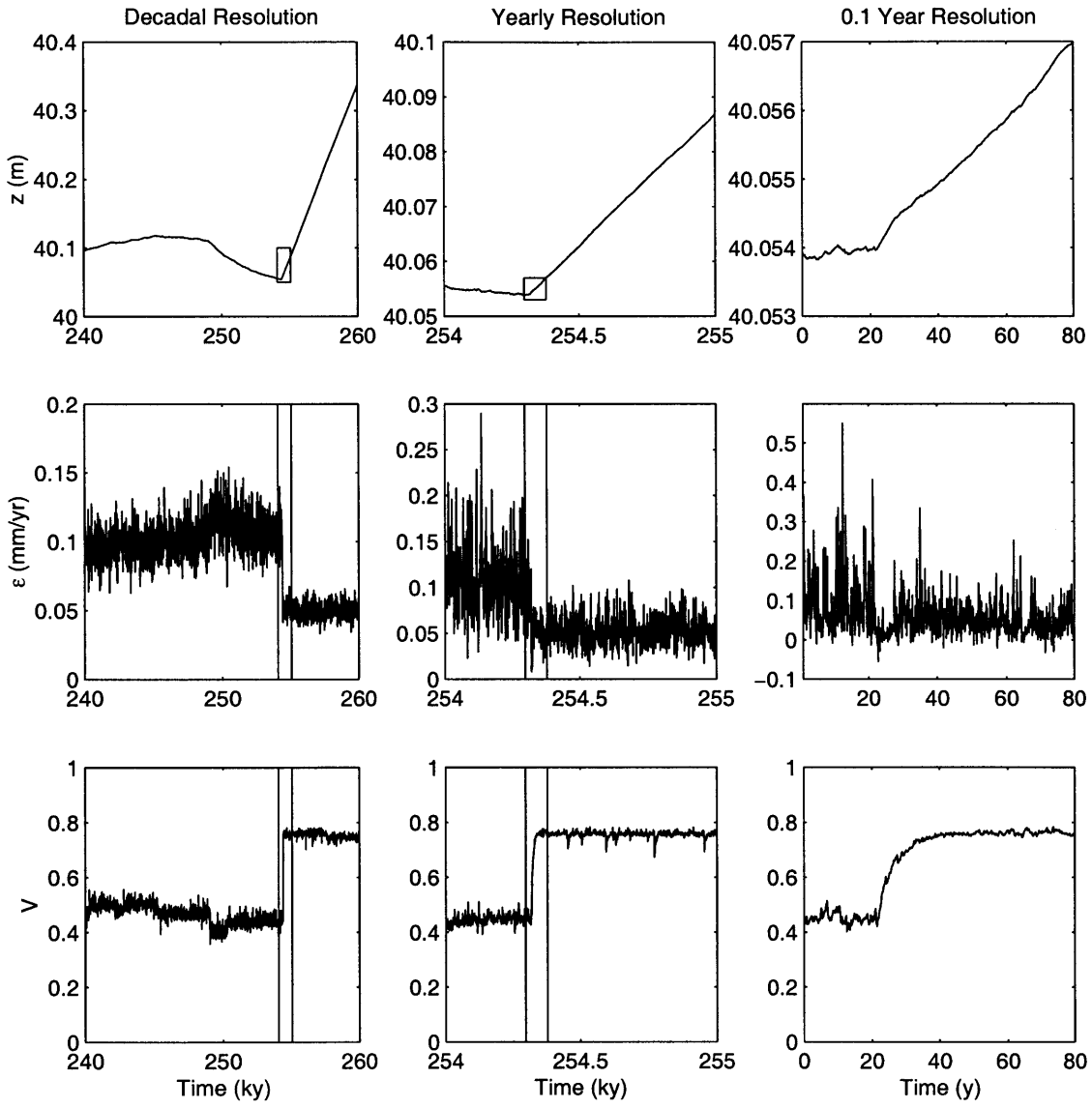

Figure 5-5: *Mean*: Ever-smaller windows of the 500,000-year time-series at increasing temporal resolution.

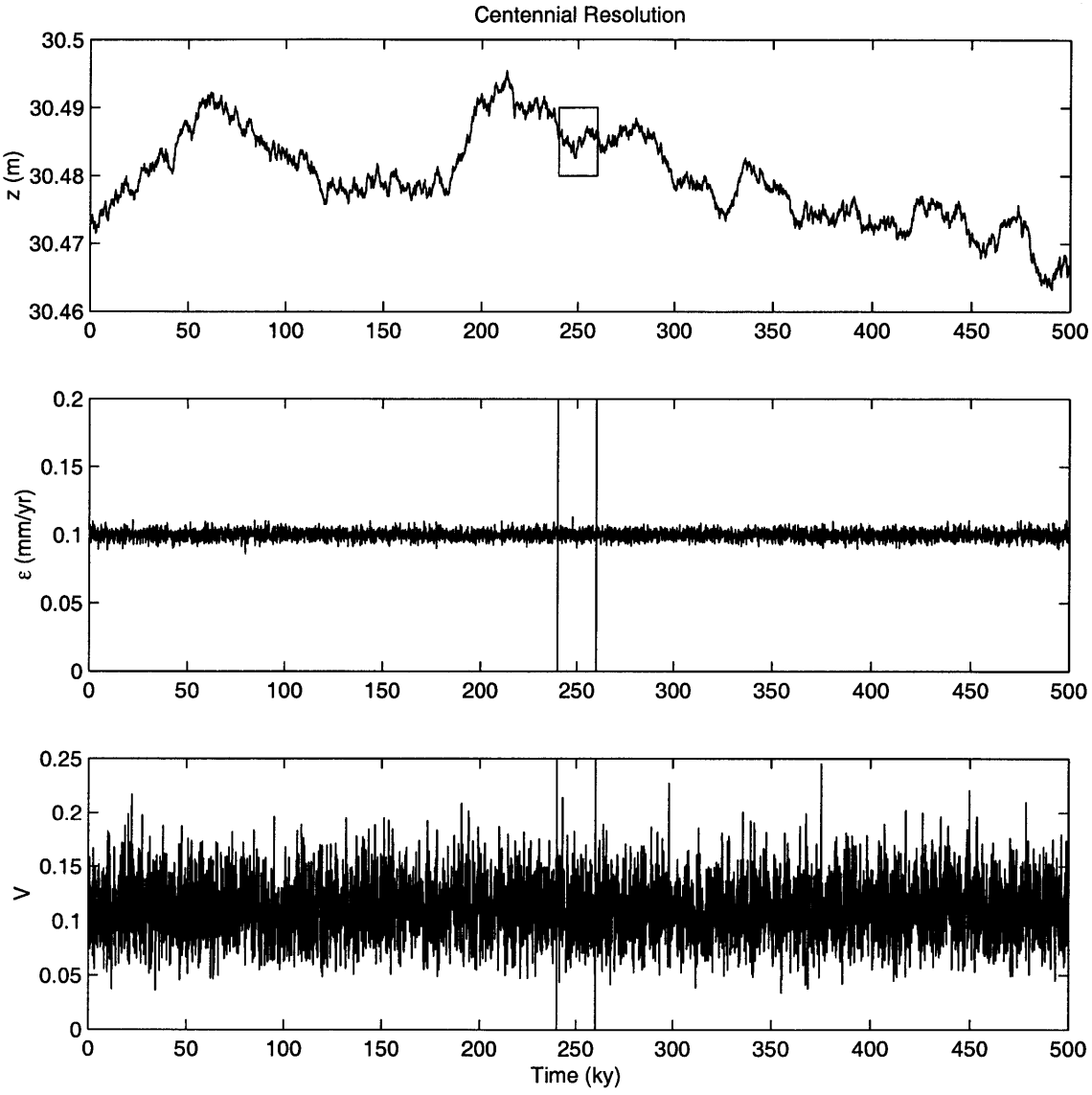

Figure 5-6: *Tau1*: 500,000-year time-series of mean elevation, erosion rate and vegetation density at 100-year resolution.

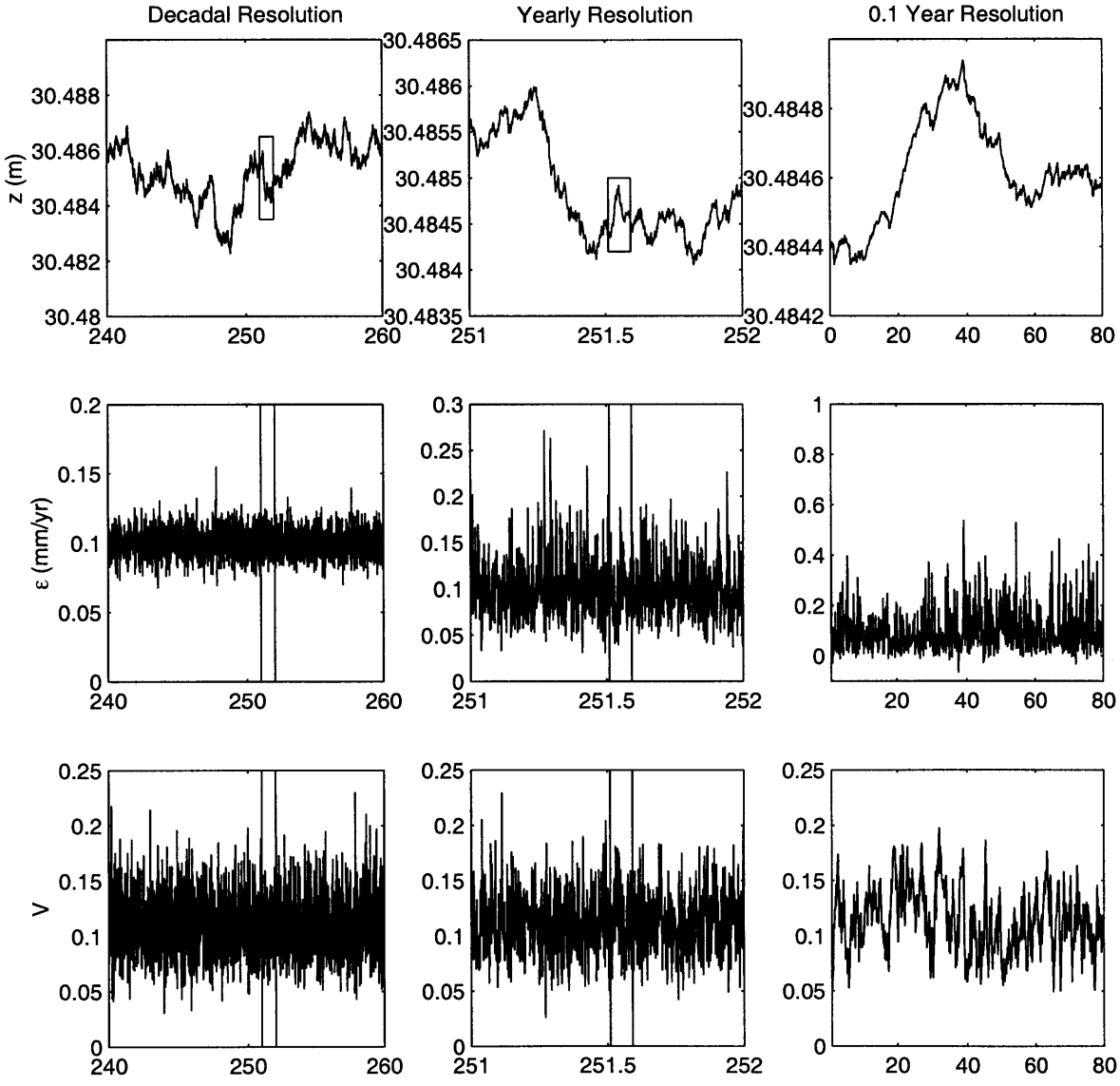

Figure 5-7: *Tau1*: Ever-smaller windows of the 500,000-year time-series at increasing temporal resolution.

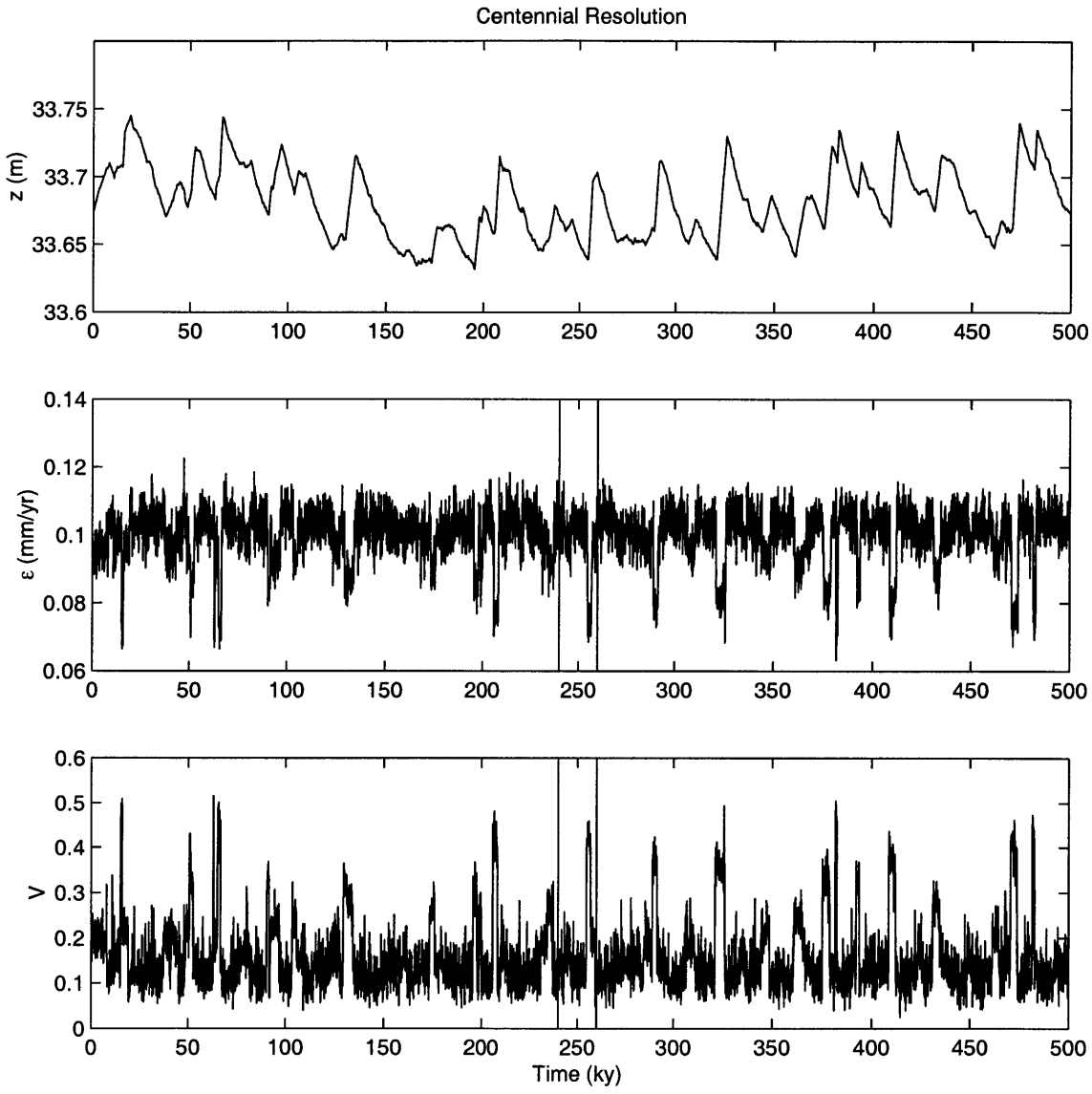

Figure 5-8: *Tau2*: 500,000-year time-series of mean elevation, erosion rate and vegetation density at 100-year resolution.

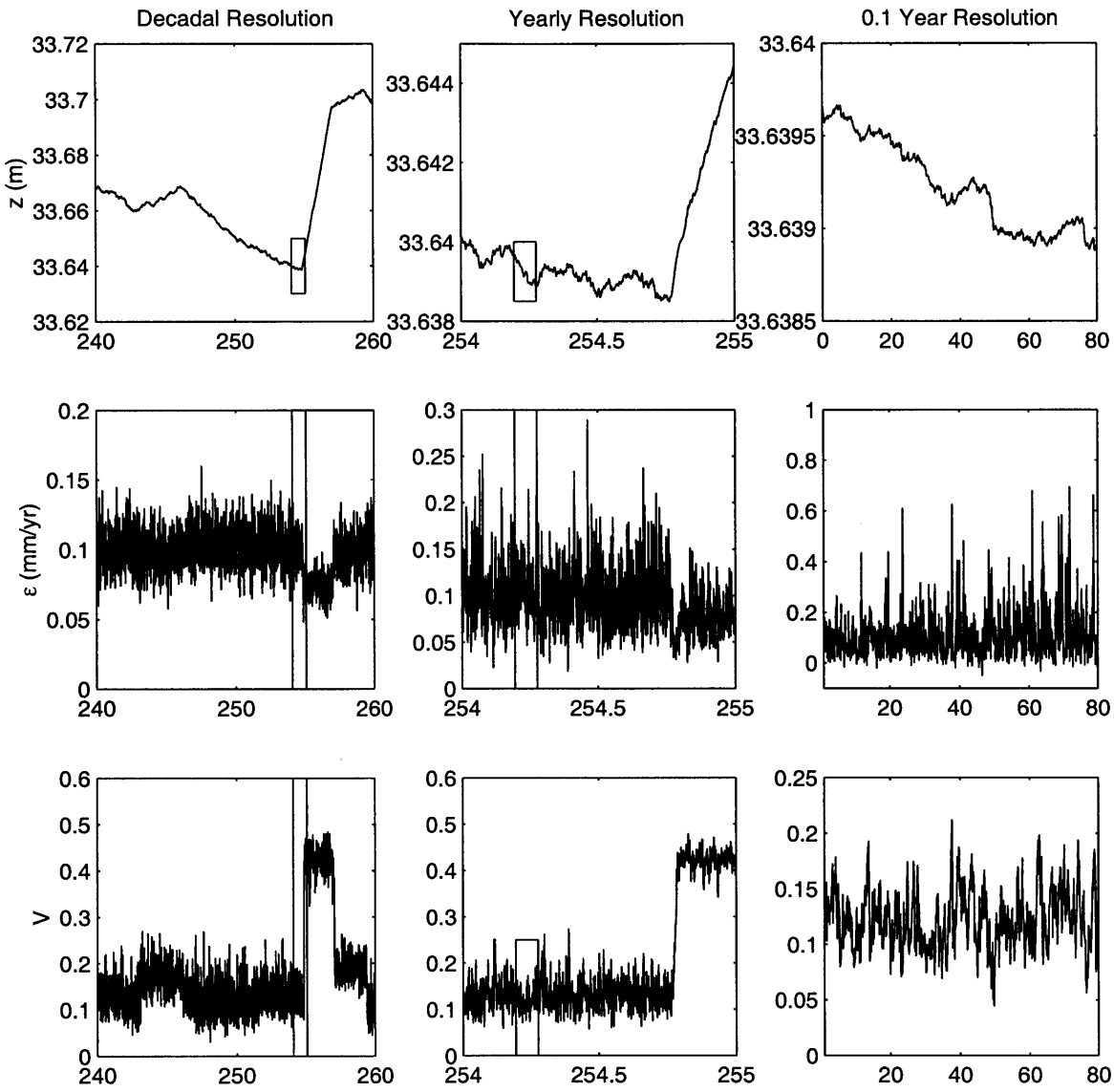

Figure 5-9: *Tau2*: Ever-smaller windows of the 500,000-year time-series at increasing temporal resolution.

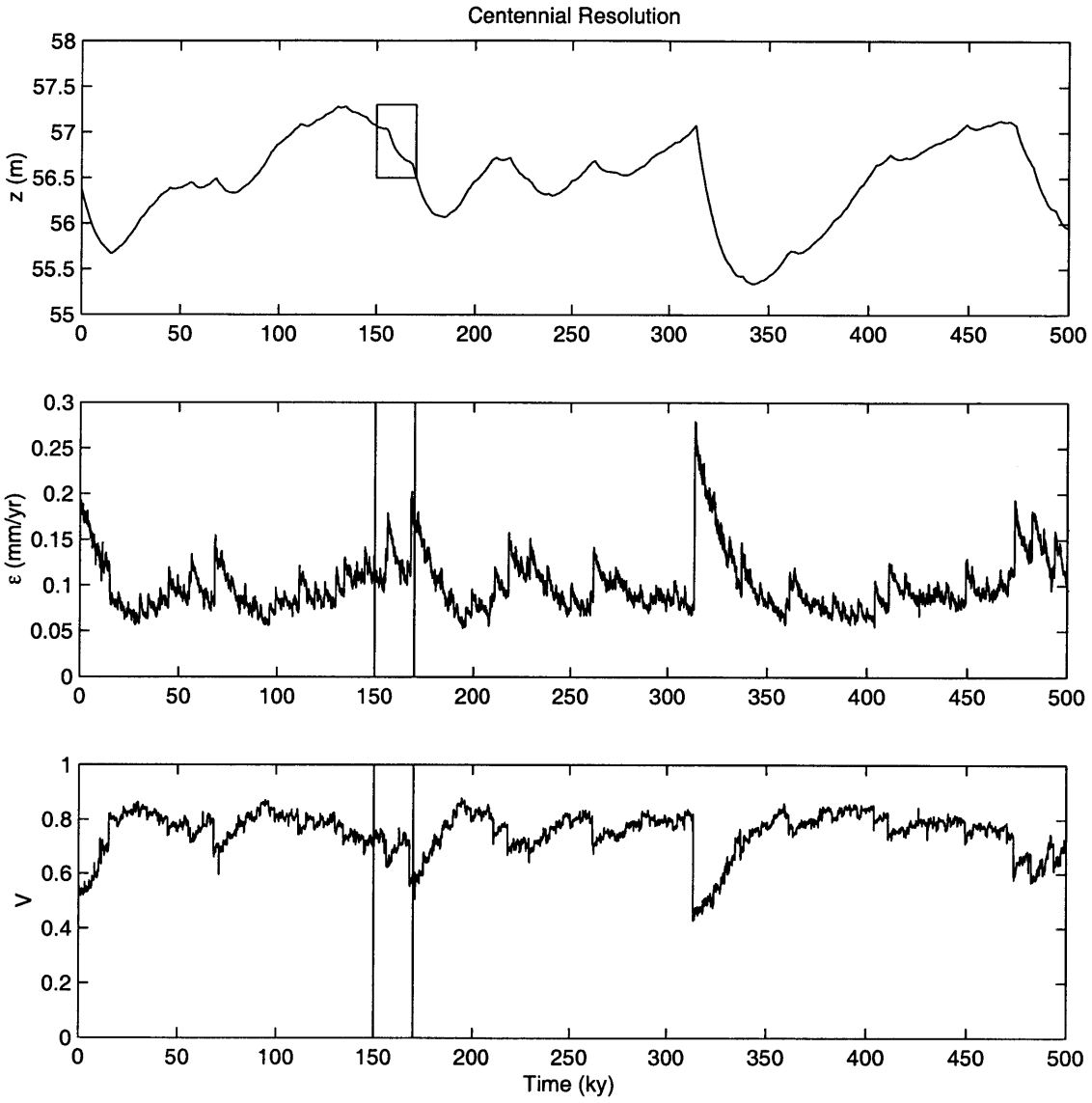

Figure 5-10: *Tau4*: 500,000-year time-series of mean elevation, erosion rate and vegetation density at 100-year resolution.

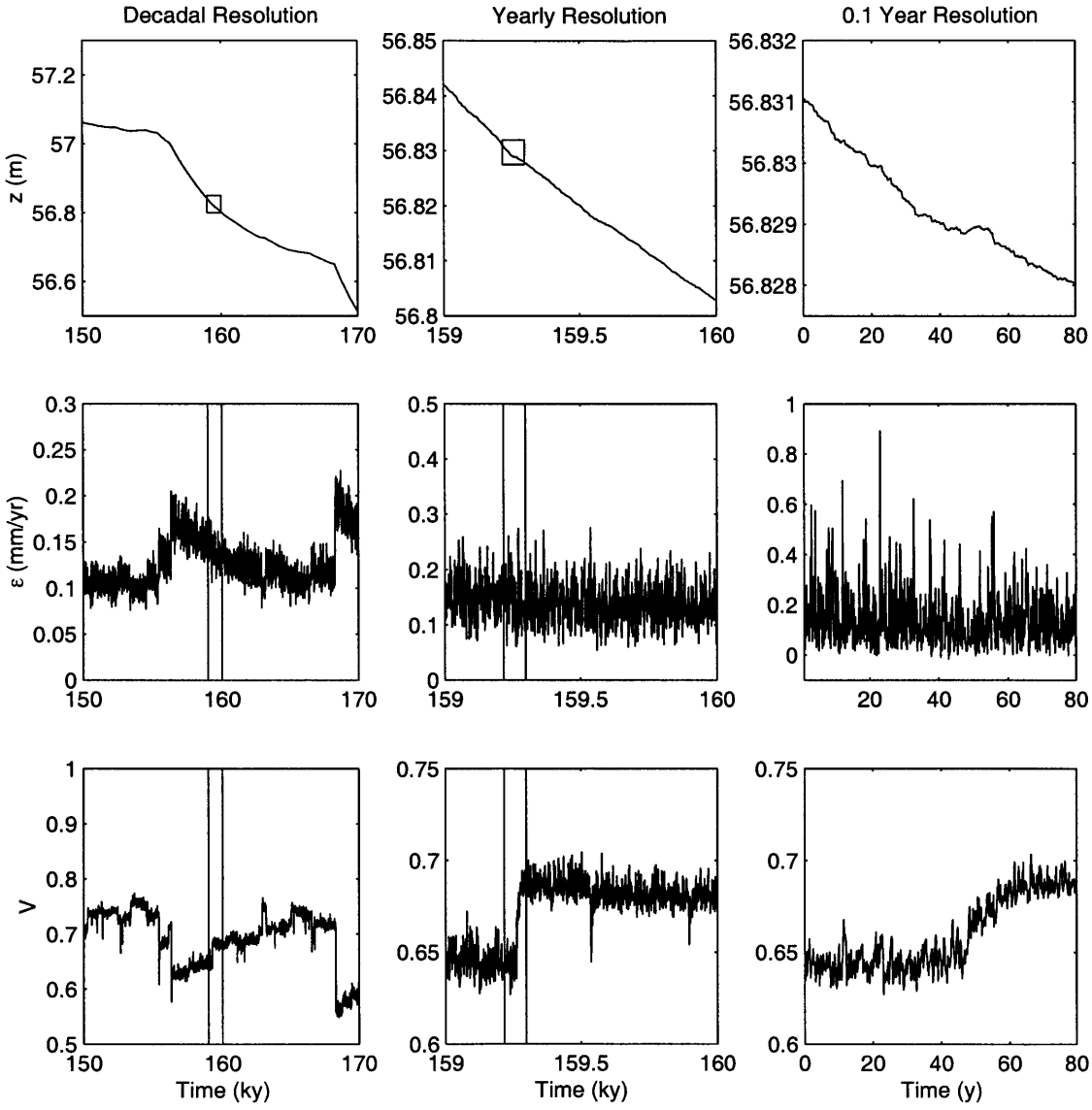

Figure 5-11: *Tau4*: Ever-smaller windows of the 500,000-year time-series at increasing temporal resolution.

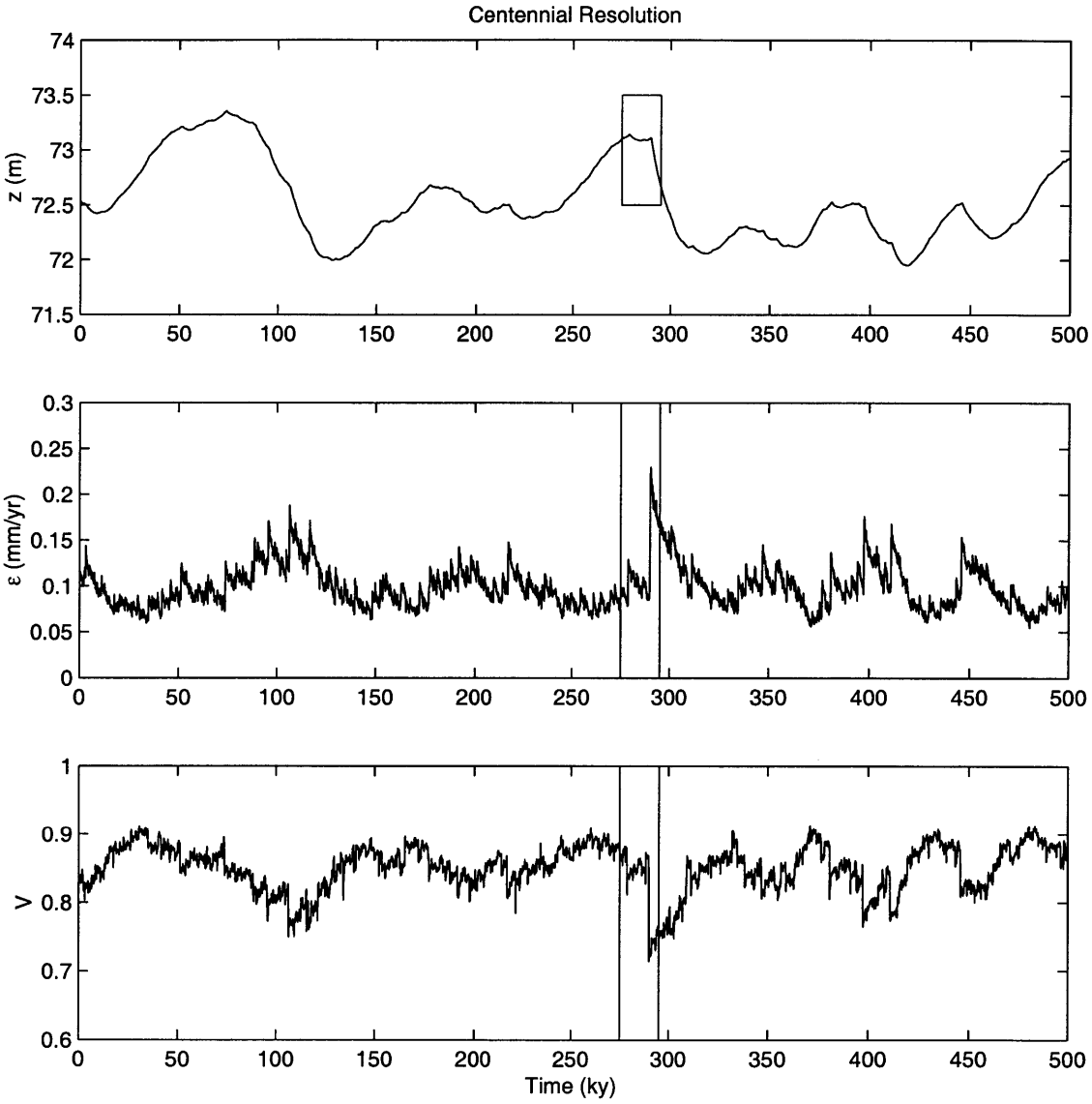

Figure 5-12: *Tau5*: 500,000-year time-series of mean elevation, erosion rate and vegetation density at 100-year resolution.

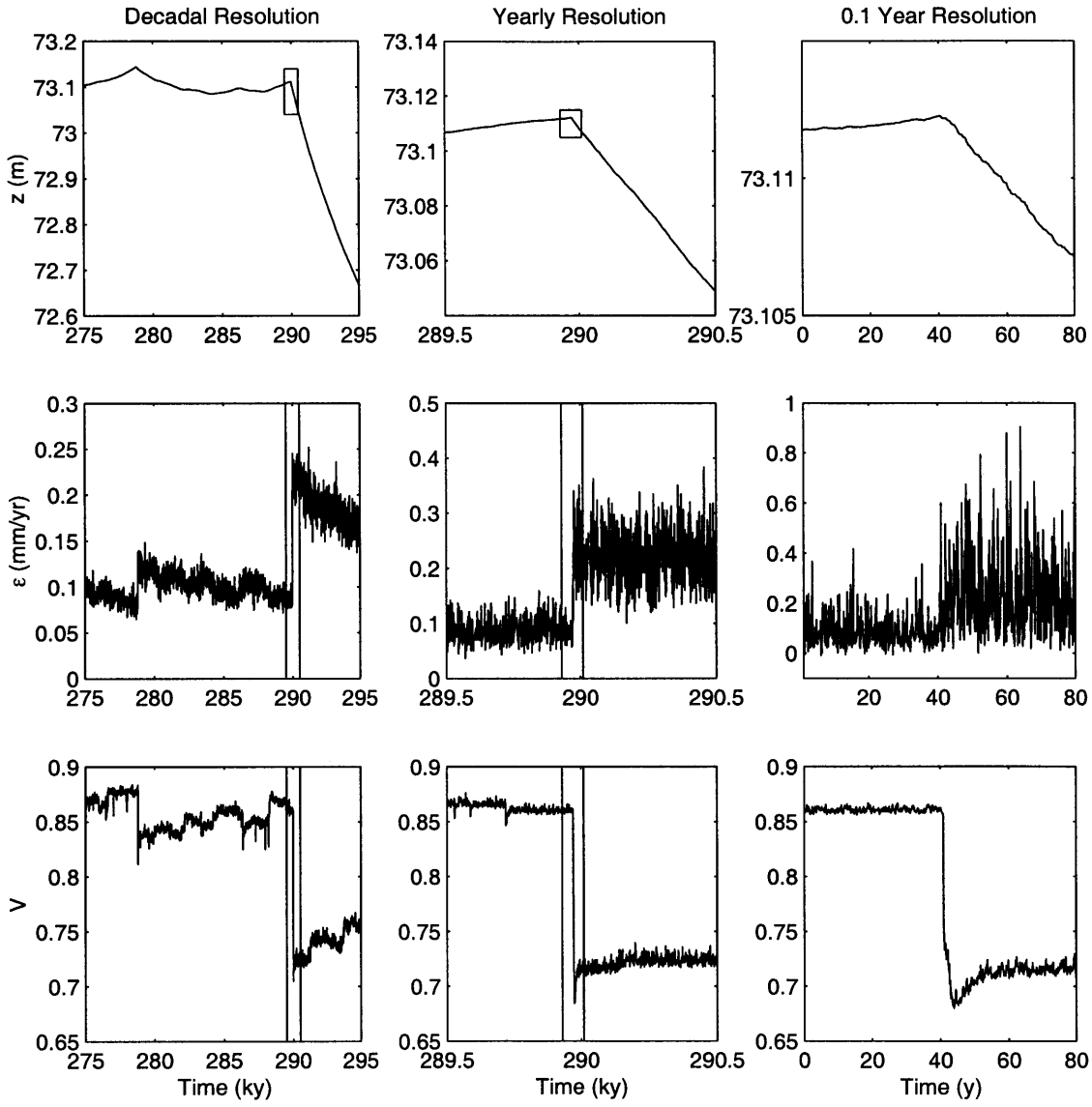

Figure 5-13: *Tau5*: Ever-smaller windows of the 500,000-year time-series at increasing temporal resolution.

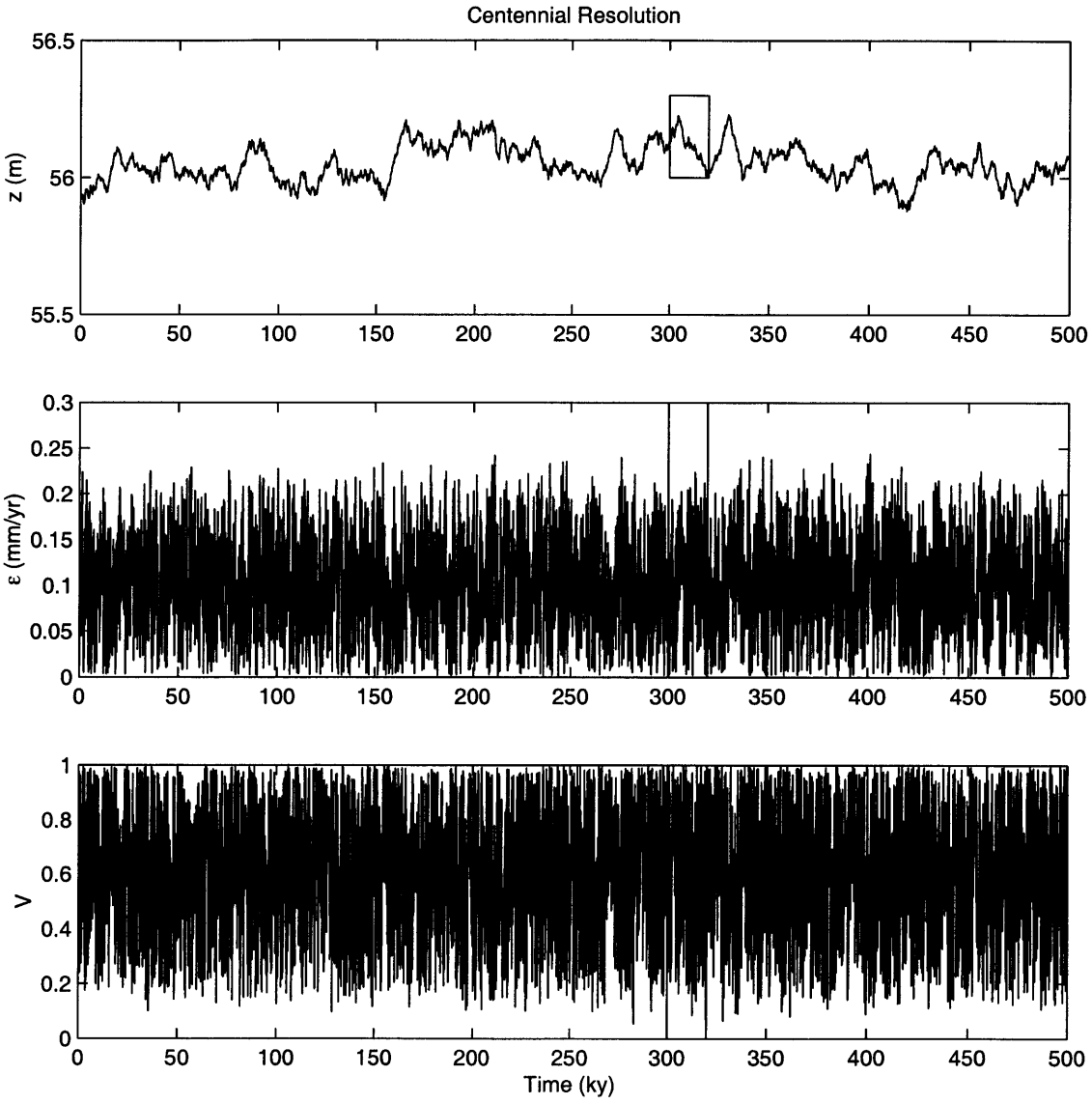

Figure 5-14: *Tv1*: 500,000-year time-series of mean elevation, erosion rate and vegetation density at 100 year resolution.

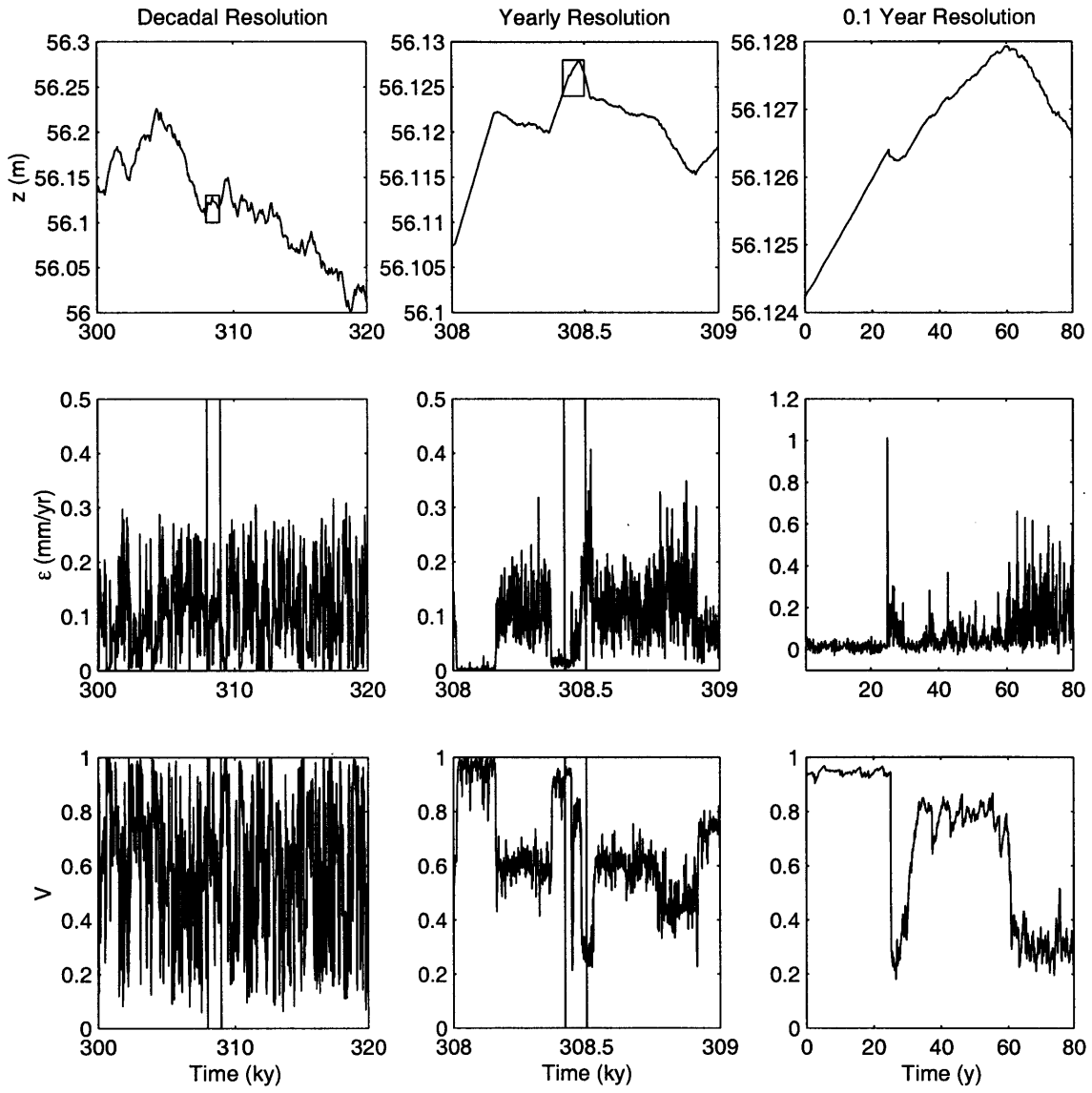

Figure 5-15: *Tv1*: Ever-smaller windows of the 500,000-year time-series at increasing temporal resolution.

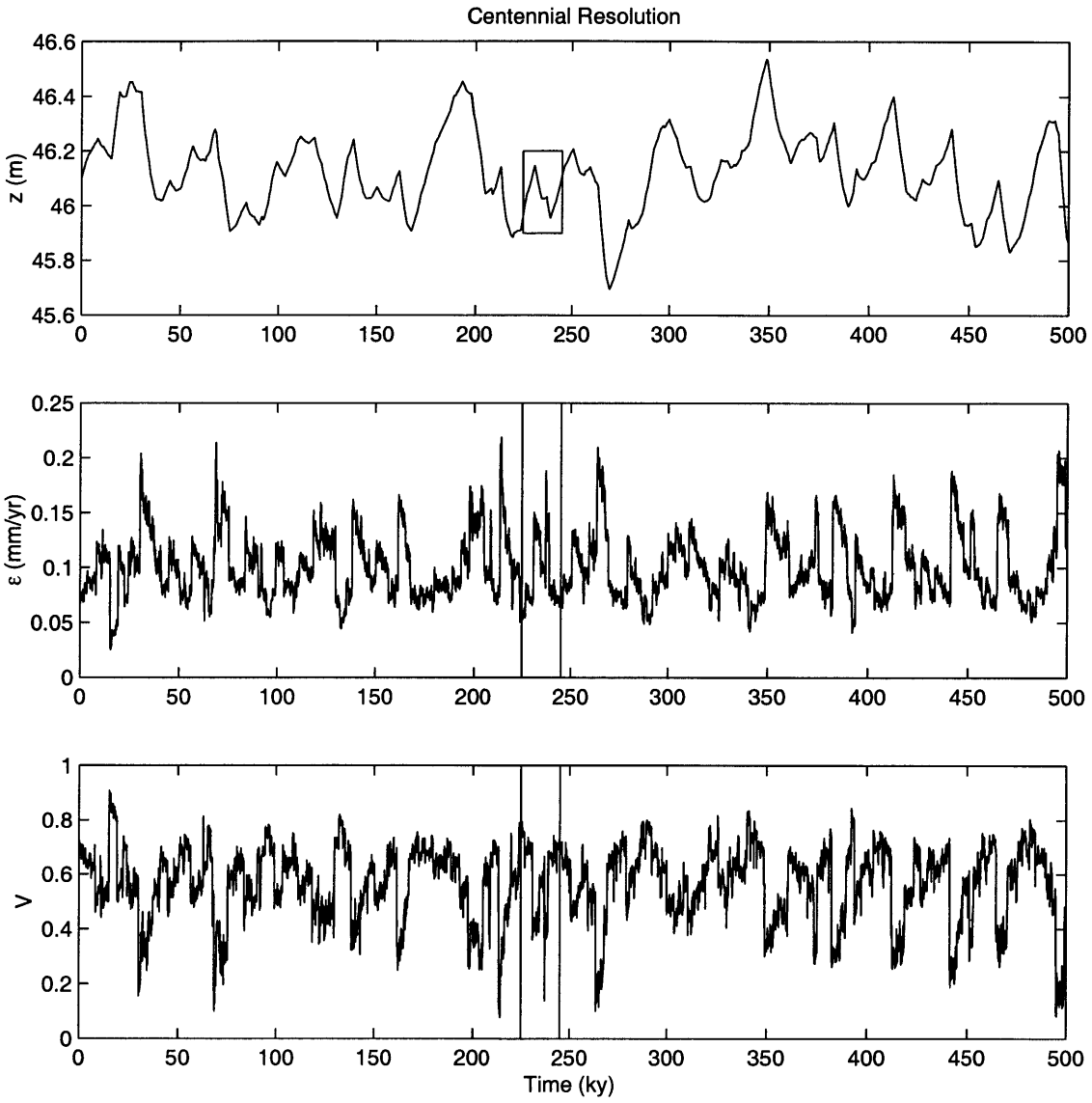

Figure 5-16: *Tv2*: 500,000-year time-series of mean elevation, erosion rate and vegetation density at 100 year resolution.

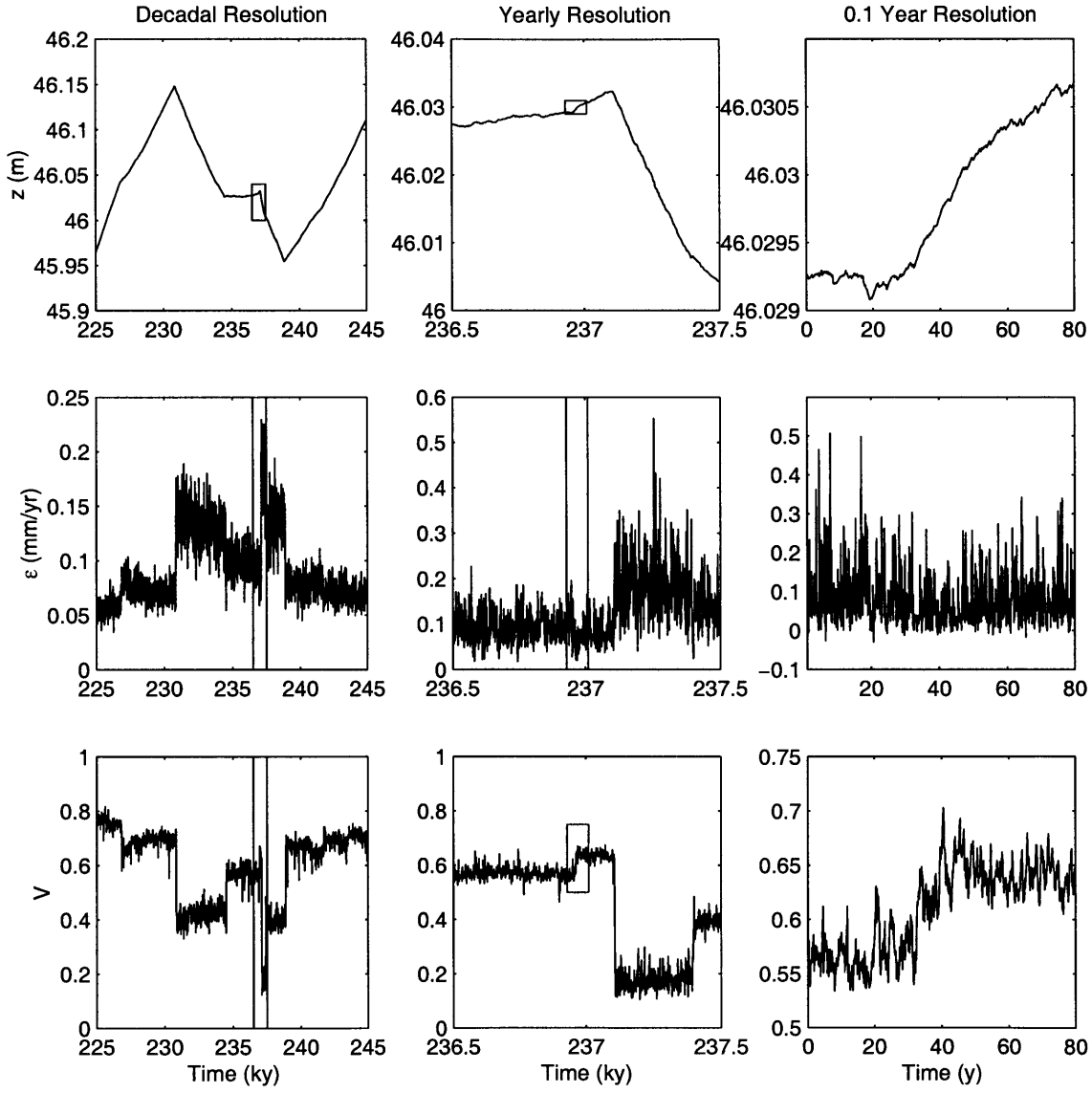

Figure 5-17: *Tv2*: Ever-smaller windows of the 500,000-year time-series at increasing temporal resolution.

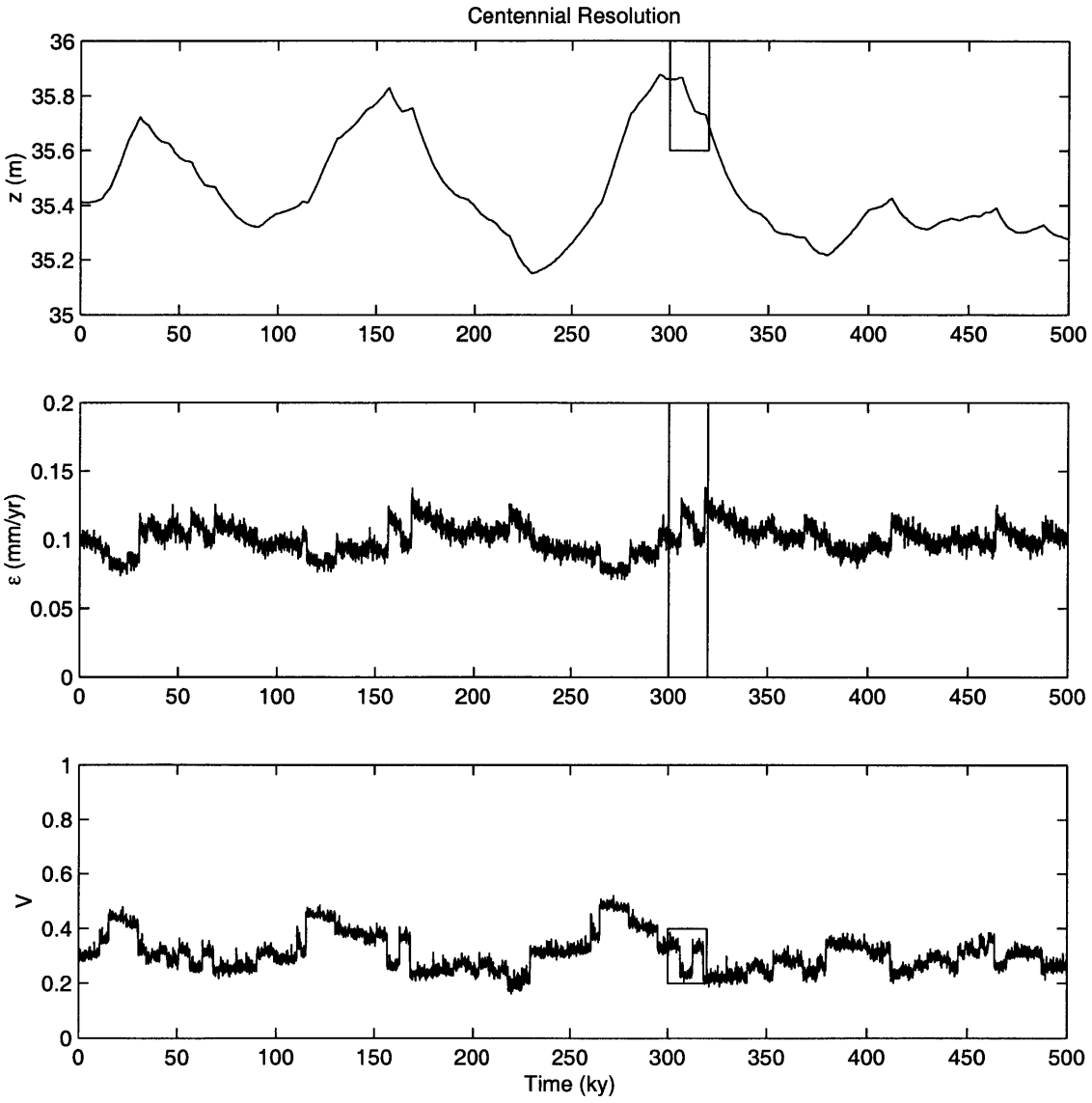

Figure 5-18: *Tv4*: 500,000-year time-series of mean elevation, erosion rate and vegetation density at 100 year resolution.

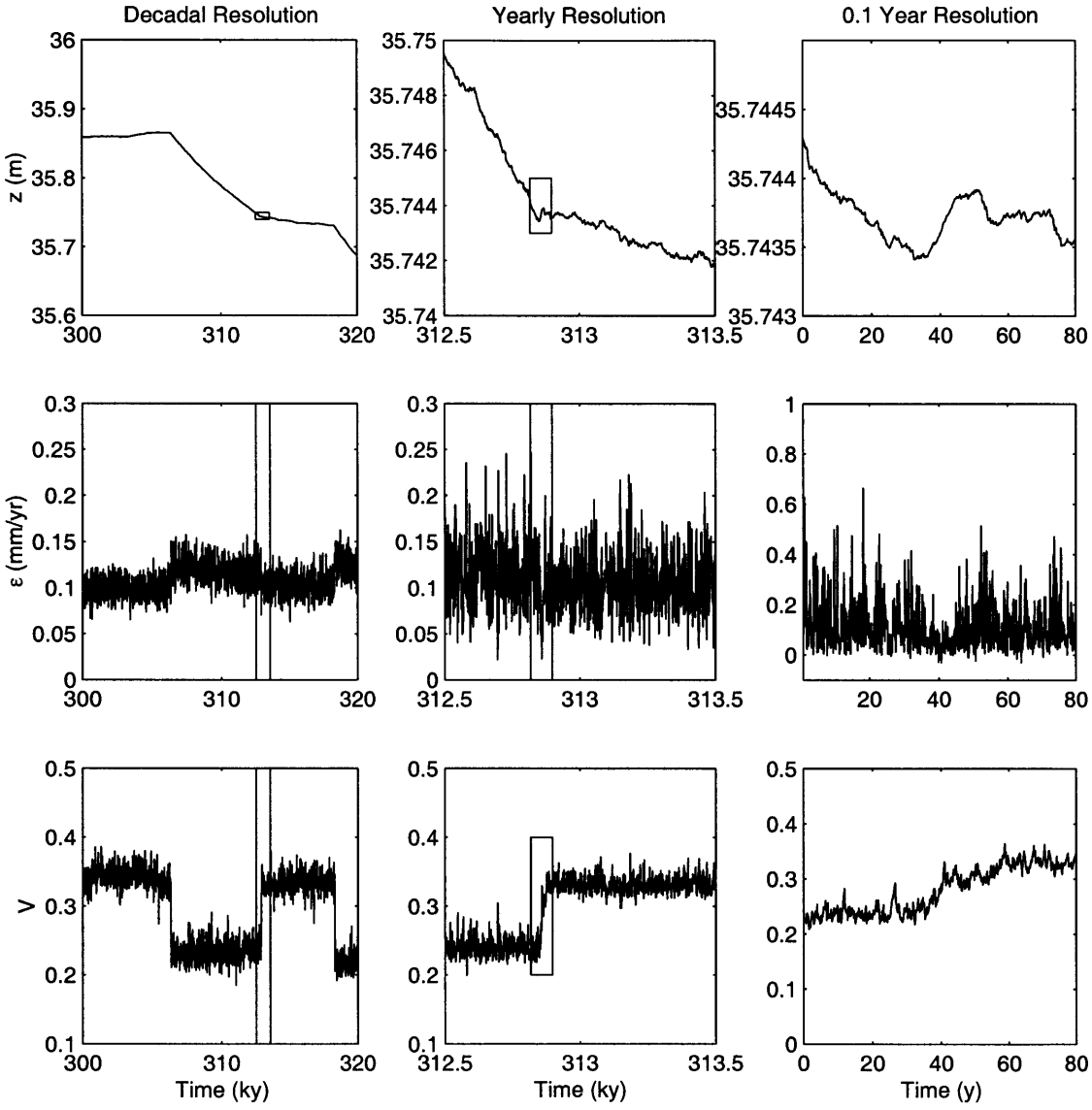

Figure 5-19: *Tv4*: Ever-smaller windows of the 500,000-year time-series at increasing temporal resolution.

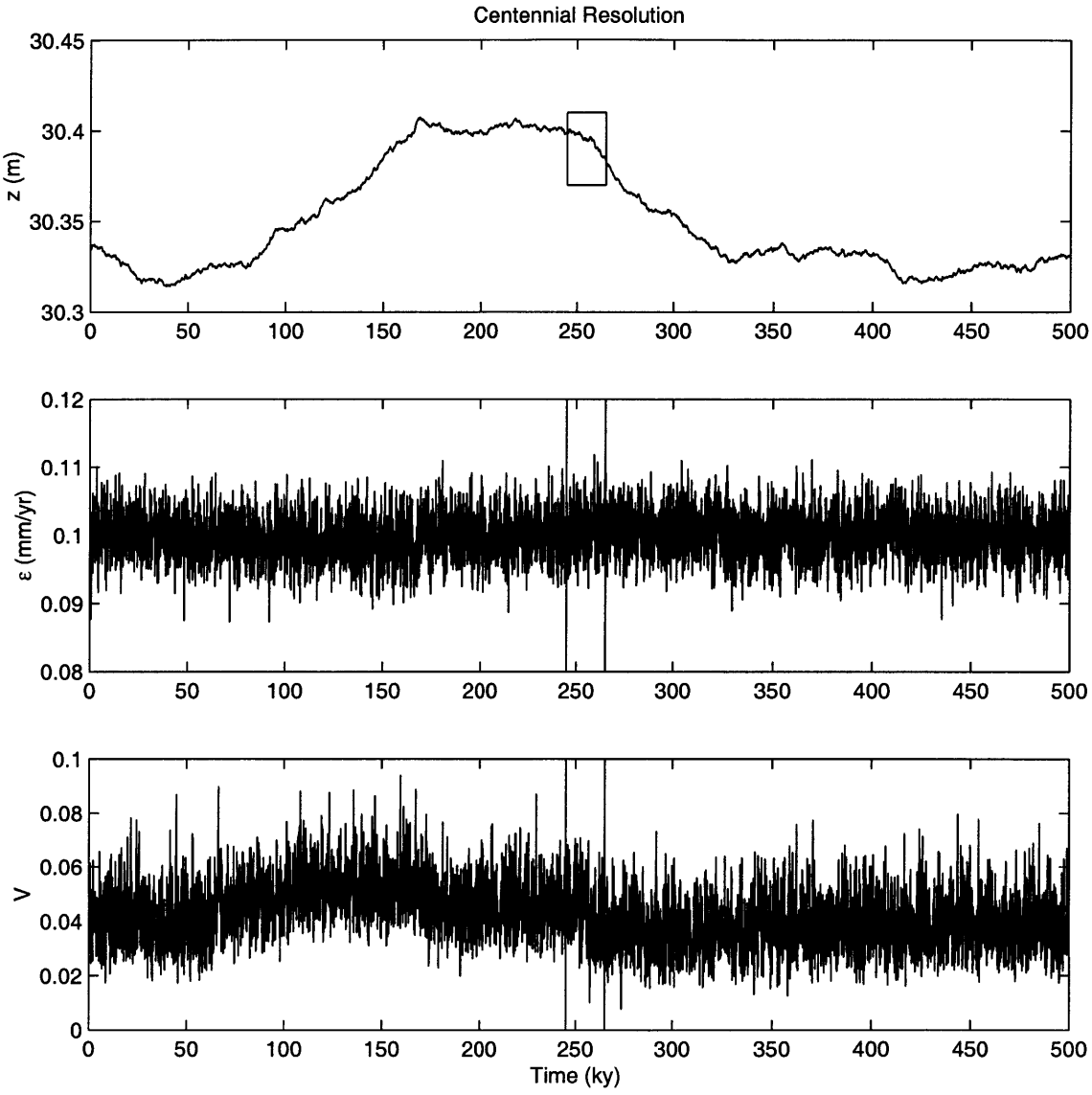

Figure 5-20: *Tv5*: 500,000-year time-series of mean elevation, erosion rate and vegetation density at 100 year resolution.

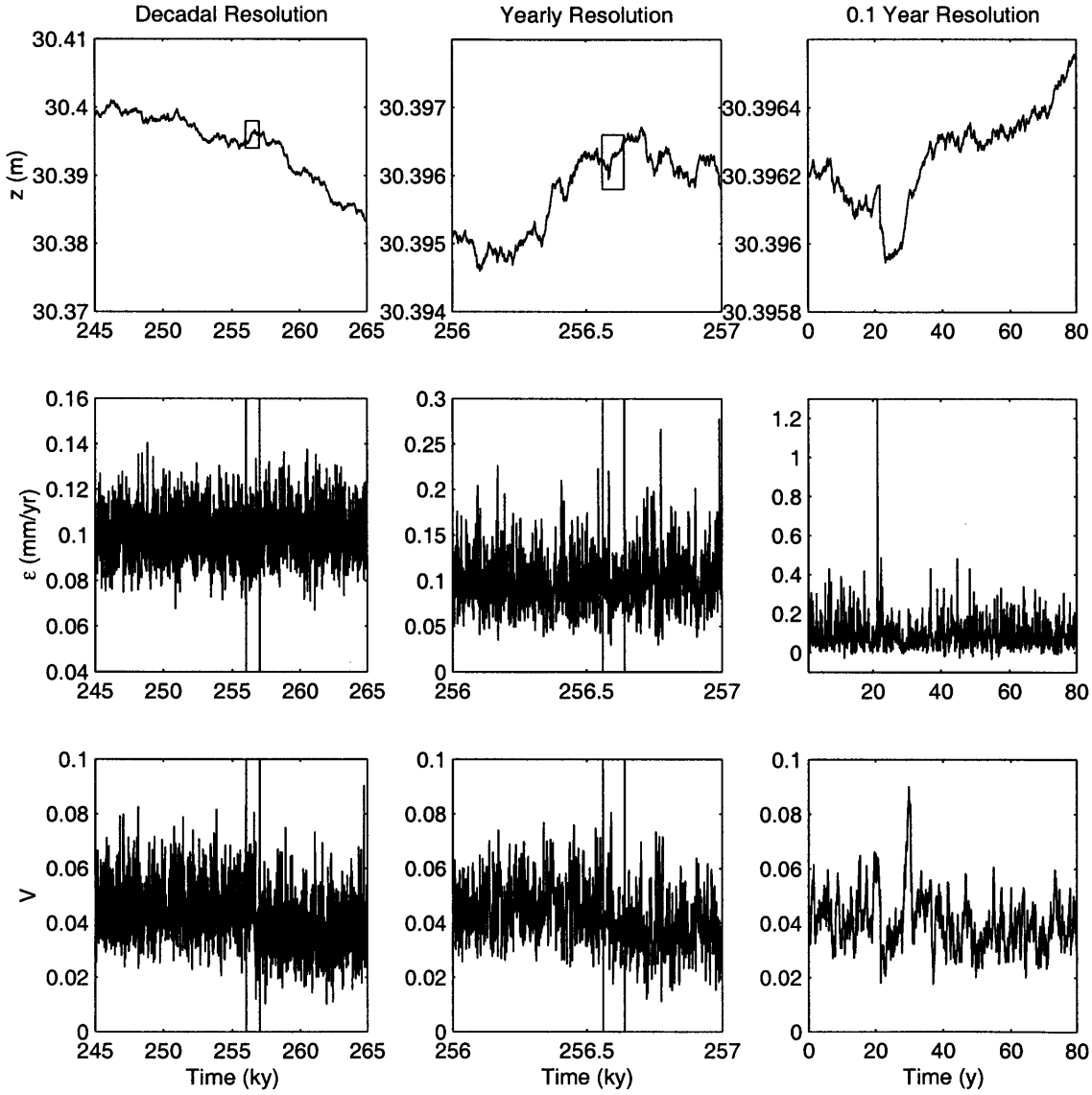

Figure 5-21: *Tv5*: Ever-smaller windows of the 500,000-year time-series at increasing temporal resolution.

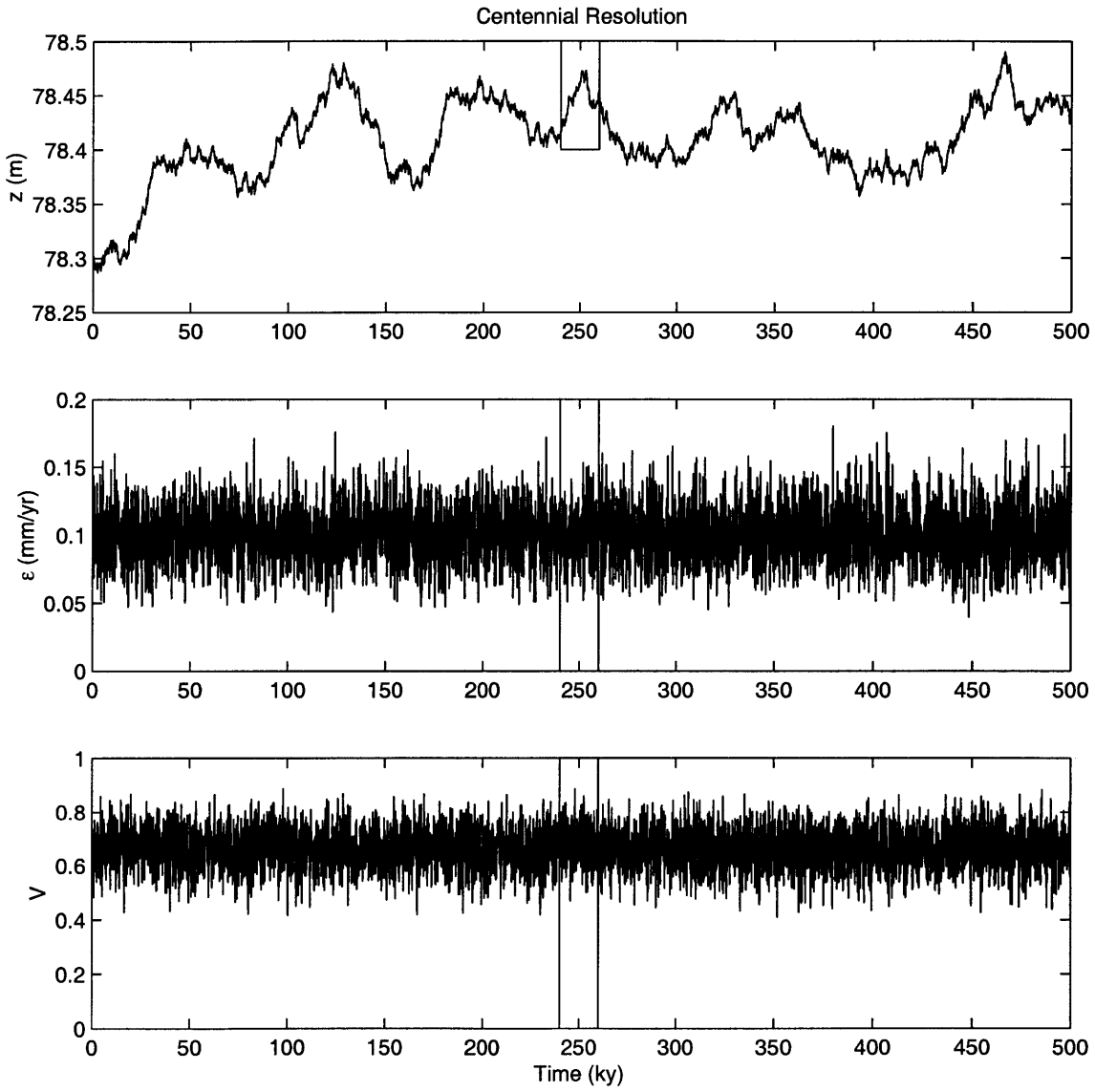

Figure 5-22: *Kv1*: 500,000-year time-series of mean elevation, erosion rate and vegetation density at 100 year resolution.

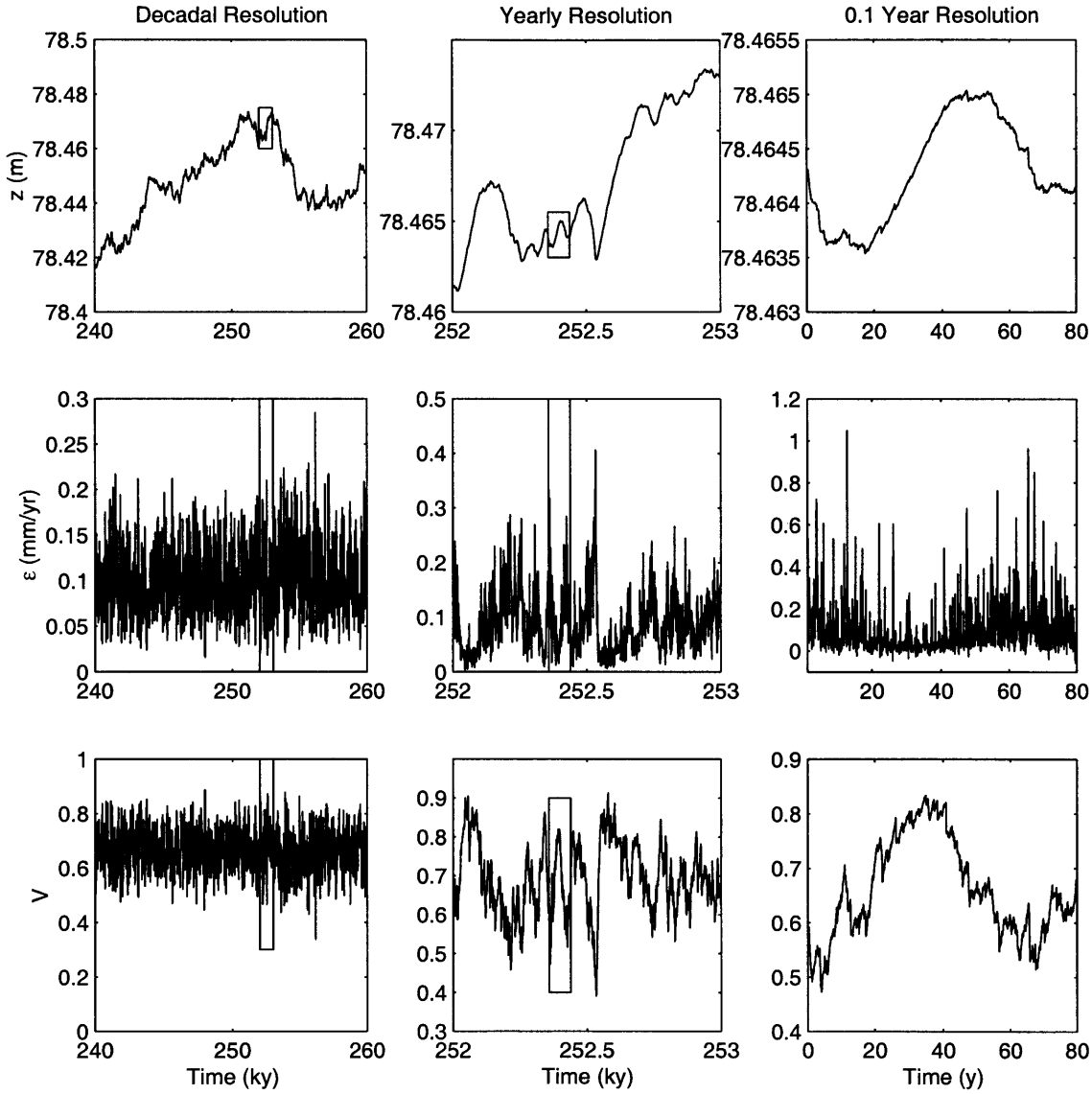

Figure 5-23: *Kv1*: Ever-smaller windows of the 500,000-year time-series at increasing temporal resolution.

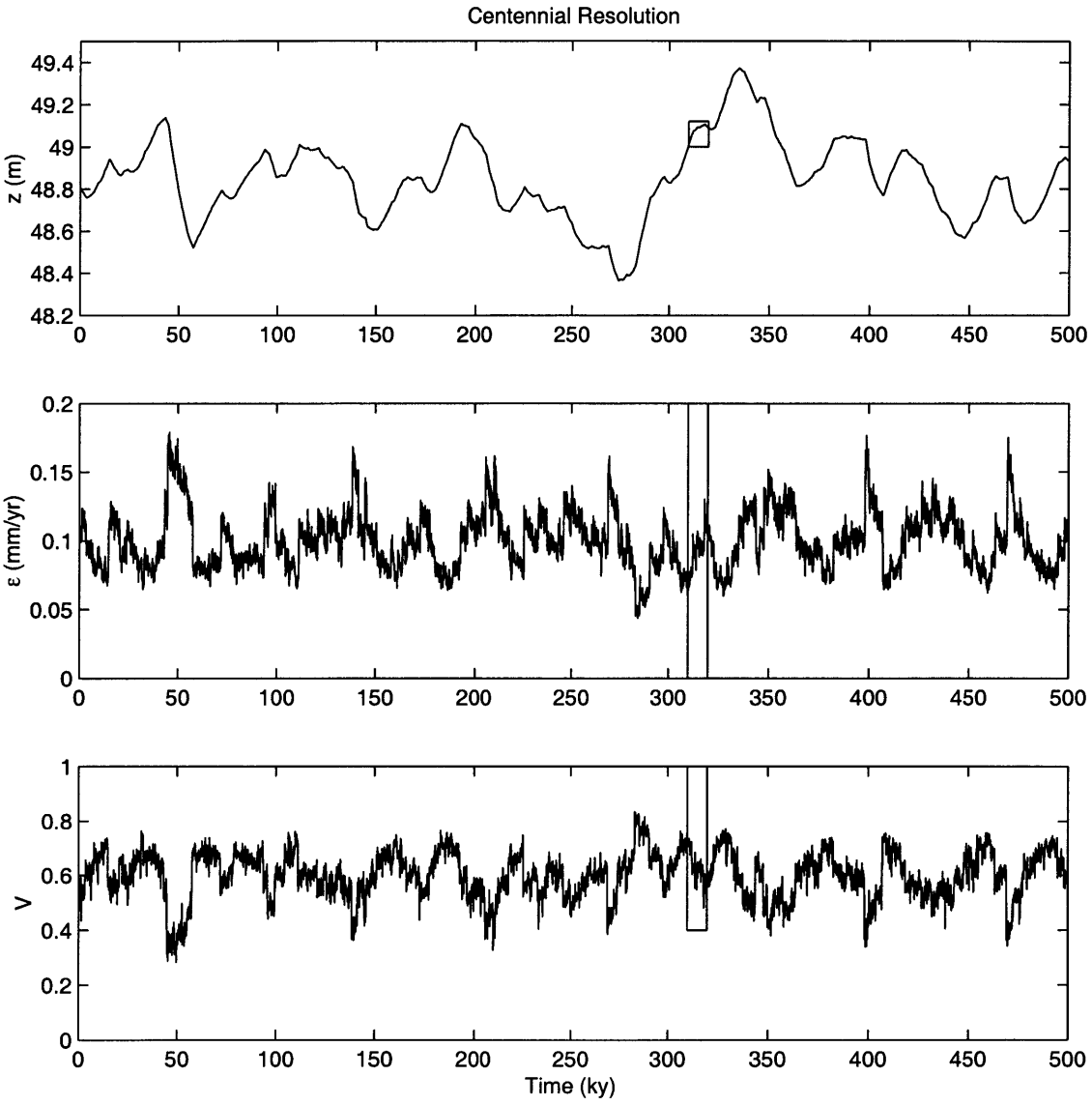

Figure 5-24: *Kv2*: 500,000-year time-series of mean elevation, erosion rate and vegetation density at 100 year resolution.

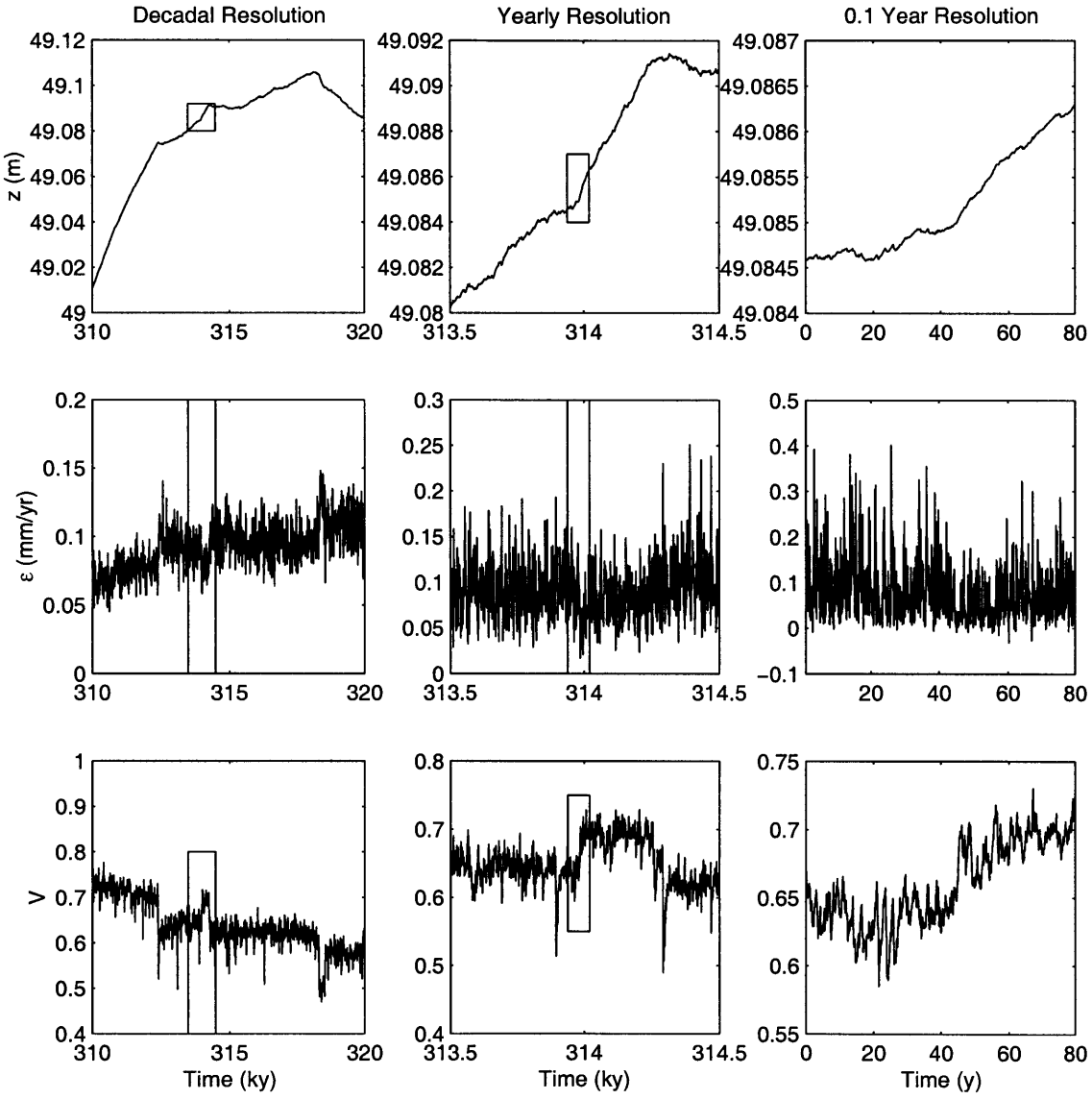

Figure 5-25: *Kv2*: Ever-smaller windows of the 500,000-year time-series at increasing temporal resolution.

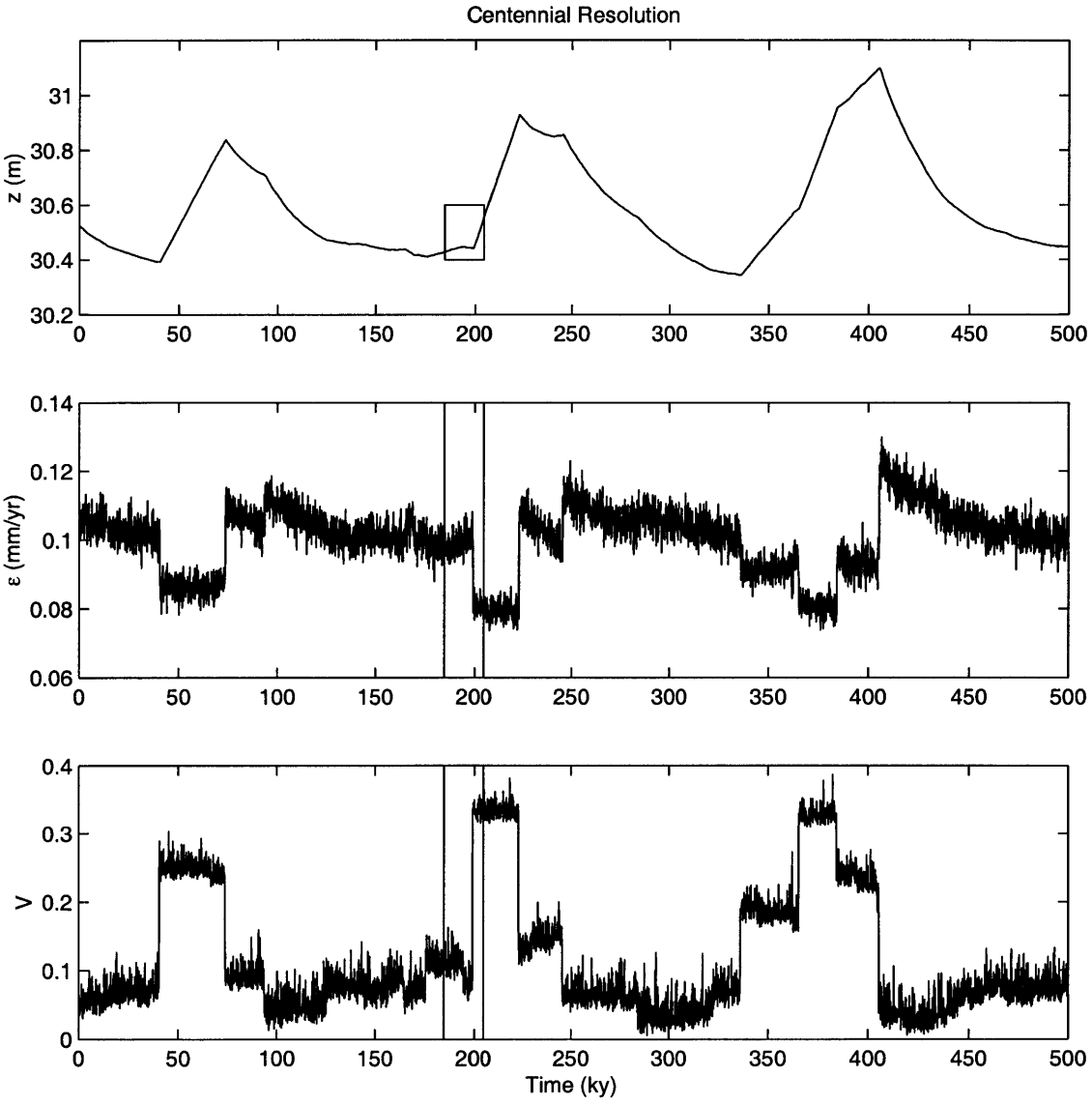

Figure 5-26: *Kv4*: 500,000-year time-series of mean elevation, erosion rate and vegetation density at 100 year resolution.

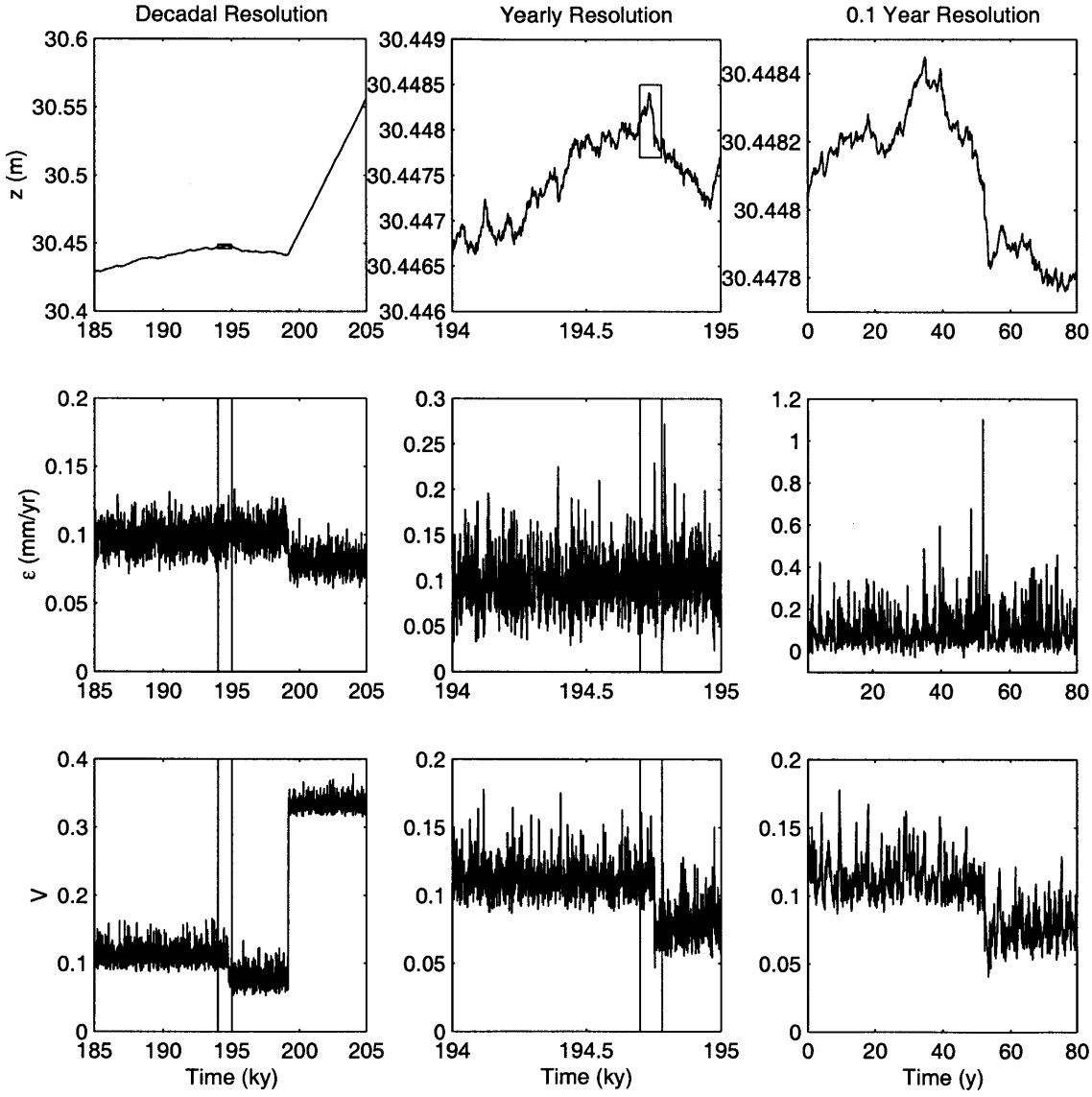

Figure 5-27: *Kv4*: Ever-smaller windows of the 500,000-year time-series at increasing temporal resolution.

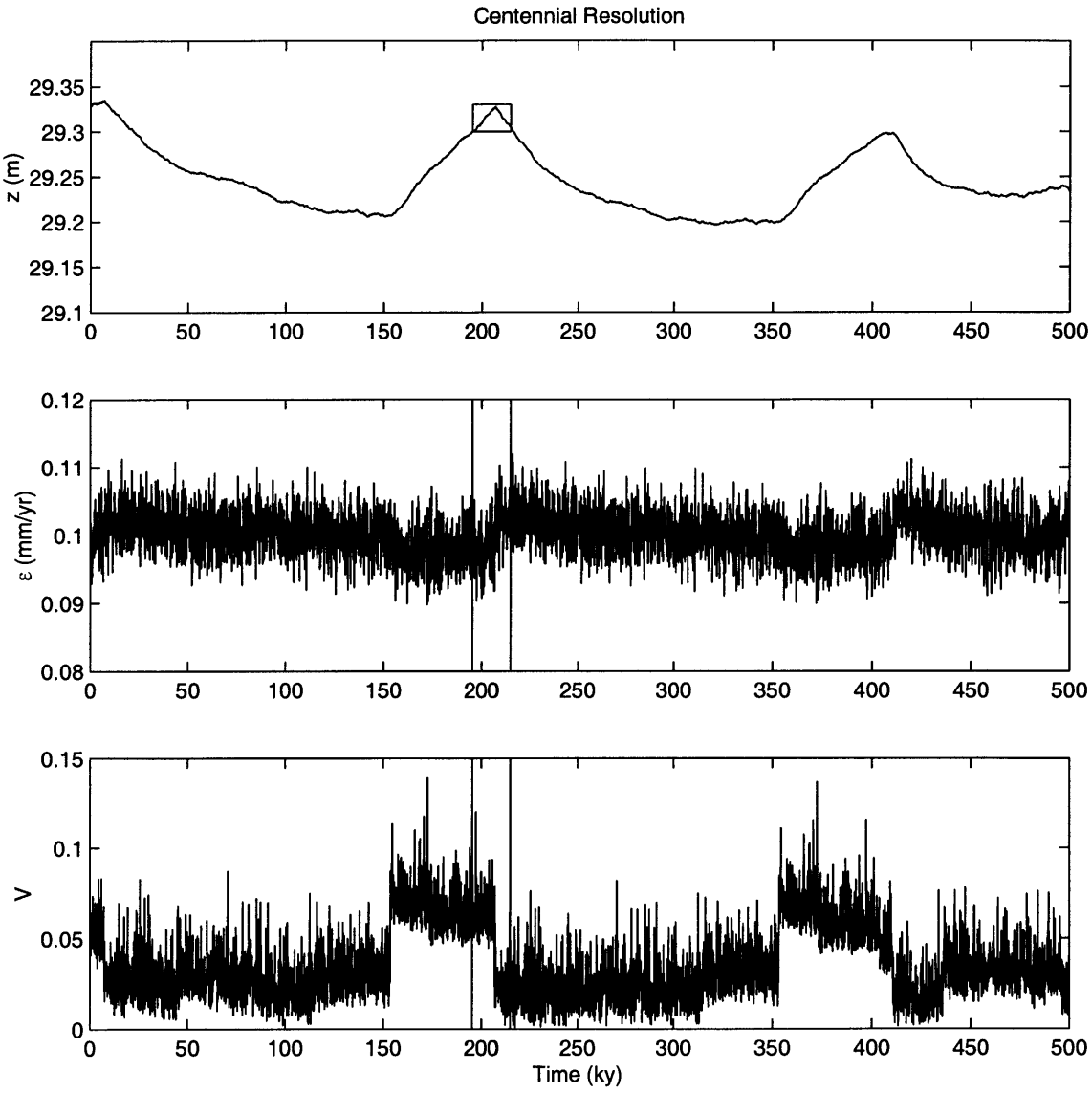

Figure 5-28: *Kv5*: 500,000-year time-series of mean elevation, erosion rate and vegetation density at 100 year resolution.

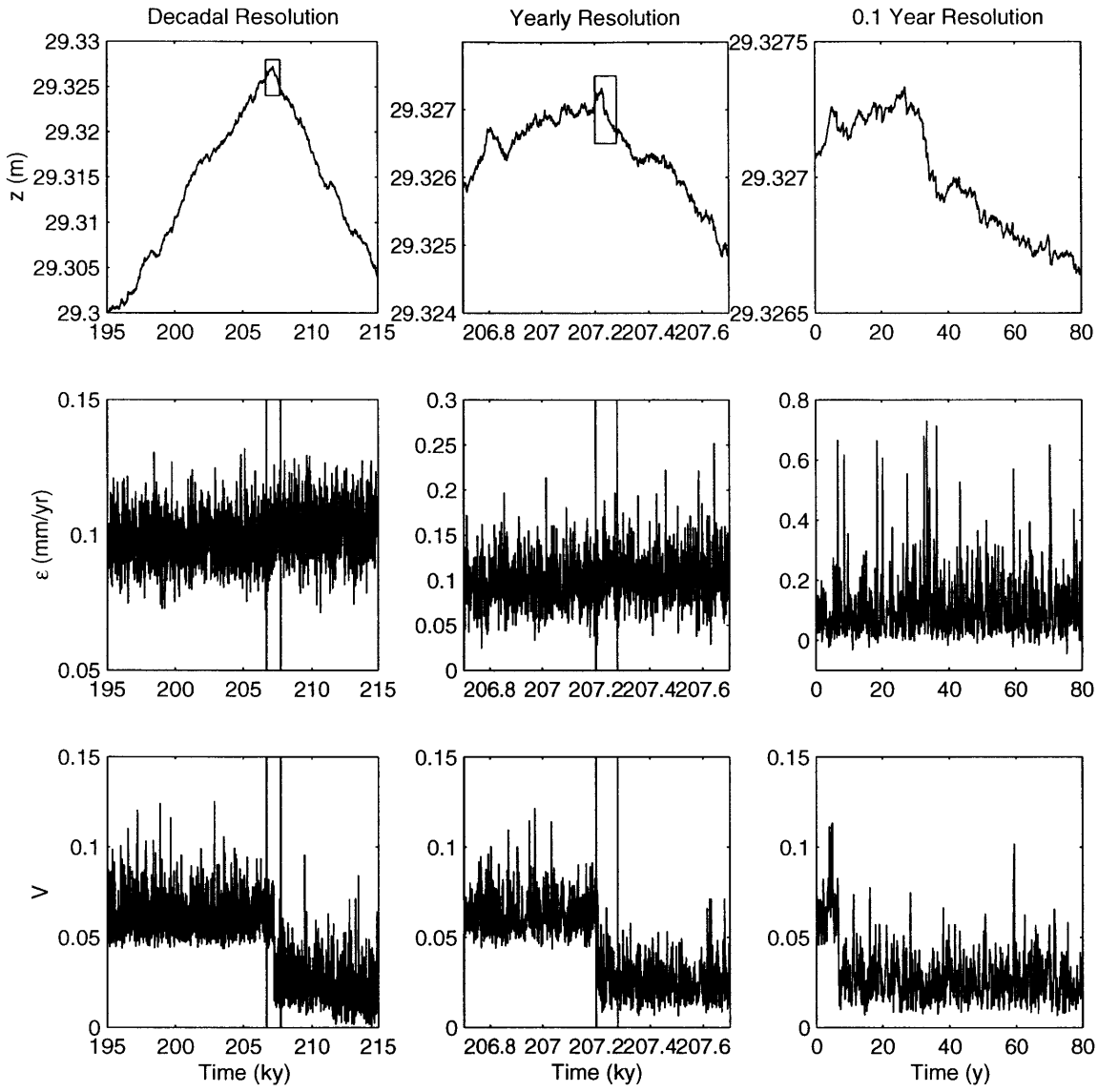

Figure 5-29: *Kv5*: Ever-smaller windows of the 500,000-year time-series at increasing temporal resolution.

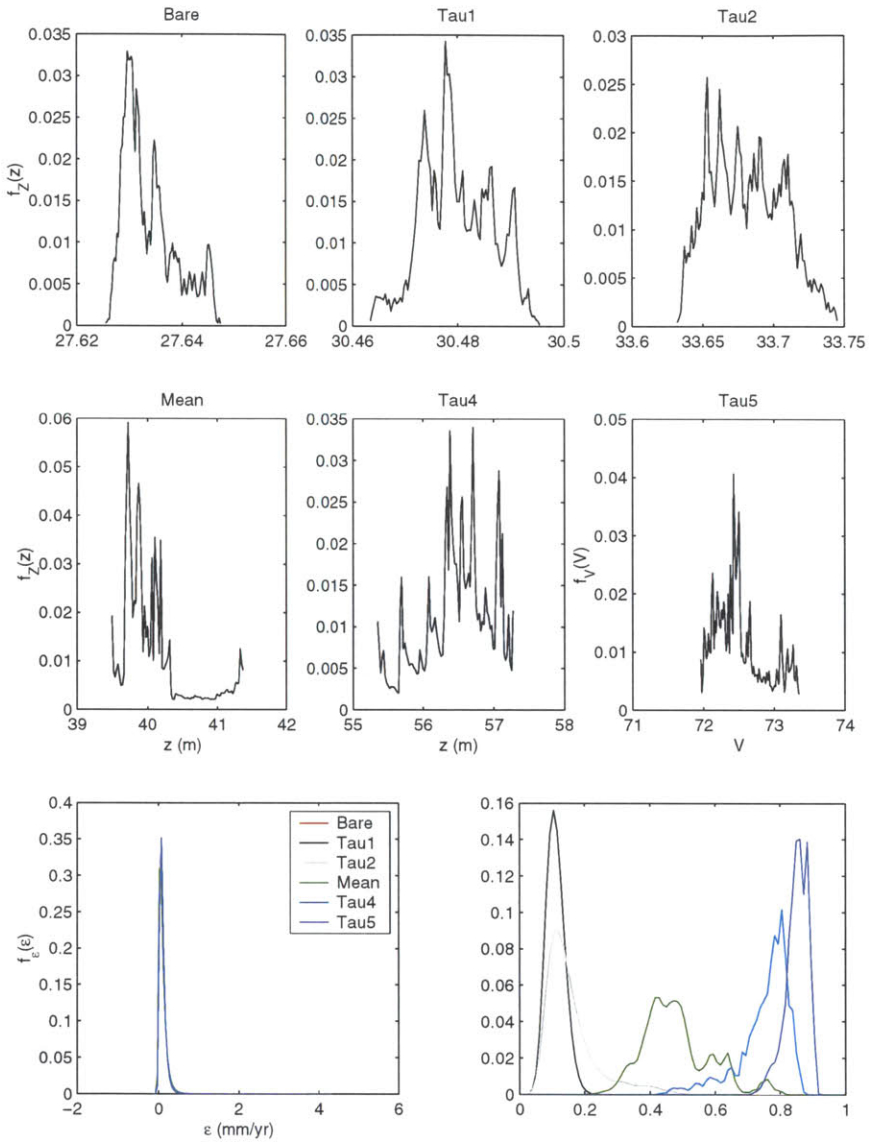

Figure 5-30: *Tau Simulations*: Distributions of mean elevation, erosion rate and vegetation density for *Bare* , *Tau1* , *Tau2* , *Mean* , *Tau4* and *Tau5*. Bin sizes for z are 0.2 mm (*Bare*), 0.4 mm (*Tau1*), 1 mm (*Tau2*), 21 mm (*Mean*), 22 mm (*Tau4*), and 16 mm (*Tau5*); for erosion, 0.05 mm/yr; for vegetation density, 1/90.

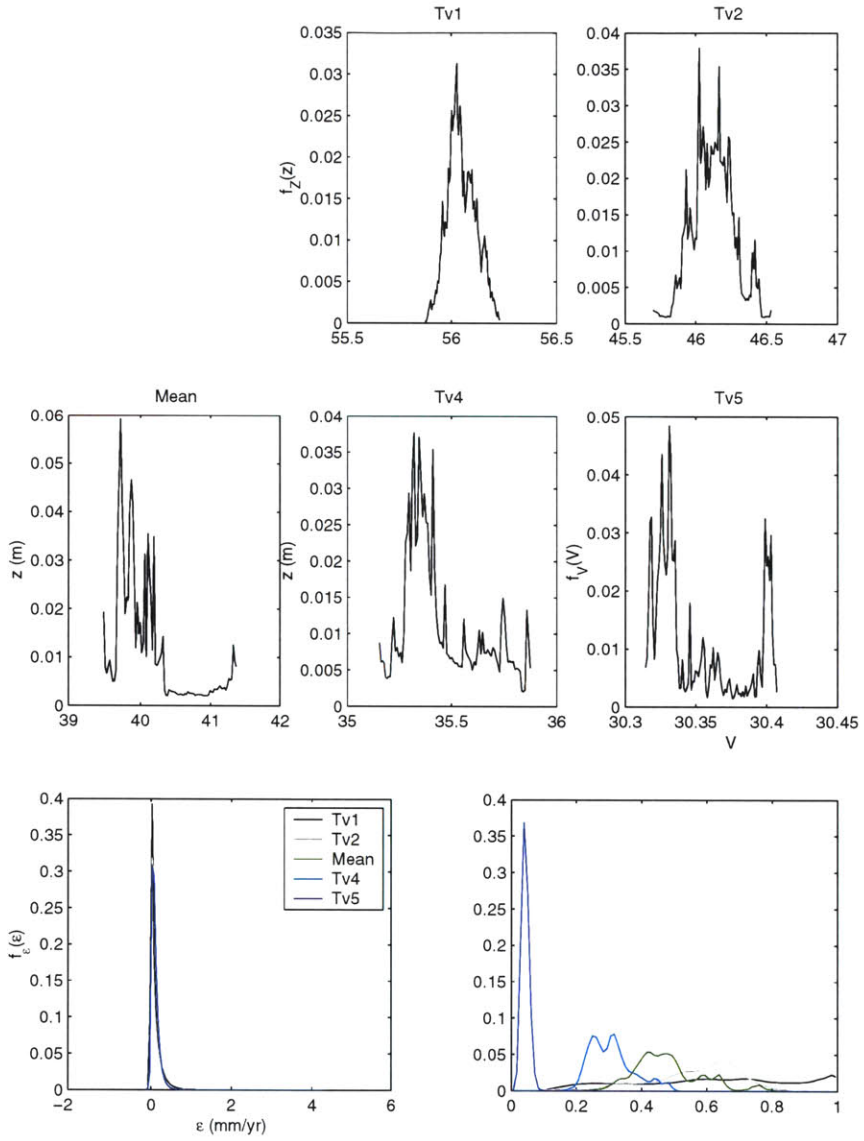

Figure 5-31: *Tv Simulations*: Distributions of mean elevation, erosion rate and vegetation density for *Tv1* , *Tv2* , *Mean* , *Tv4* and *Tv5*. Bin sizes for z are 4 mm (*Tv1*), 9 mm (*Tv2*), 21 mm (*Mean*), 8 mm (*Tv4*), and 1 mm (*Tv5*); for erosion, 0.05 mm/yr; for vegetation density, 1/90.

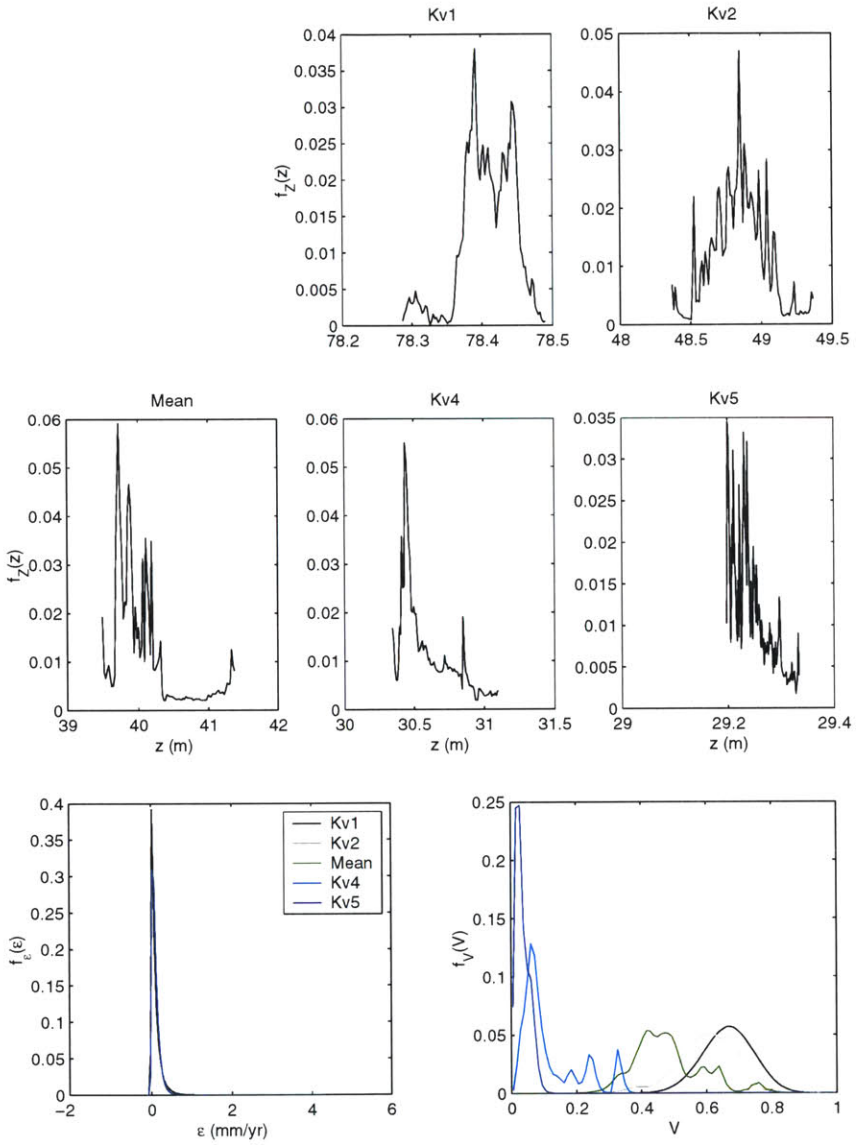

Figure 5-32: *Kv Simulations*: Distributions of mean elevation, erosion rate and vegetation density for *Kv1* , *Kv2* , *Mean* , *Kv4* and *Kv5*. Bin sizes for z are 2 mm (*Kv1*), 11 mm (*Kv2*), 21 mm (*Mean*), 8 mm (*Kv4*), and 2 mm (*Kv5*); for erosion, 0.05 mm/yr; for vegetation density, 1/90.

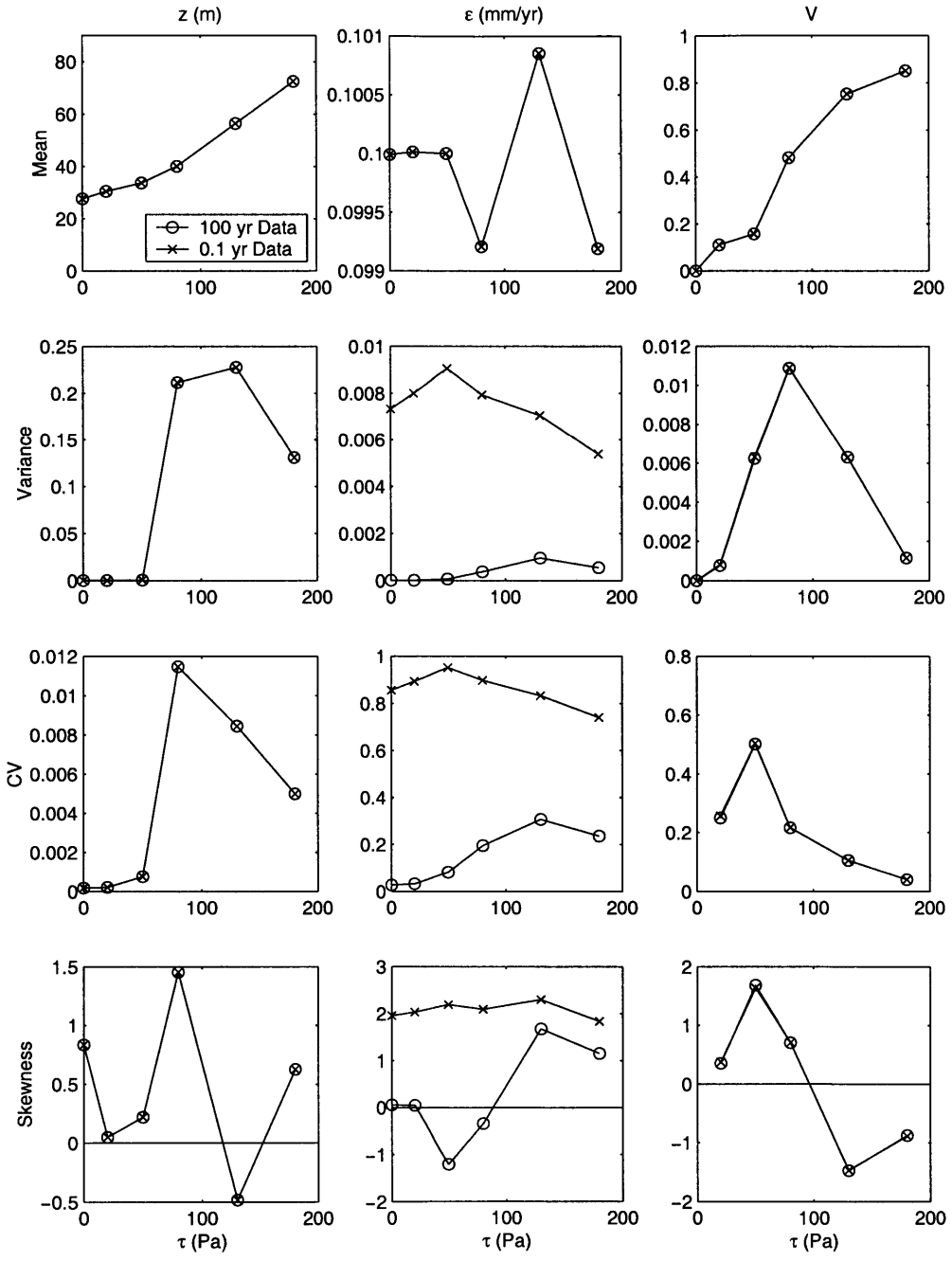

Figure 5-33: *Tau Simulations*: Variation of statistics with varying $\tau_{c,v}$, at the centennial and 0.1 year resolutions.

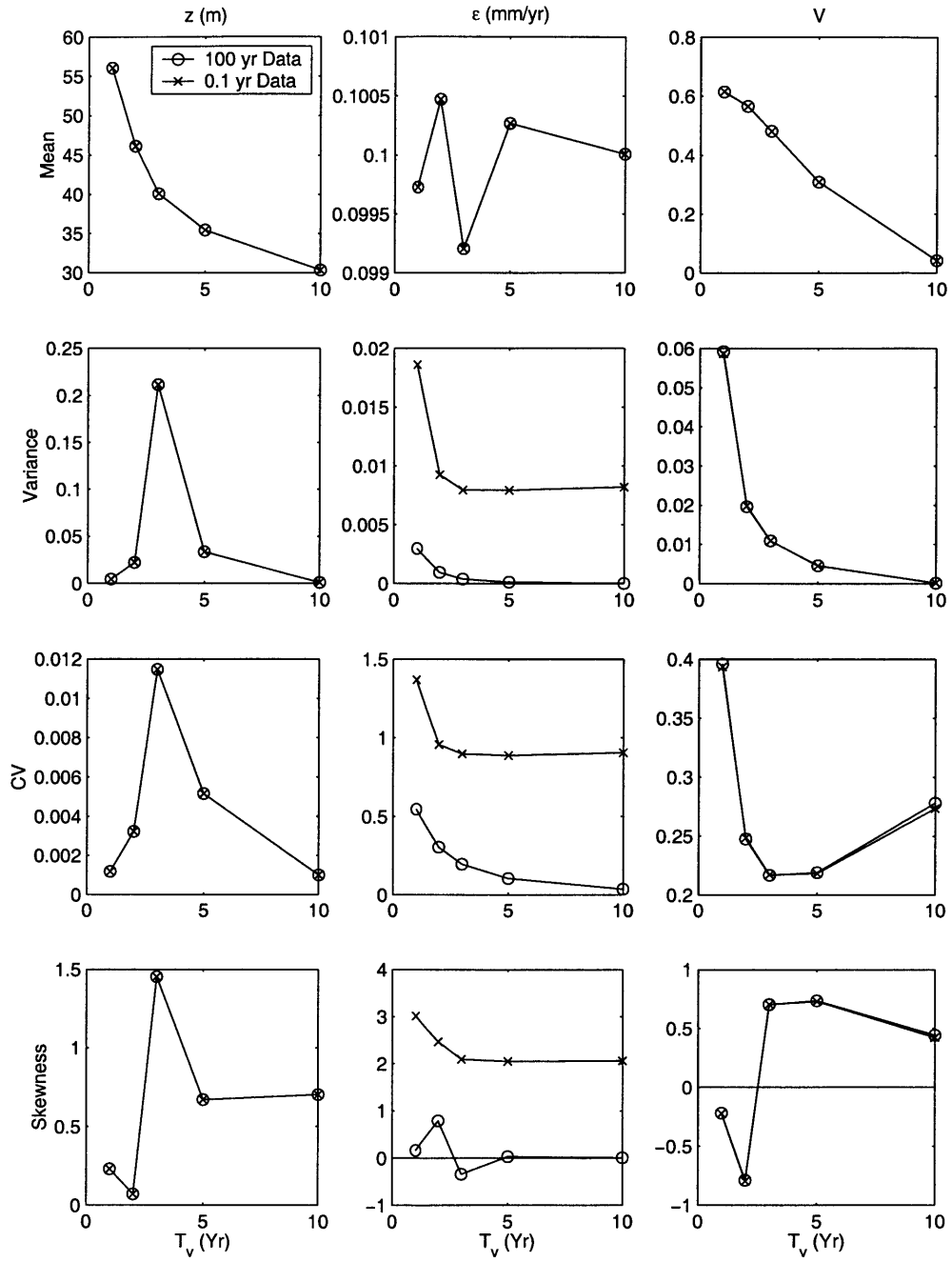

Figure 5-34: *Tv Simulations*: Variation of statistics with varying T_v, at the centennial and 0.1 year resolutions.

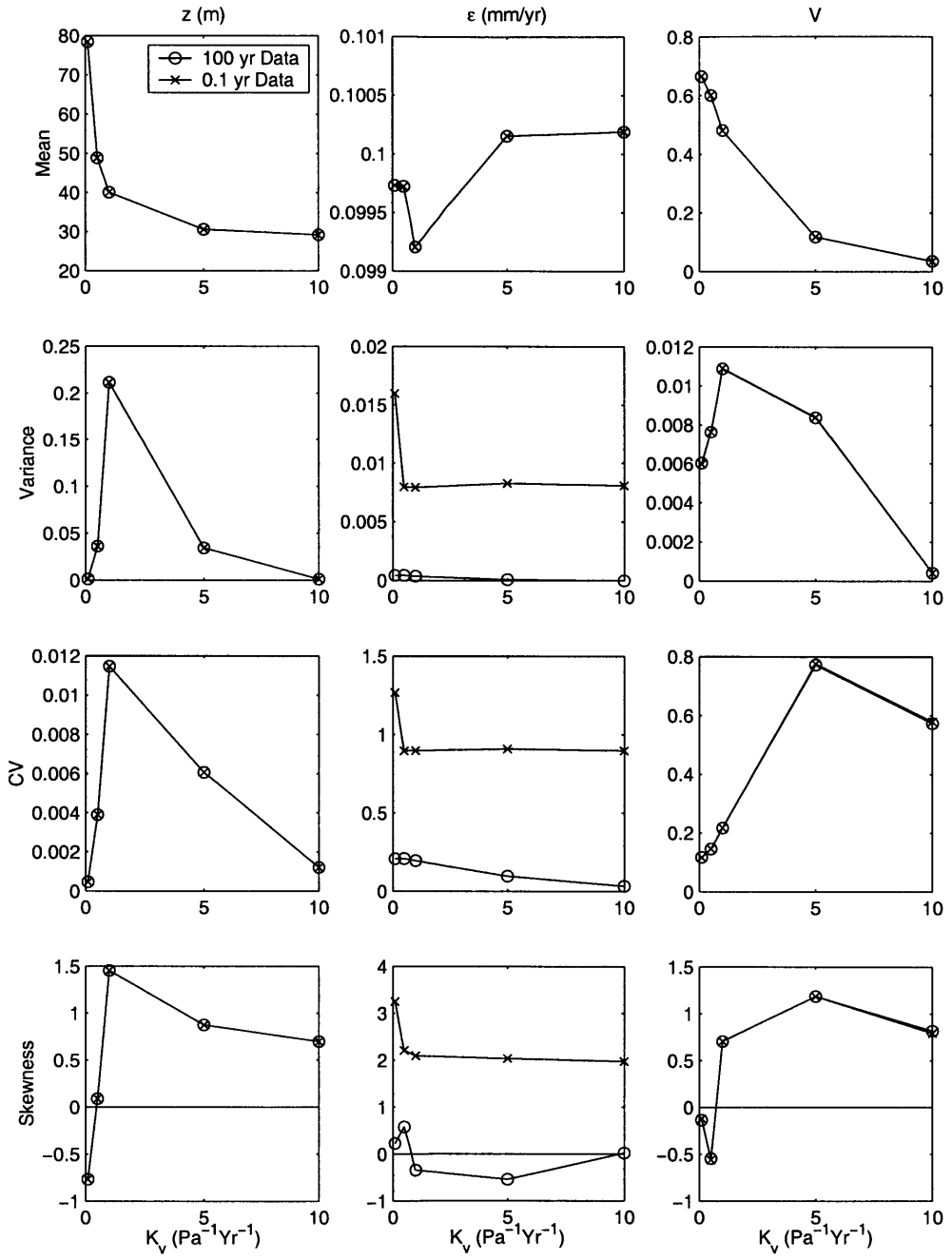

Figure 5-35: *Kv Simulations*: Variation of statistics with varying K_v, at the centennial and 0.1 year resolutions.

5.2 Vegetation-Erosion Relationship

The clear relationship between erosion rate, ϵ, and vegetation density[1], $\bar{V}$, in both the annual and centennial time-scales are considered more deeply. Figures 5-37, 5-39 and 5-41 illustrate bivariate histograms of this $\epsilon - V$ relationship at the yearly scale; Figures 5-36, 5-38 and 5-40 show the same at the centennial scale. The latter show a consistent monotonic dependence for most simulations (*Mean, Tau2, Tau4, Tau5, Tv1, Tv2, Tv4, Kv2,* and *Kv4*), while the former suggest the relationship is better represented by a probability distribution for smaller time scales.

An analytic relation qualitatively similar to the linear, centennial trends in Figures 5-36, 5-38 and 5-40 is obtained as follows. Consider the local, cell-based, non-zero erosion rate corresponding to a constant vegetation cover

$$\epsilon_{local} = K_b(\tau - \tau_c)^p, \tag{5.2}$$

$$\frac{\partial V_{local}}{\partial t} = \frac{1}{T_v}(1 - V_{local})\frac{\bar{T}_b}{\bar{T}_b + \bar{T}_r} - K_v V_{local}(\tau - \tau_c)\frac{\bar{T}_r}{\bar{T}_b + \bar{T}_r} = 0. \tag{5.3}$$

Given the bimodality of spatial vegetation states, the vegetation density corresponding best to active erosion is V_*, the lower, analytically-derived mode. Combining (5.2) and (5.3), by eliminating τ, one gets an estimate of the local erosion rate:

$$\epsilon_{local} = k_b \left(\frac{1 - V_*}{T_v K_v V_*} \frac{\bar{T}_b}{\bar{T}_r} \right)^p. \tag{5.4}$$

This rate applies only to actively eroding regions, not necessarily the entire domain. The fraction of area actively eroding, β, is estimated by again recognizing mean vegetation to be a weighted combination of low and high vegetation densities:

$$V = \beta \bar{V}_{low} + (1 - \beta)\bar{V}_{high}, \tag{5.5}$$

which is rearranged, taking $\bar{V}_{low} = V_*$ (eroding regions are similarly vegetated with

[1]Note that the value of vegetation density is that at the beginning of the time over which erosion is measured, and not the temporal mean.

the lower mode) and $\bar{V}_{high} = 1$ (non-eroding regions are fully vegetated), to become

$$\beta = \frac{1 - \bar{V}}{1 - V_*}. \tag{5.6}$$

This gives a spatial average erosion rate of

$$\epsilon = \beta \epsilon_{local}, \tag{5.7}$$

or

$$\epsilon = k_b \frac{1 - \bar{V}}{1 - V_*} \left(\frac{1 - V_*}{T_v K_v V_*} \frac{\bar{T}_b}{\bar{T}_r} \right)^p, \tag{5.8}$$

showing a linear relationship between mean vegetation cover and spatial average erosion rate. This is reasonable since $\epsilon \to 0$ as $\bar{V} \to 1$. Thus, with a measure of the meta-stable spatial mean vegetation density, one can estimate the global erosion rate. Furthermore, by equating ϵ to the long-term mean erosion rate, equivalent to the uplift rate, U, one gets an estimate of the long-term mean vegetation density

$$\bar{V} = 1 - \frac{U}{K_b}(1 - V_*) \left(\frac{1 - V_*}{T_v K_v V_*} \frac{\bar{T}_b}{\bar{T}_r} \right)^{-p}, \tag{5.9}$$

which is compared with the numeric results in Figure 5-42.

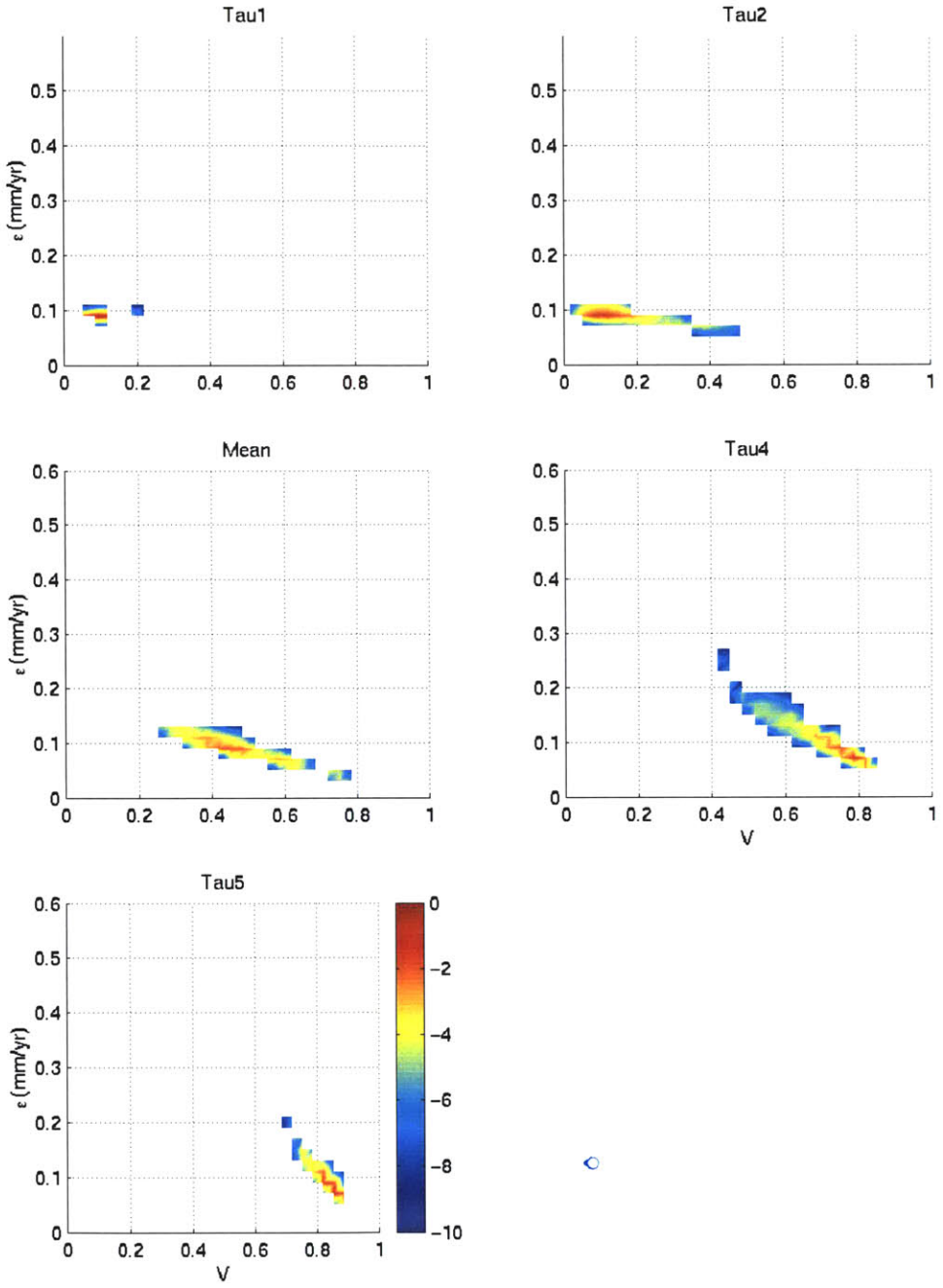

Figure 5-36: *Tau Simulations*: Bivariate histograms of $\epsilon - V$ dependence at the yearly time-scale. The normalized frequencies are expressed as log_{10}. The white regions correspond to zero probability. The bin size for ϵ is 1/150 mm/yr, and 1/90 for V.

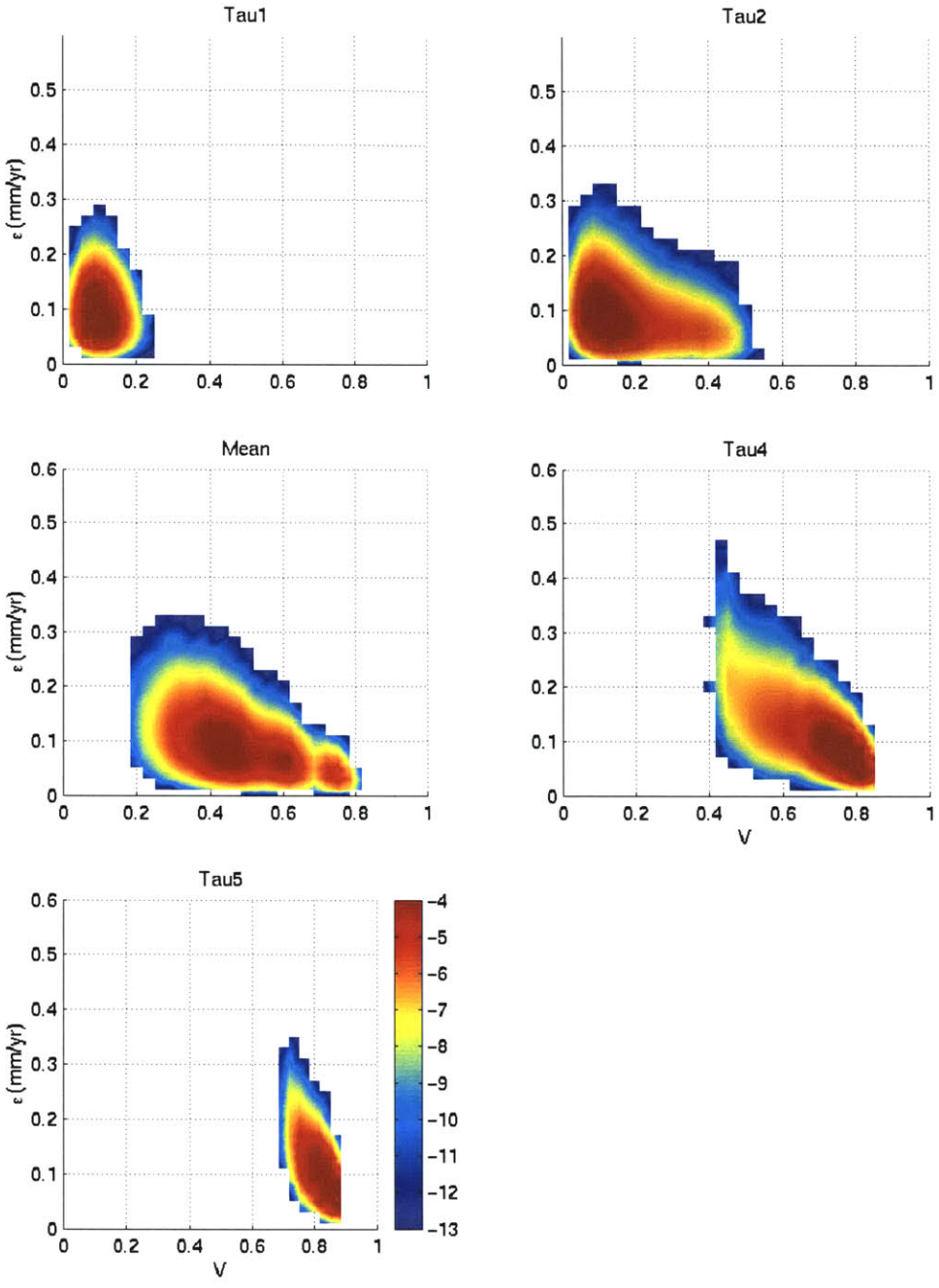

Figure 5-37: *Tau Simulations*: Bivariate histograms of $\epsilon - V$ dependence at the yearly time-scale. The normalized frequencies are expressed as log_{10}. The white regions correspond to zero probability.

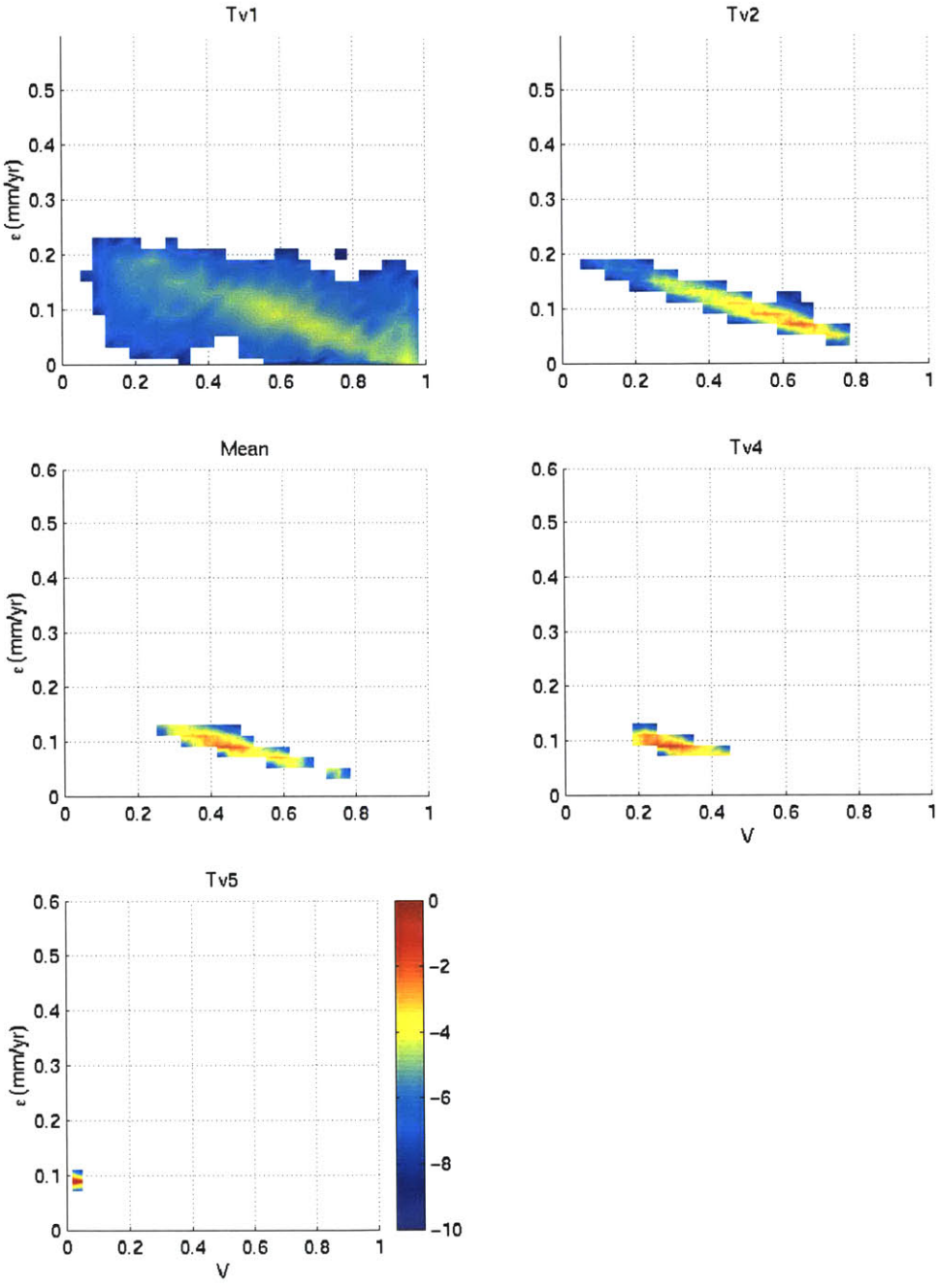

Figure 5-38: *Tau Simulations*: Bivariate histograms of $\epsilon - V$ dependence at the yearly time-scale. The normalized frequencies are expressed as log_{10}. The white regions correspond to zero probability.

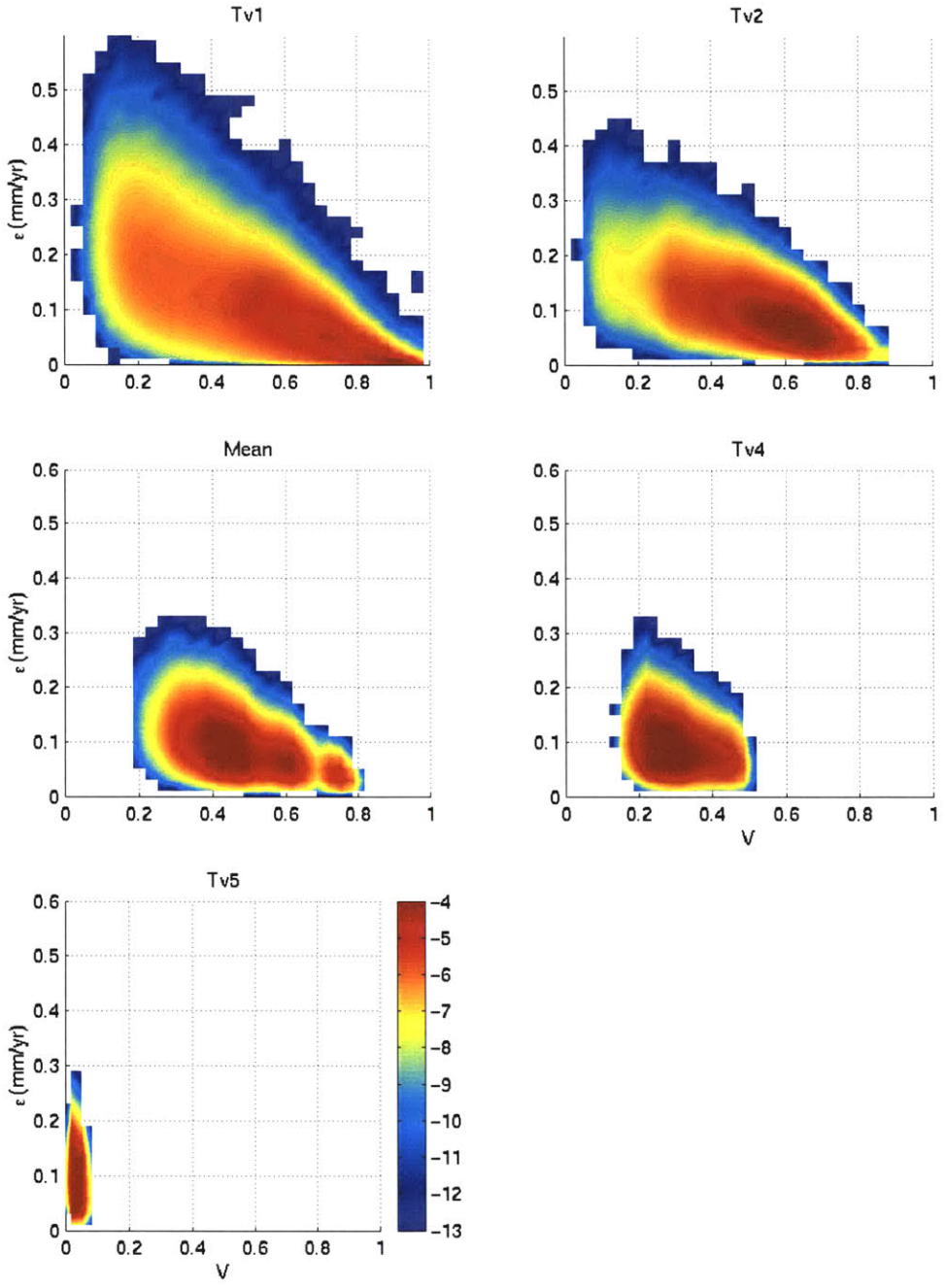

Figure 5-39: *Tau Simulations*: Bivariate histograms of $\epsilon - V$ dependence at the yearly time-scale. The normalized frequencies are expressed as log_{10}. The white regions correspond to zero probability.

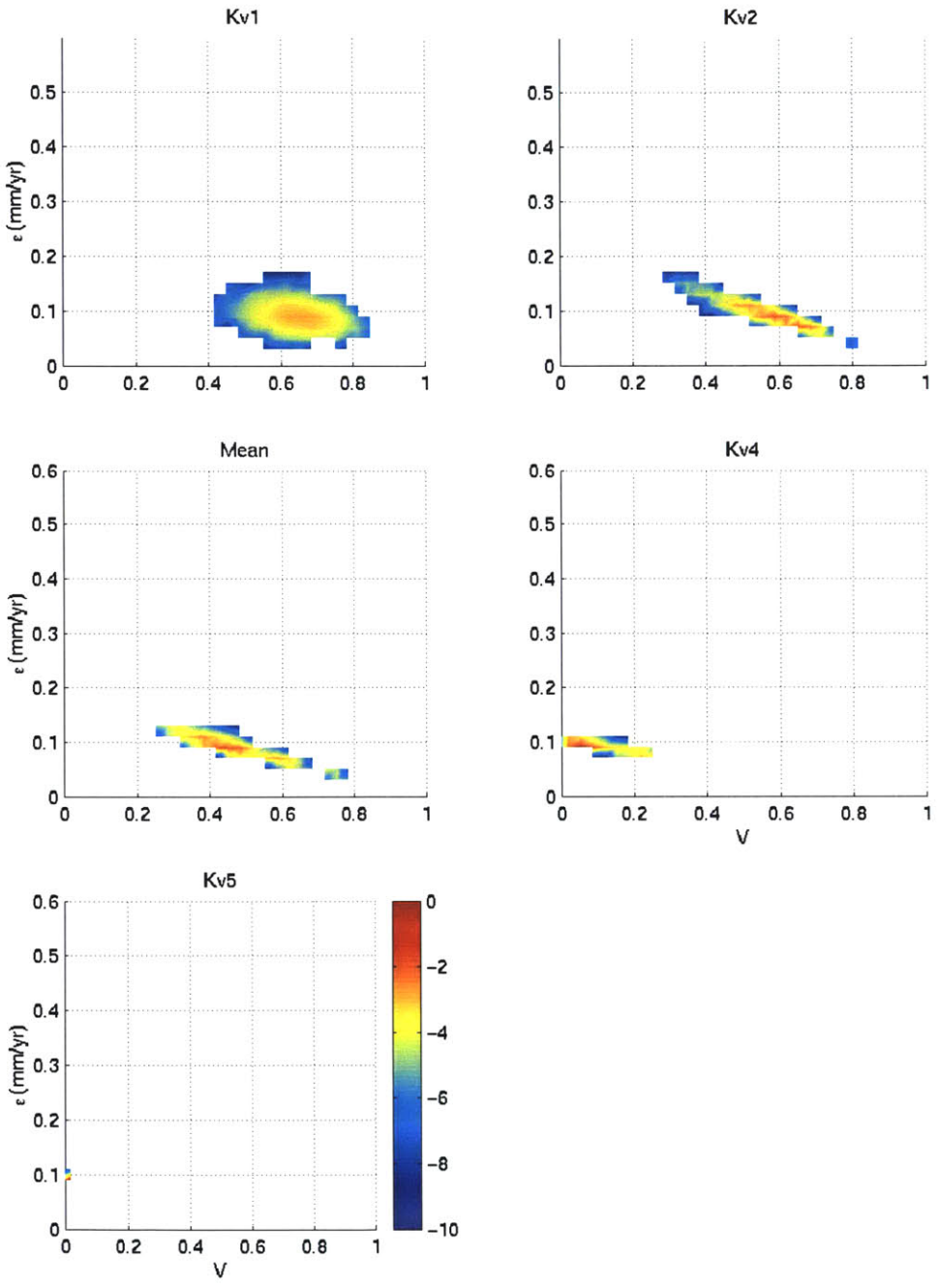

Figure 5-40: *Tau Simulations*: Bivariate histograms of $\epsilon - V$ dependence at the yearly time-scale. The normalized frequencies are expressed as log_{10}. The white regions correspond to zero probability.

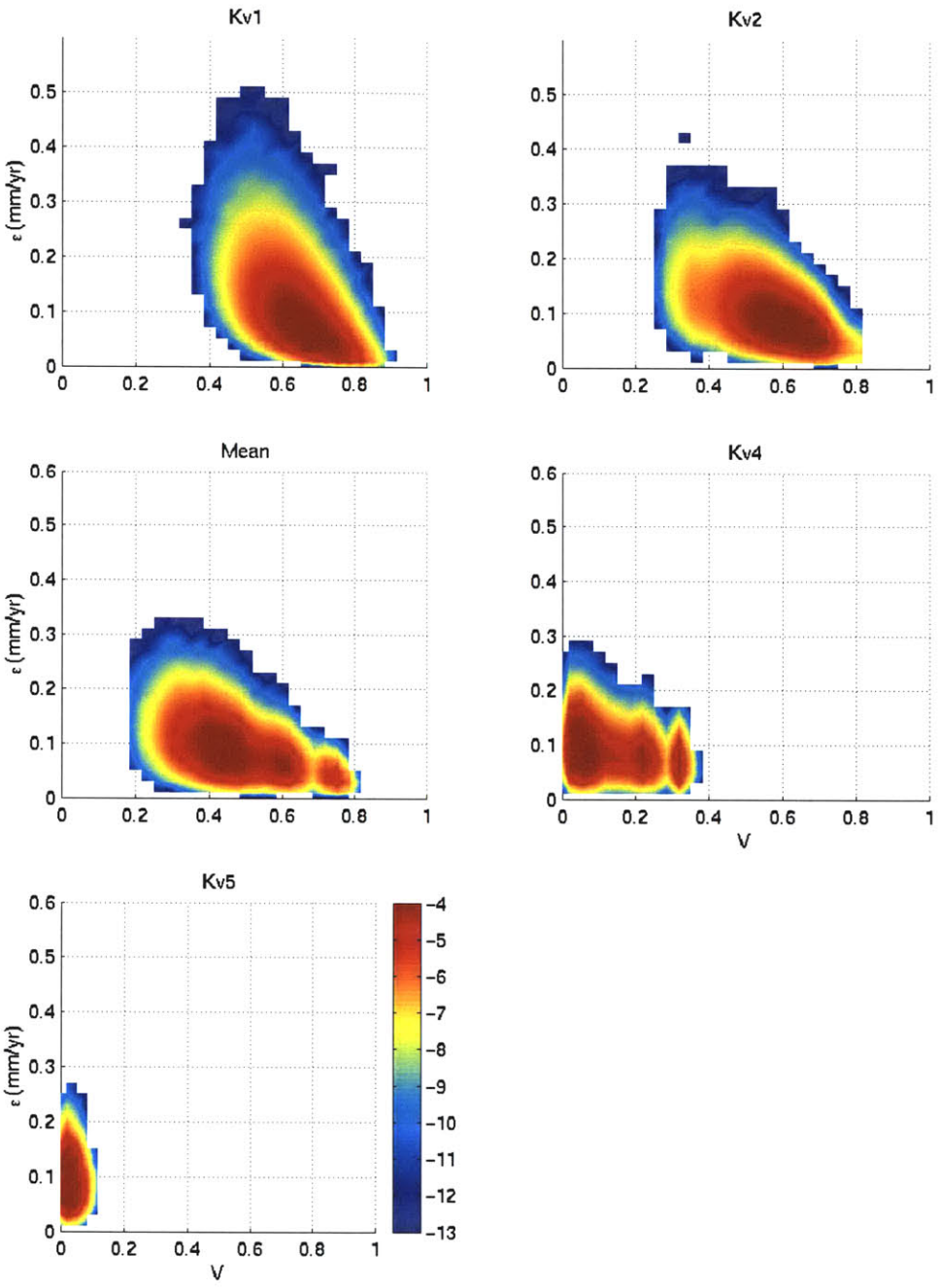

Figure 5-41: *Tau Simulations*: Bivariate histograms of $\epsilon - V$ dependence at the yearly time-scale. The normalized frequencies are expressed as log_{10}. The white regions correspond to zero probability.

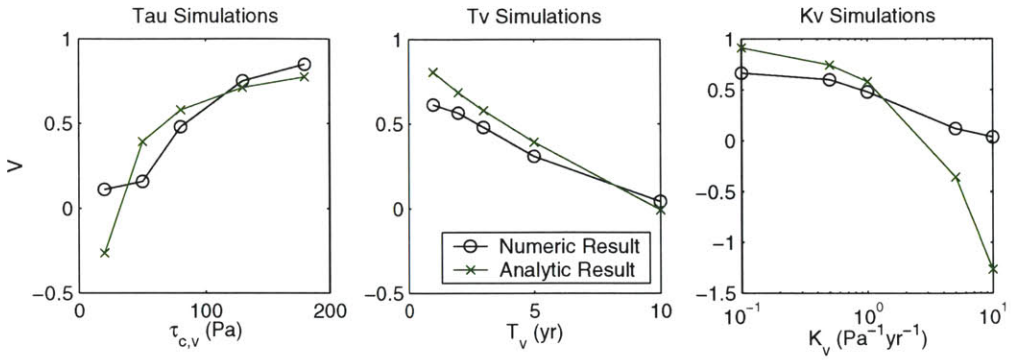

Figure 5-42: Long-term mean vegetation densities for the numeric and analytic (Equation 5.9) results.

The analytic result does not capture the approach to bare cover as $\tau_{c,v} \rightarrow 0$, nor as T_v and $K_v \rightarrow \infty$, although the general trends agree. This is understandable since the bivariate histograms show weak dependence for these parameter values. When a landscape becomes ever more bare, the high frequency variability becomes relatively more significant, putting more weight on the nature of erosive, and hence storm, events. The simplifications that led to the above result were that each storm and interstorm duration equaled their mean, and each storm had the same erosive potential. In the poisson rainfall model, all storms are not created equal, nor what takes place during them.

5.3 Summary

Of the results obtained from solely temporal analyses, conclusions are as follows:

1. Most simulations show medium- and long-term persistence. The medium are meta-stable states, with roughly constant vegetation and erosion magnitudes. The longer patterns are periods of consistent net uplift or net erosion. Durations of these patterns differ among the simulations;

2. The large-scale trends are composed of step-changes between the meta-stable states, and may be periodic or aperiodic;

3. Simulations that exhibit non-positive erosion rate skewness at the centennial scale, which correspond to a net uplift time-scale that is no longer than that of net erosion, exhibit periodic oscillations. The exception is *Mean*, which has an anomalous drop in erosion rate.

4. Simulations with positive erosion skewness for all scales show aperiodic fluctuations.

5. Erosion rate variability is proportional to vegetation density magnitude.

6. High frequency fluctuations in erosion rate and vegetation density are visible at all scales, superposed on larger scale trends.

7. 0.1 year erosion rate probabilities are insensitive to $\tau_{c,v}$, but respond to changes in both T_V and K_v, suggesting the latter parameters have a temporal control on erosion dynamics, as opposed to $\tau_{c,v}$ (suggested also by their units).

8. For most simulations (those with large scale persistence) there is a clear near-linear, negative relationship between vegetation density and mean millennial erosion rate;

9. The above ϵ-V relationship may be approximated analytically, and extended to provide a reasonable estimate for the long-term mean vegetation density, for simulations that do exhibit the ϵ-V dependence.

Chapter 6

Dynamic Biophysiography

Landscape evolution is intrinsically both spatial and temporal in nature — changes in one dimension affect changes in the other. Knowledge garnered from their combined study is thus greater than the sum of their separate studies, revealing differences in erosion and vegetation variability between cells and changes in drainage direction. These phenomena are first illustrated with the *Kv4* simulation specifically, and then generally with the remaining simulations.

6.1 Individual Node Time series

The spatially-distributed data of the *Kv4* simulation were recorded for another 200,000 years, after the initial 500,000, at a resolution of 2,000 years. This gave 101 equispaced time-slices, permitting reasonable assessment of individual node evolution spanning one macroscale oscillation. Of the total 841 active nodes comprising the landscape, the elevation and vegetation density time series of 20 nodes, identified in Figure 6-1, are considered (Figures 6-2 and 6-3). The landscape's spatially-averaged time series are also presented in Figure 6-1. The nodes were chosen to compare among first order channels, among basins, between basins, and in the vicinity of avulsions[1].

Compared with the average elevation variability of 0.8 m, individual node variations range from 0.02 m to 3 m. Those with variations greater than 2 m (1d, 3a,

[1]In this thesis, the term 'avulsion' is used interchangeably with 'stream capture'.

3c, 4a, 5a and 5c) show abrupt changes between net erosion and net uplift, and are completely vegetated only during the latter. For all other nodes, vegetation density is generally less than 0.1. Furthermore, the behavior of only three nodes (3a,3c and 5a) resemble the large-scale behavior. Others may have two or three peaks rather than one, decay differently, or are out of phase — some nodes are eroding while others are not. This begs the question: Which nodes are dominating macroscale behavior? Of course it is likely to be those whose elevations vary the most, given that each node represents roughly the same area. However, three out of six nodes that fit this criterion are clearly not in tune, in either phase or period. Their local effects must therefore be counterbalanced by the integrated effects of other nodes evolving differently, leading to destructive interference. It thus remains unclear what the characteristics are that determine which cells dominate the macroscale behavior, if it is not partially random.

Considering now just first order channels (1a-e, 3a, 3c, 4a, 4c, 5a, 5c, 5d), they include all, but are not limited to, nodes with the largest fluctuations. The neighboring nodes 1c and 1d show similar trends, and 1e to a lesser extent despite being in a completely different sub-basin. Nodes separated any further show no such similarities. Close inspection of the vegetation signals, however, reveals almost identical fluctuations, albeit with marginally different magnitudes. While there appears no diagnostic test to separate first order from larger channels based on elevation, such a test exists with vegetation. The sequence of maxima and minima are alike among the first order channels, and among the larger channels, while clear differences exist between the two sets.

While nodes 2a, 2b and 2c, selected as having comparable drainage areas, are in separate drainage basins, they have similar elevation variation ranges of 0.2 m. Within basins, there is no clear similarity between elevation changes within the largest sub-basin on the right (5d, 2c and 1e), and within the central, main sub-basin (5b, 4d, 4b, 2b, and 1a-e). Nor are there similarities along the domain front (5a-d). Thus, there is no indication that basins behave more or less differently from each other than individual nodes.

The remaining nodes to discuss are those associated with avulsions. Node 3c

flows to either 3b or 3d at some stage during its evolution. Similarly, 4a flows to both 4b and 4d. Both avulsing nodes 3c and 4a are at some stage well-vegetated. Non-avulsing nodes 3a and 4c, on the opposite side of the larger channel, which are also first order channels, are provided for comparison. The only difference appears in the direction of the larger channel to which they flow — away from the un-avulsing node. A total of 13 nodes change their drainage direction during the course of the simulation.

As suggested by the vegetation state distributions of Chapter 4 (Figures 4-5-4-6), the poorly-vegetated states are not all alike. Their means fluctuate in the vicinity of $V_* = 0.05$, but do not seem attracted to it.

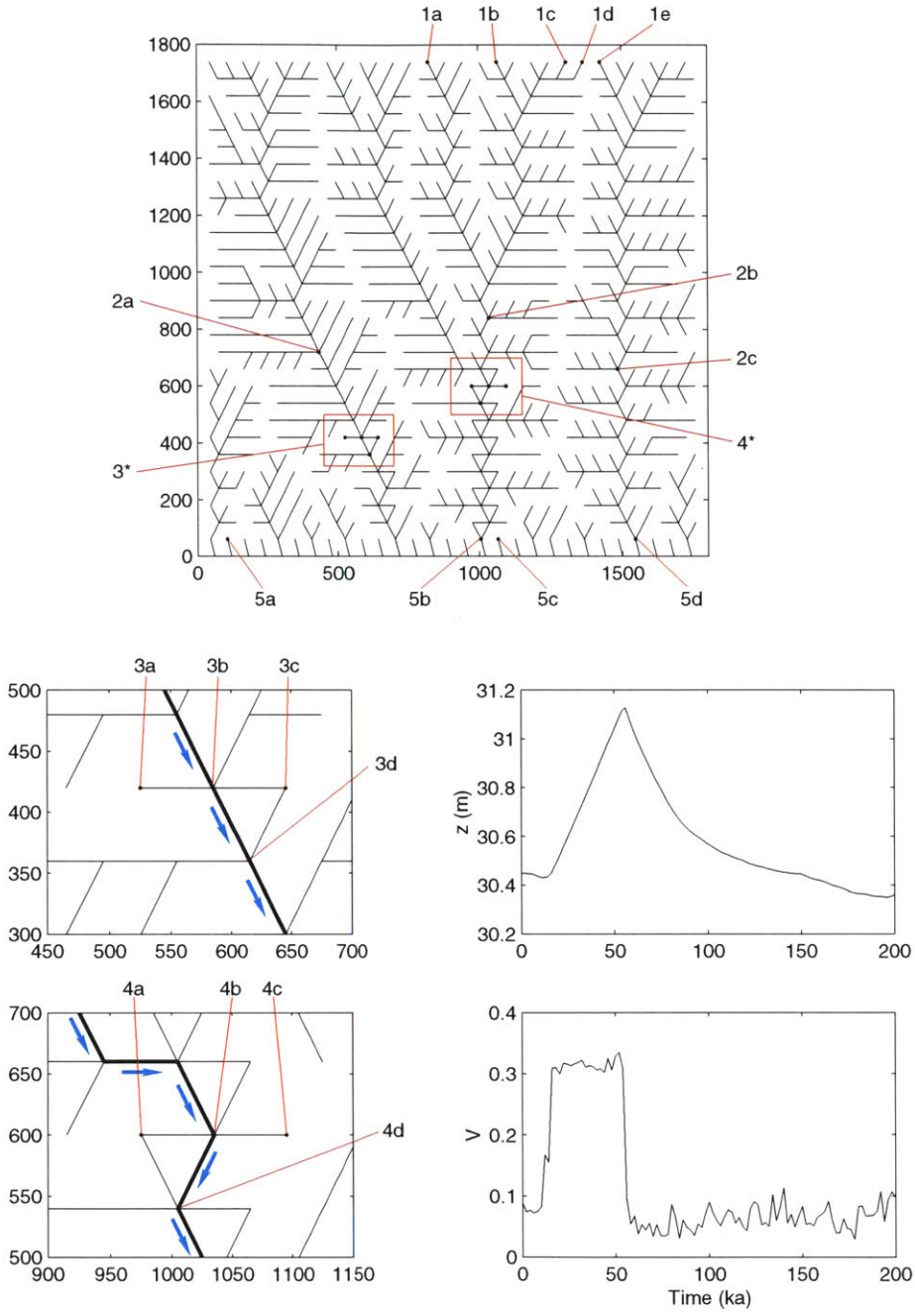

Figure 6-1: Top and lower left: Overlapped drainage networks of the 101 equispaced time-slices of the *Kv4* simulation. Sites of channel changes (avulsions) appear as closed loops of connected nodes — there are 13 such changes. Nodes whose individual time series are displayed in figures 6-2 and 6-3 are identified. Lower right: Time series of the spatial mean elevation and vegetation density at 200 year resolution, the same as individual time series.

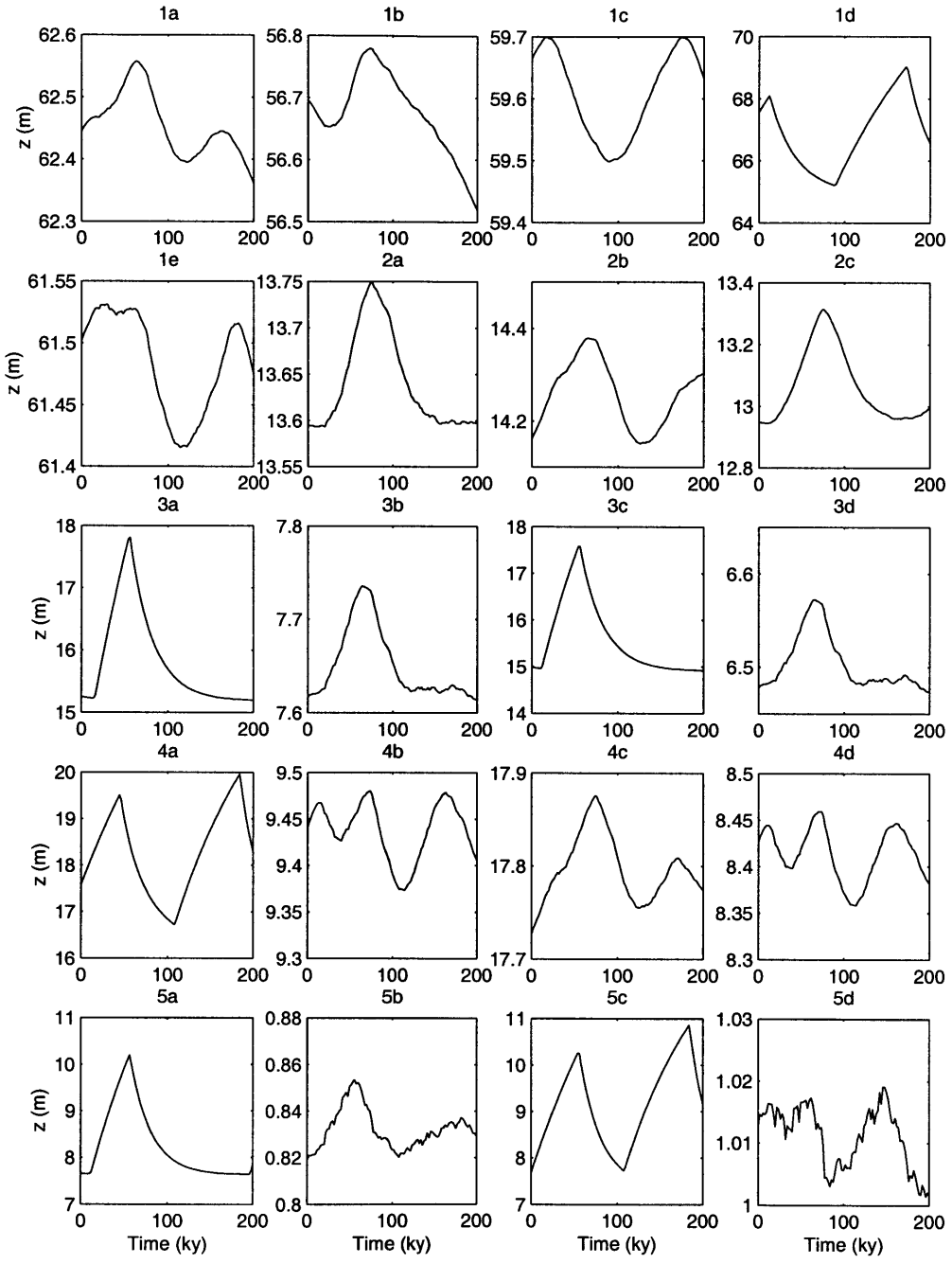

Figure 6-2: Individual node elevation time series at 200-yr resolution. Node locations are identified in figure 6-1.

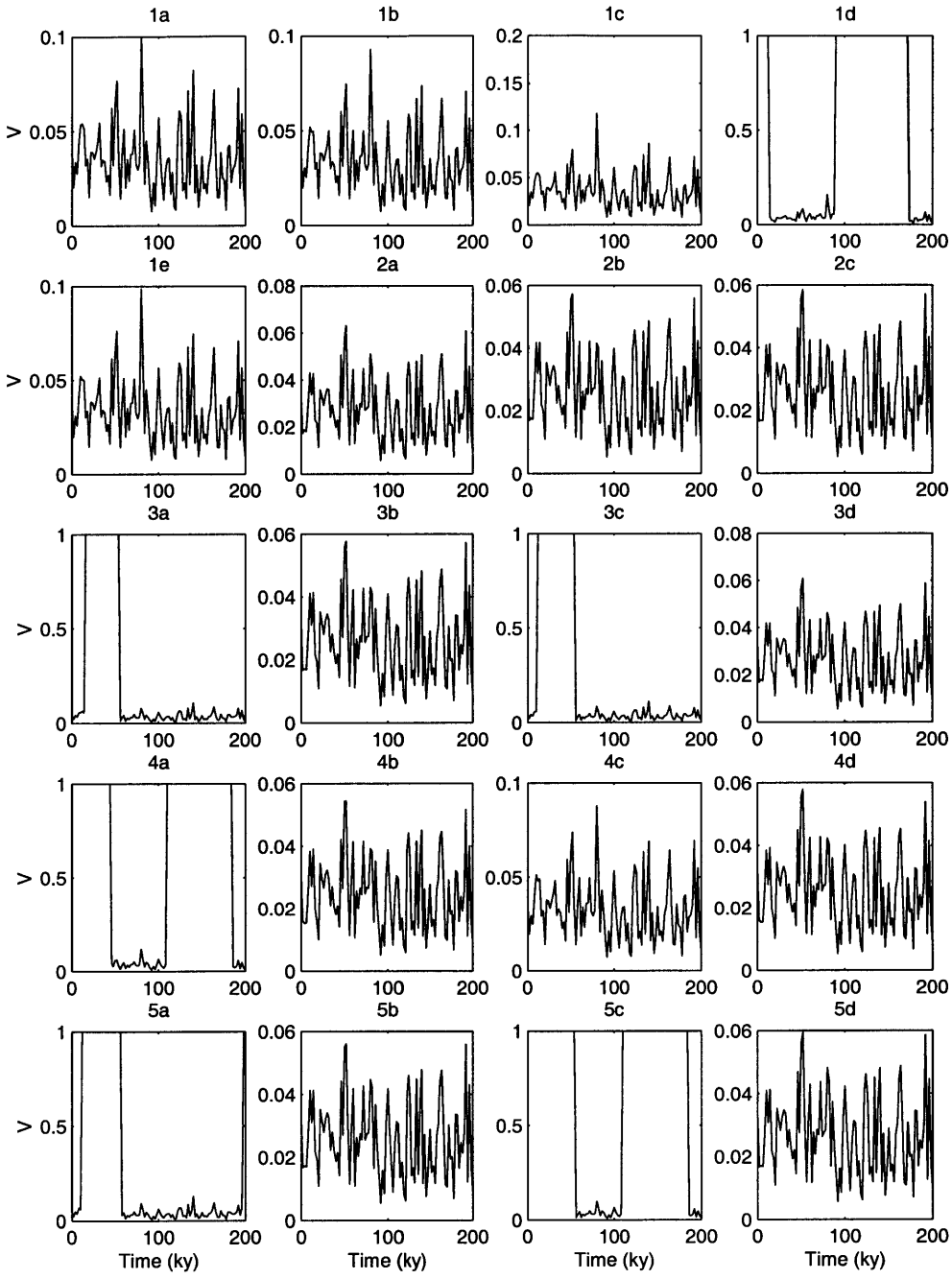

Figure 6-3: Individual node vegetation time series at 200-yr resolution. Node locations are identified in figure 6-1.

6.2 Stream Capture and Differential Elevation Changes

Simulations other than *Kv4* also exhibit stream capture, with the exception of *Bare*, *Tau1*, *Tau2* and *Tv5*. Both minor channel changes (fluctuating first order channel directions) and major stream capture take place over the course of the other simulations. During *Tau5*, a large branch of the central sub-basin is gradually consumed, proceeding from high to low elevations, mainly by the sub-basin to the left (Figure 6-4).

To understand the conditions that lead to stream capture, consider three nodes arranged as in Figure 6-5. Node *1* may flow to either *2* or *3*. For the purposes of the illustration, *2* always flows into *3*, and itself drains other nodes, although neither need be universally true. The general trend is thus for channels to flow down the page, i.e. from *1* to *3*. For *1* to flow instead to *2*, the slope from *1* to *2* must be larger than that to *3*:

$$\frac{z_1 - z_3}{|\mathbf{x_1} - \mathbf{x_3}|} > \frac{z_1 - z_2}{|\mathbf{x_1} - \mathbf{x_2}|}, \tag{6.1}$$

which leads to an *avulsion criterion*,

$$C_A = \frac{z_3}{|\mathbf{x_1} - \mathbf{x_3}|} - \frac{z_2}{|\mathbf{x_1} - \mathbf{x_2}|} - z_1 \frac{|\mathbf{x_1} - \mathbf{x_2}| - |\mathbf{x_1} - \mathbf{x_3}|}{|\mathbf{x_1} - \mathbf{x_2}||\mathbf{x_1} - \mathbf{x_3}|}. \tag{6.2}$$

If $C_A > 0$, node *1* flows to *3*; if $C_A < 0$, node *1* flows to *2*. Alternatively, if $z_2 > z_3$ and $|\mathbf{x_1} - \mathbf{x_2}| = |\mathbf{x_1} - \mathbf{x_3}|$ $\forall$ time, avulsions are impossible. If the second constraint were not true but z_1 variability is sufficiently low, avulsions will also not occur. On the other hand, large variations in z_1 cause C_A to become negative, provided the differences in elevation between the two lower nodes is not too great.

These avulsion principles are illustrated in Figure 6-6 for sets of nodes in the 2000-yr resolution *Kv4* data. For nodes within A, the main channel elevations are comparable after scaling by the horizontal distances, and the tributary variation is large. C_A occasionally drops below zero at which time the drainage direction changes. For nodes within B, the main channel elevations are less similar (they are steeper as

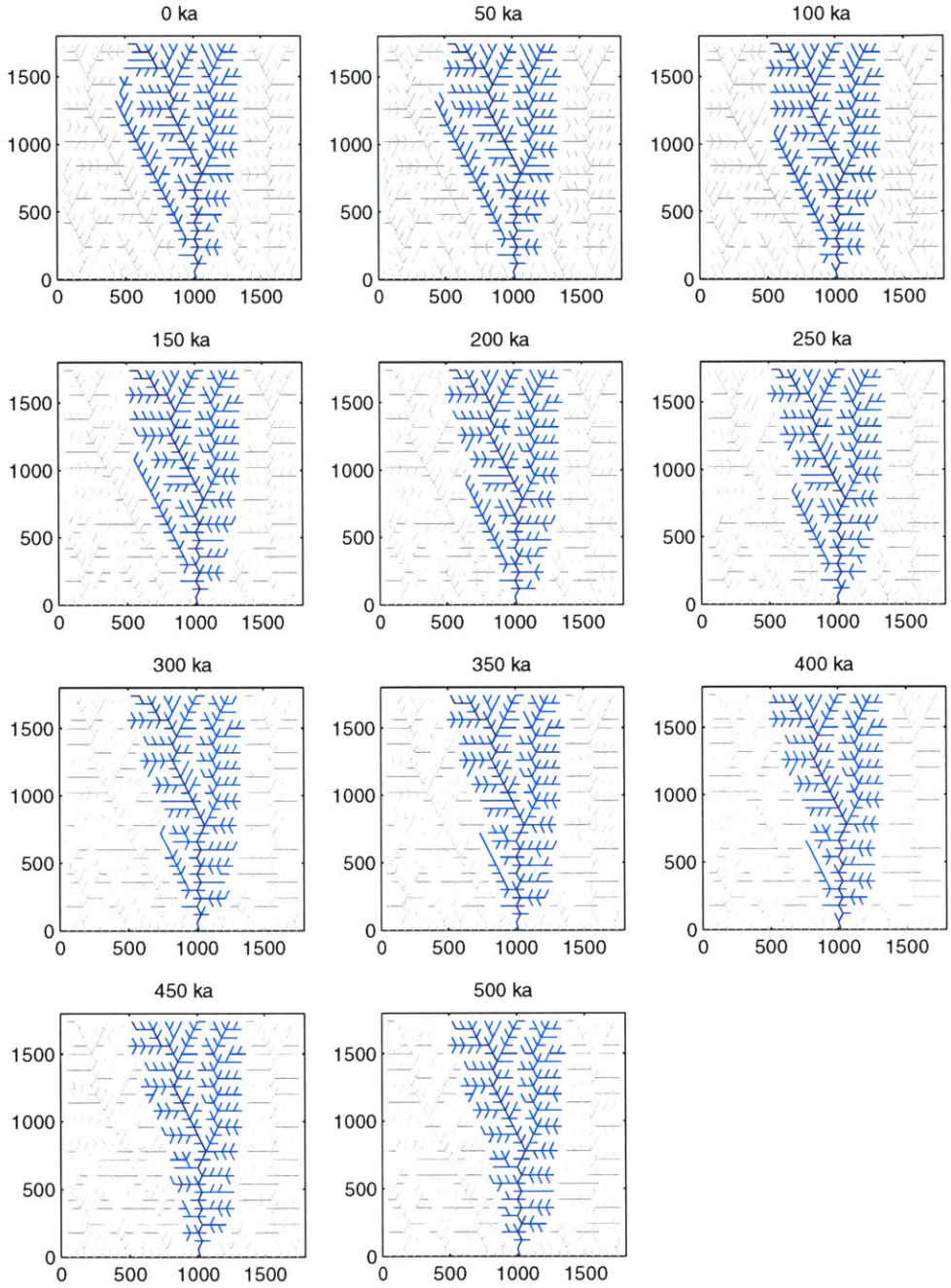

Figure 6-4: Dynamic drainage network of the *Tau5* simulation over 500,000 years at 50,000-yr intervals. While minor channels changes occur everywhere, the large left-most branch of the largest basin (blue) is gradually being captured from its source by the neighboring sub-basin.

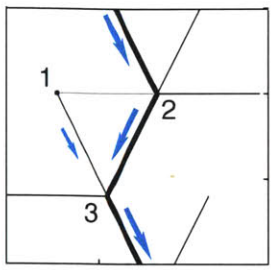

Figure 6-5: Flow net to illustrate avulsions. Node A may flow to either B or C, depending on inter-node distances and node elevations.

a result of being further upstream). While variations in the tributary channel are large, they are not sufficient to cause $C_A < 0$, and no avulsions occur.

Given that the magnitude of elevation changes is instrumental to avulsion propensity, and that individual node time series for *Kv4* show a diverse range of such magnitudes, all simulations will be analyzed in this way. The variable considered is the difference between the maximum and minimum elevations for each node, Δz (Figure 6-7). There is a marked tendency for the range of Δz to increase with $\tau_{c,v}$, while for K_v, Δz subtly decreases. For T_v, Δz is greatest for intermediate parameter values. *Tau4* and *Tv1* have similar mean elevations, yet the node ranges are clearly not, indicating that topography alone does not determine elevation fluctuations. These trends are akin to avulsion frequency and extent (Figure 6-8, Table 6.1). While some simulations may be approaching a steady state network (*Tv1* and *Kv5*), most suggest channel changes are a regular occurrence, while being confined to low order channels. Both the number of avulsions (frequency) and the number of avulsing nodes (extent) increase with $\tau_{c,v}$, but the latter does so at a slower rate — avulsions are more likely for high $\tau_{c,v}$ and are more evenly distributed. For T_v, avulsion frequency and extent also increase, but in this case avulsions become relatively more localized until they are eliminated in *Tv5*. The trends for Kv are less clear. None of the trends are monotonic, after accounting for *Mean*, although there is a general decrease in both frequency and extent. Avulsion concentration is greatest for intermediate K_v values.

Predicting stream capture likelihood is thus largely tantamount to predicting node elevation variation. A greater erosion threshold, with higher $\tau_{c,v}$, allows longterm

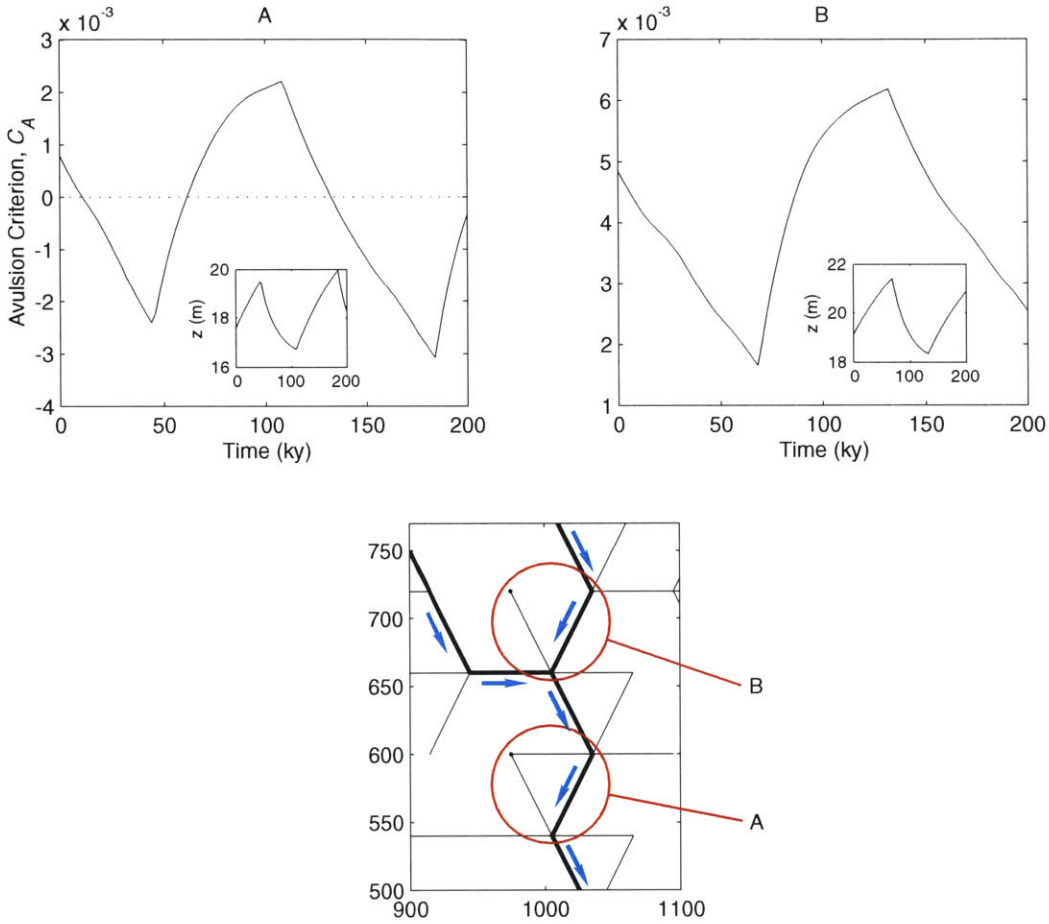

Figure 6-6: If the *avulsion criterion*, C_A, changes sign, channel direction changes. This occurs in the A nodes but not in the B nodes further upstream. These nodes are part of the 200-yr resolution *Kv4* data.

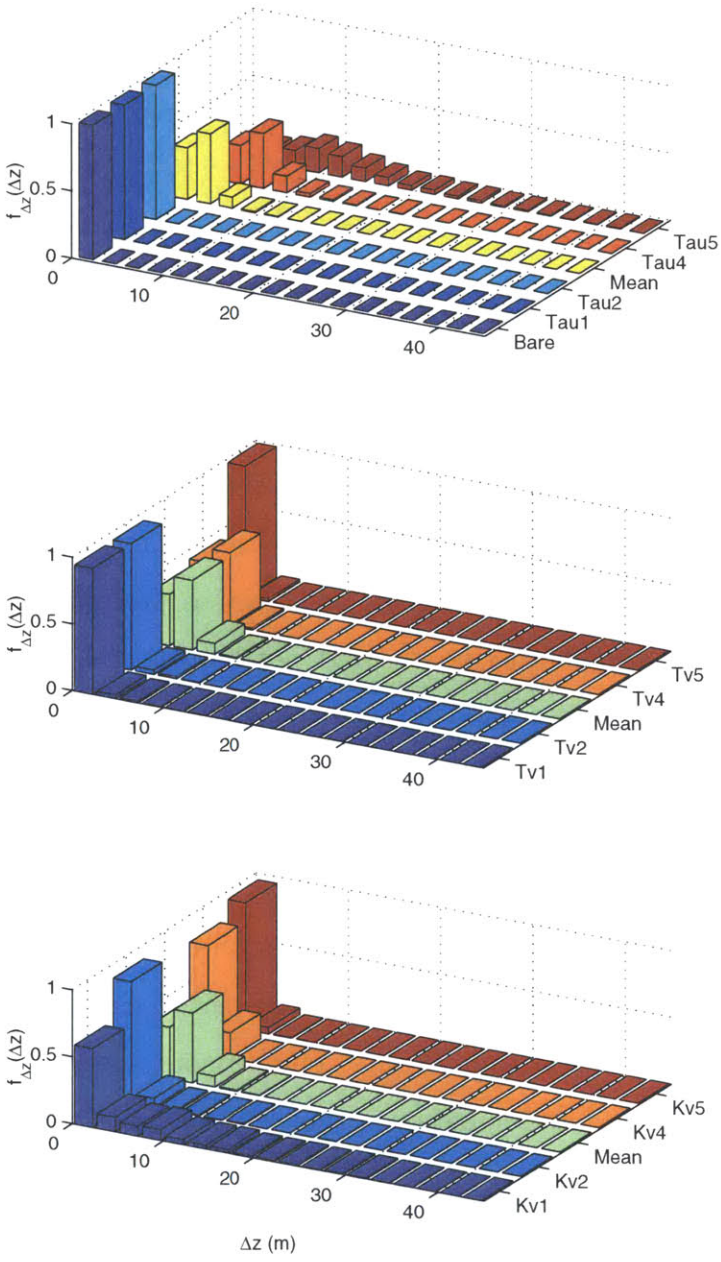

Figure 6-7: Distribution of individual node elevation ranges, Δz, for each simulation.

persistence to develop, where vegetated slopes may be stable for a longer time. This allows Δz, and therefore avulsions, to increase. Δz is low, and avulsions few, for *Tv1* because the rapidity with which the vegetation recovers is too high for longterm persistence in erosion to develop. For *Tv5*, Δz is low because vegetation ceases to play an important role in erosion prevention, again eliminating significant persistence, and stream capture altogether. Low K_v acts similarly to high $\tau_{c,v}$, by restricting the compound effects of erosive events. High persistence may then develop, leading to marginally higher Δz and avulsion rates.

Δz is constrained in part by the duration of the large scale oscillations. The greater the period, T, the longer the contiguous time a cell may be subject to uplift. This leads to the inequality

$$\Delta z < UT. \tag{6.3}$$

For *Tau5*, $T \sim 400,000$ years, which matches the maximum Δz of about 40 m. Thus, the longer the oscillations, the more likely stream capture becomes.

However, large Δz is not alone sufficient to precipitate stream capture. The fluctuations of neighboring nodes must not be identical - they must be eroding at different rates. With a fixed critical shear stress and a spatially uniform applied shear stress, fluvial landscapes would achieve an equilibrium state in which the entire domain is subject to the same excess shear stress during any given storm. In this study, the critical shear stress can vary spatially, allowing excess shear stress to do the same, in turn driving neighboring nodes with different erosion rates. Given that vegetation is generally bimodal, that which partitions cells between the two modes is also responsible for stream capture. Furthermore, the differential erosion rates are suggestive of cut-fill cycles, although the elevation gains come solely from uplift.

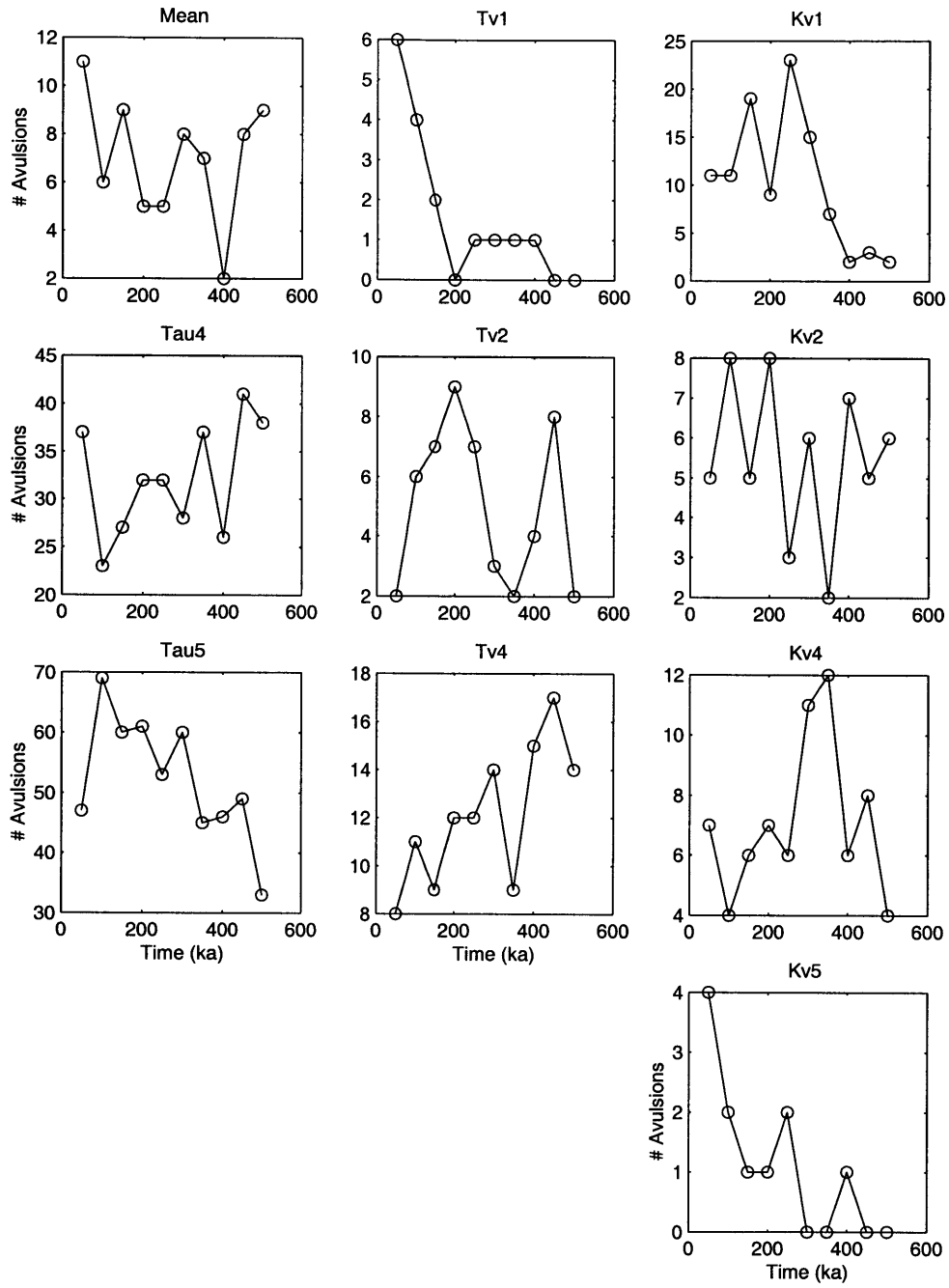

Figure 6-8: Avulsion time series at 50,000-yr resolution (*Tau1*, *Tau2* and *Tv5* exhibit constant channel positions). There is no consistent pattern among simulations. *Tv4*, *Kv1* and *Kv5* may be belatedly achieving steady state, while variability in other simulations is on the order of the actual measurements.

Table 6.1: Avulsion statistics for each 500,000 year simulation.

Simulation	Number of Avulsions	Number of Avulsed Nodes	Average Avulsions Per Node
Bare	0	0	-
Mean	70	26	2.7
Tau1	0	0	-
Tau2	0	0	-
Tau4	321	115	2.8
Tau5	523	234	2.2
Tv1	16	10	1.6
Tv2	50	21	2.4
Tv4	121	29	4.2
Tv5	0	0	-
Kv1	102	93	1.1
Kv2	55	23	2.4
Kv4	71	14	5.1
Kv5	11	11	1.0

6.3 Dynamic Biogeography and Meta-Stable Variations

The spatial mean vegetation density is calculated as

$$\bar{V} = \frac{\sum_{x,y} V(x,y)A(x,y)}{\sum_{x,y} A(x,y)}. \tag{6.4}$$

Recognizing that local vegetation is either approximately, or notably less than, unity, and that local cell areas are essentially identical, this expression simplifies to

$$\bar{V} \simeq \frac{\text{Number of well-vegetated cells}}{\text{Total number of cells}}, \tag{6.5}$$

giving a slight under-prediction. The error arises from the omission of the poorly-vegetated contribution. Meta-stable state changes are therefore changes in the areal extent of active erosion, and so the large scale trends are driven by the partitioning between vegetation modes, with the well-vegetated cells providing a lower bound for the mean density. Superposed on this is the high frequency fluctuations of the eroding, poorly-vegetated cells. These phenomena are observed in *Kv4*'s vegetation density time series (Figure 6-10), corresponding to its evolving biogeography (Figure 6-9). Other simulations show the same behavior (Figure 6-11).

As suggested by the *Kv4* vegetation density time series, lower order channels are more likely to be vegetated, although the frequencies also depend on the vegetation parameters. As vegetation importance increases, so does the number of well-vegetated cells, as well as the duration spent well-vegetated (Figure 6-12). Landscapes are therefore vegetated more often, and so erode less often, in turn causing instantaneous erosion rates to increase. For this to be possible, slopes must increase. Precisely the same conclusion was reached in Section 4.1. Figures 6-13 through 6-16 show that across all simulations, the lower order, steeper channels are those more often vegetated, although the maximum duration a cell is well-vegetated depends on the vegetation parameters. As vegetation importance increases, so do local slopes, leading

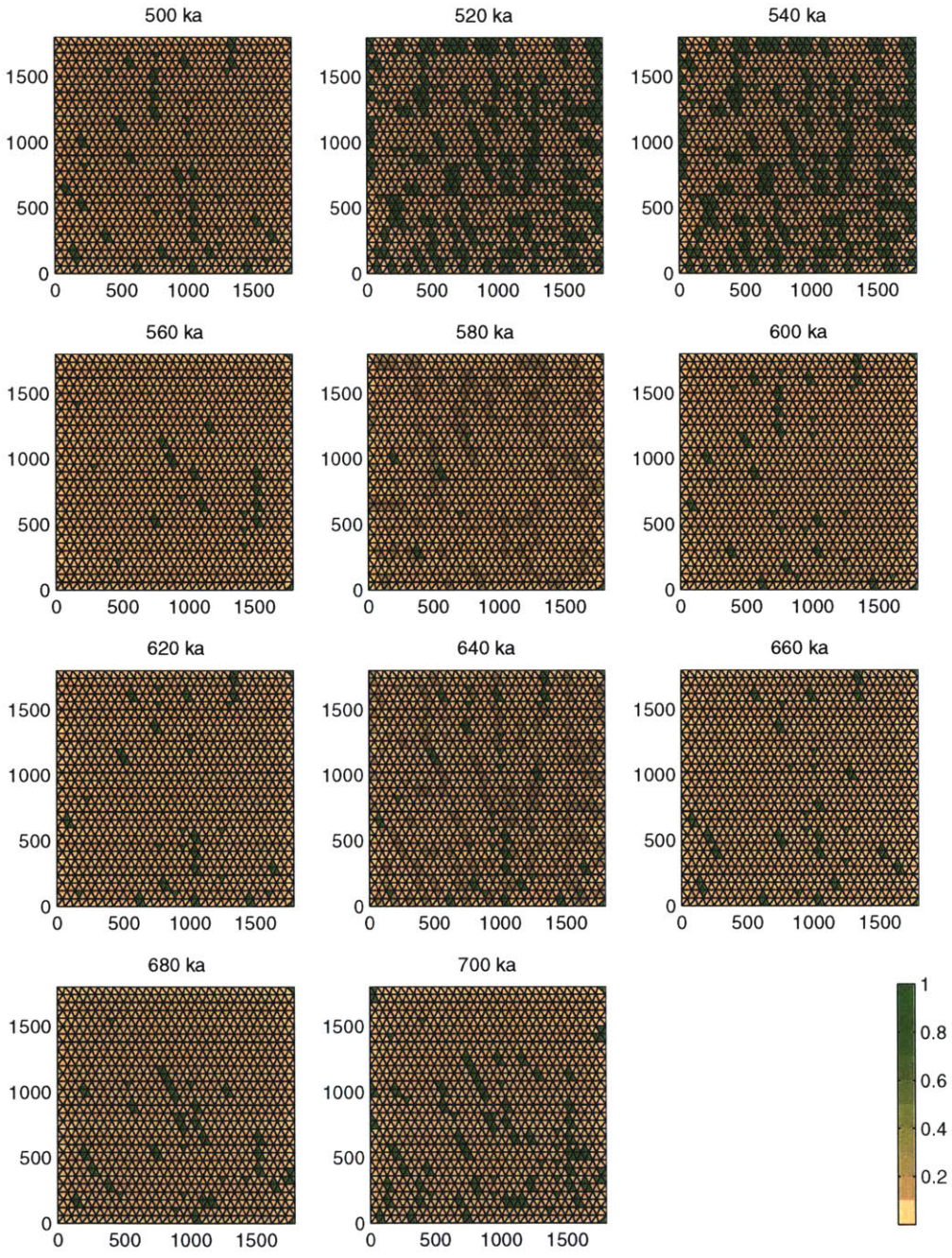

Figure 6-9: Spatial vegetation distribution at intervals of 20,000 years, for the *Kv4* simulation. There is notable re-vegetation by 520 ka, which reverts by 560 ka.

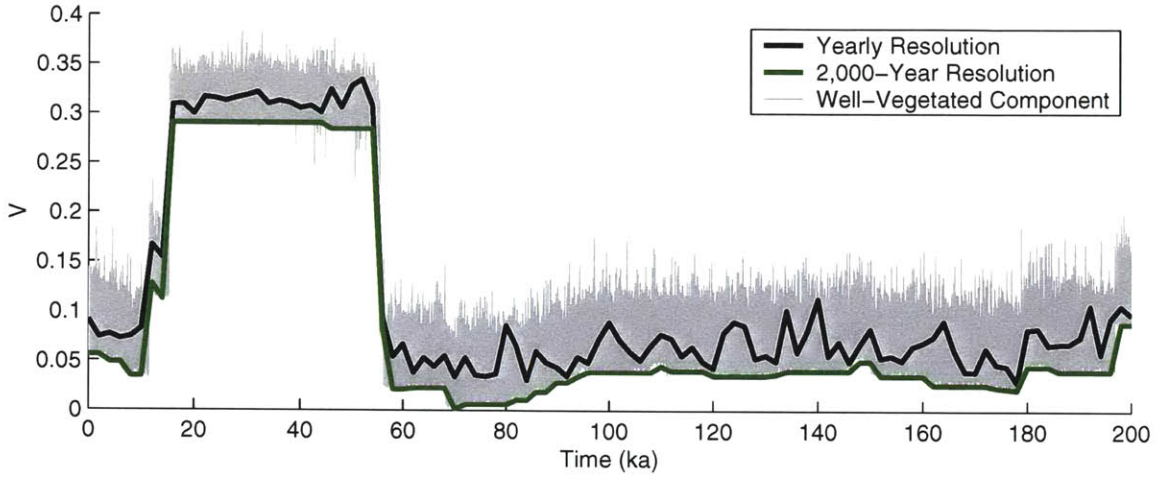

Figure 6-10: From the yearly data (gray line) the 200-yr data (black line) is extracted. The proportion of mean vegetation contributed solely from the well-vegetated cells (green line) closely tracks the total value, albeit marginally lower. It also bounds the lower range of yearly data, implying the high frequency fluctuations are due solely to poorly-vegetated cells.

to greater drainage areas being well-vegetated - a wave of dense vegetation thus descends the channels.

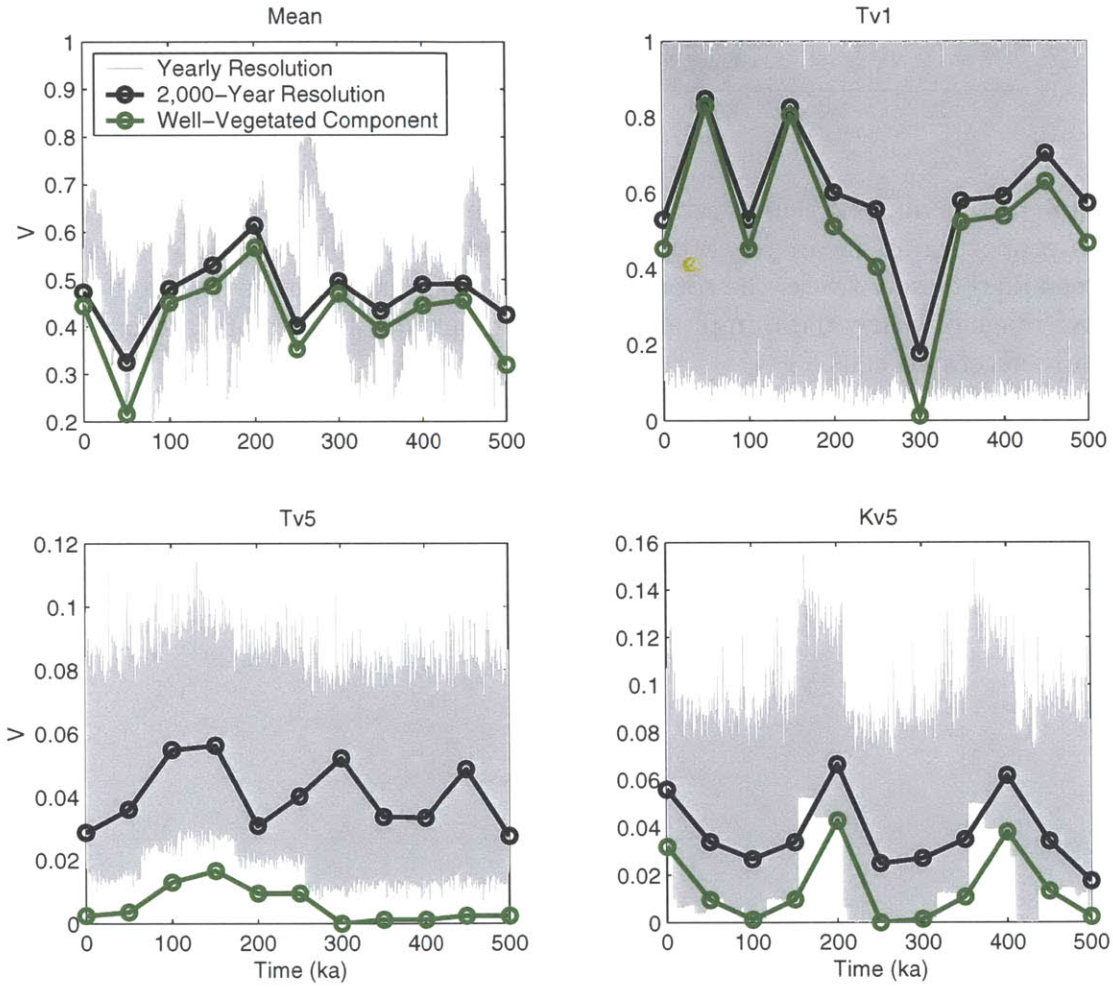

Figure 6-11: As with the last 200,000 years of *Kv4* (Figure 6-10), the proportion of total mean vegetation cover contributed solely by the well-vegetated regions (green) tracks the total value (black) for the 500,000-yr simulations of *Mean*, *Tv1*, *Tv5* and *Kv5* .

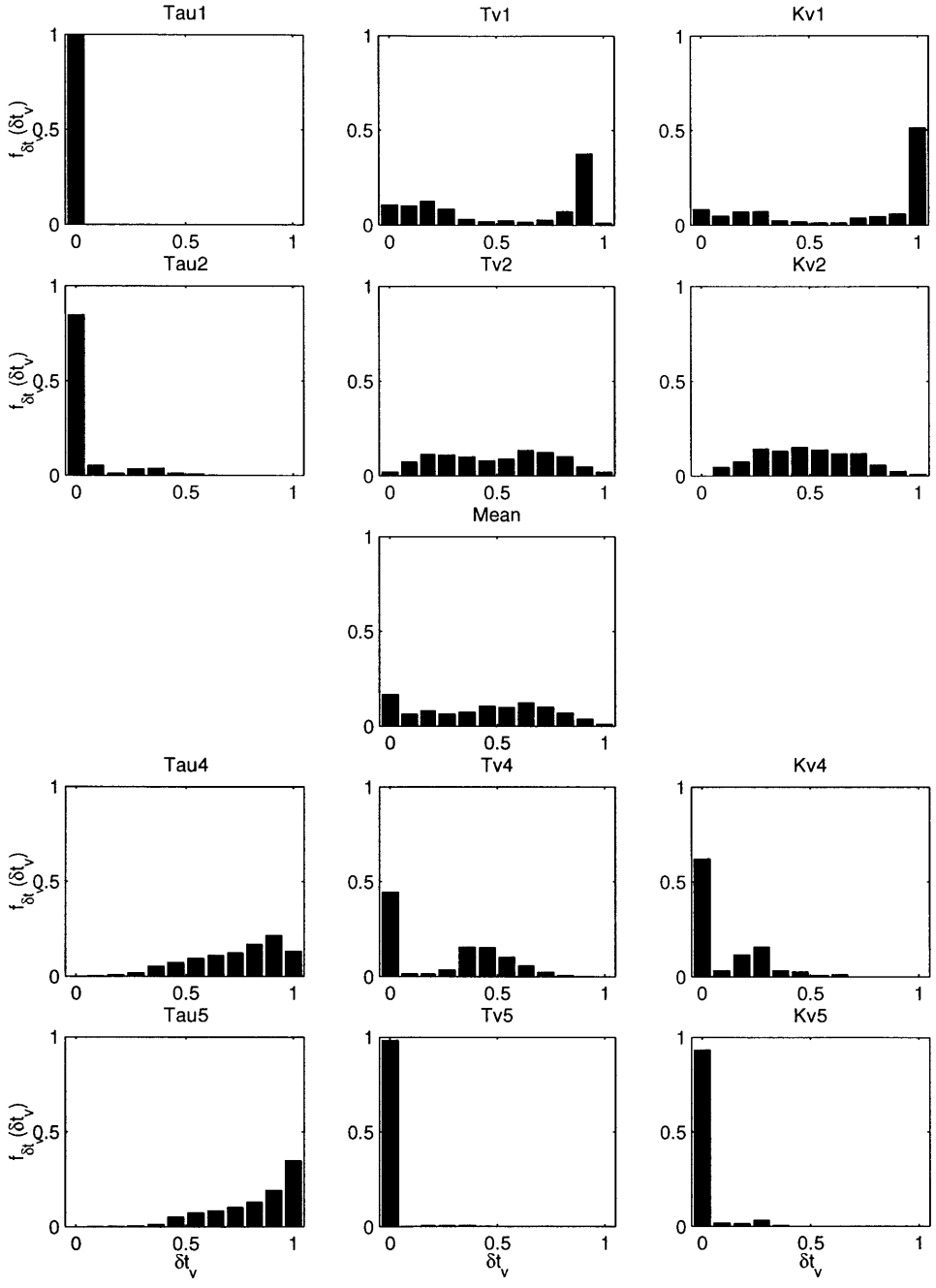

Figure 6-12: Distribution of the fraction of time, δt_v, cells are well-vegetated.

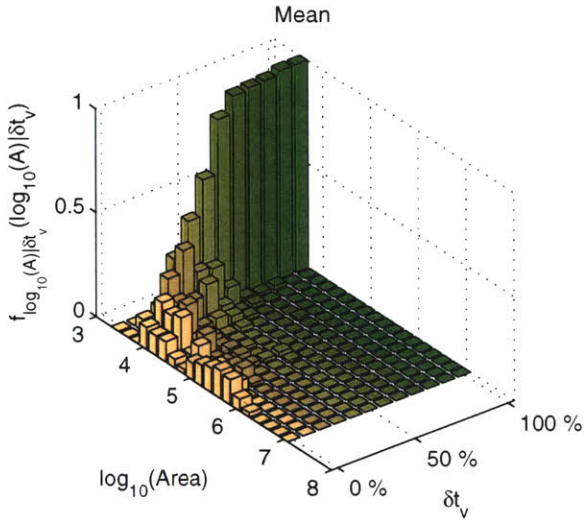

Figure 6-13: Conditional distribution of drainage areas ($log_{10}(A)$) associated with the duration a cell is well-vegetated (δt_V) for the *Mean* simulation. The probabilities sum to unity along the area-axis.

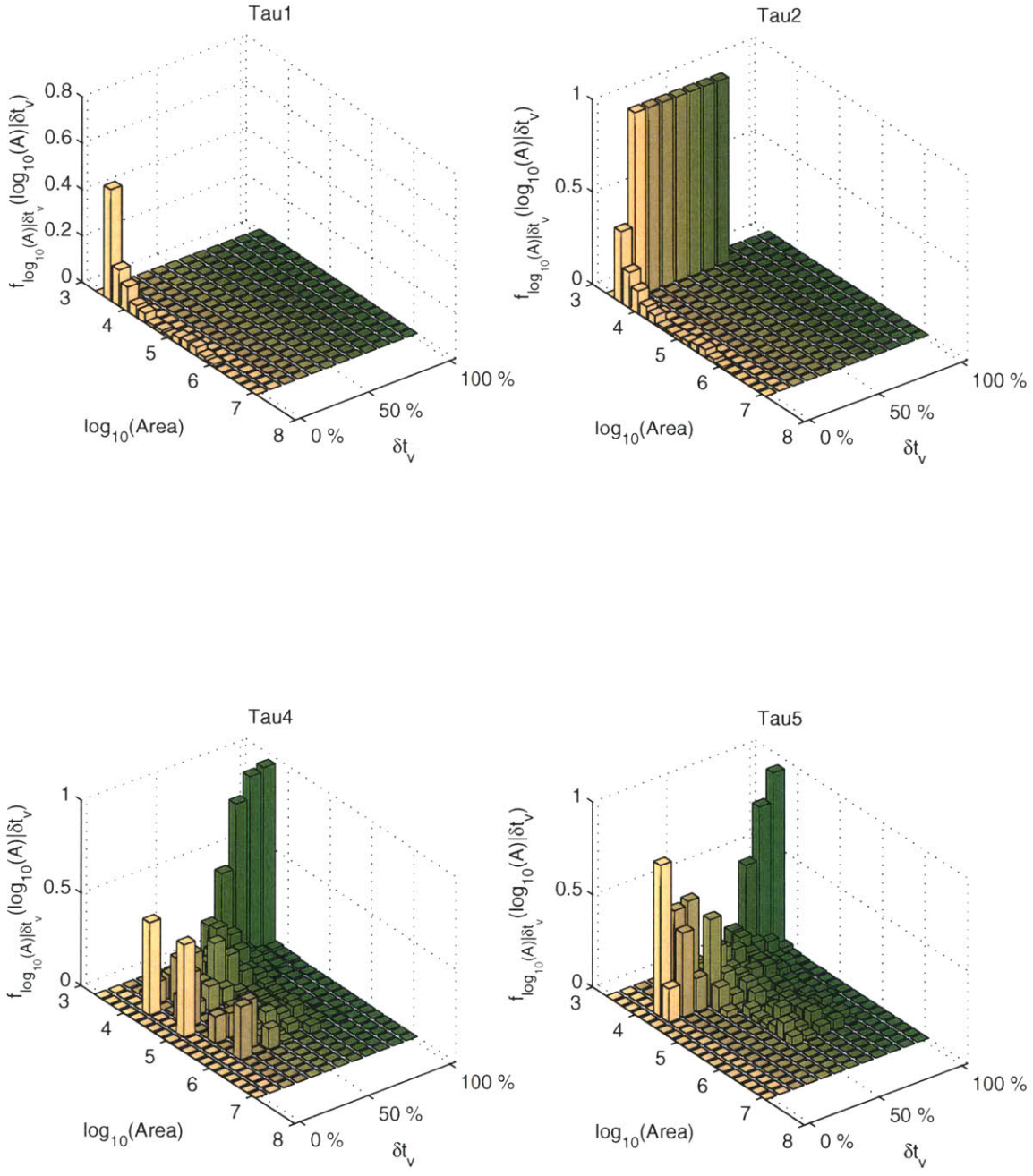

Figure 6-14: Conditional distribution of drainage areas ($log_{10}(A)$) associated with the duration a cell is well-vegetated (δt_V) for the *Tau* simulations. The probabilities sum to unity along the area-axis.

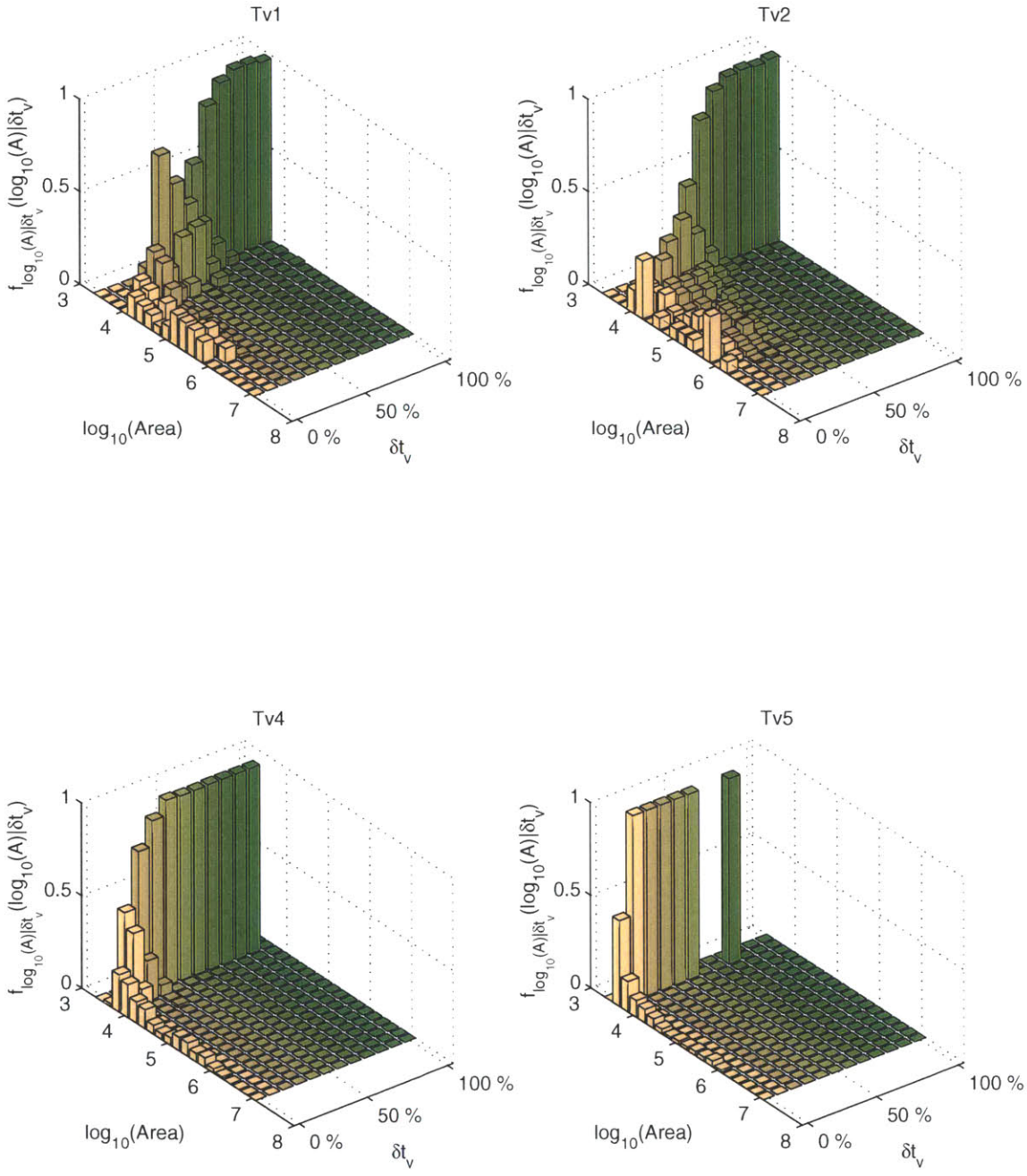

Figure 6-15: Conditional distribution of drainage areas ($log_{10}(A)$) associated with the duration a cell is well-vegetated (δt_V) for the Tv simulations. The probabilities sum to unity along the area-axis.

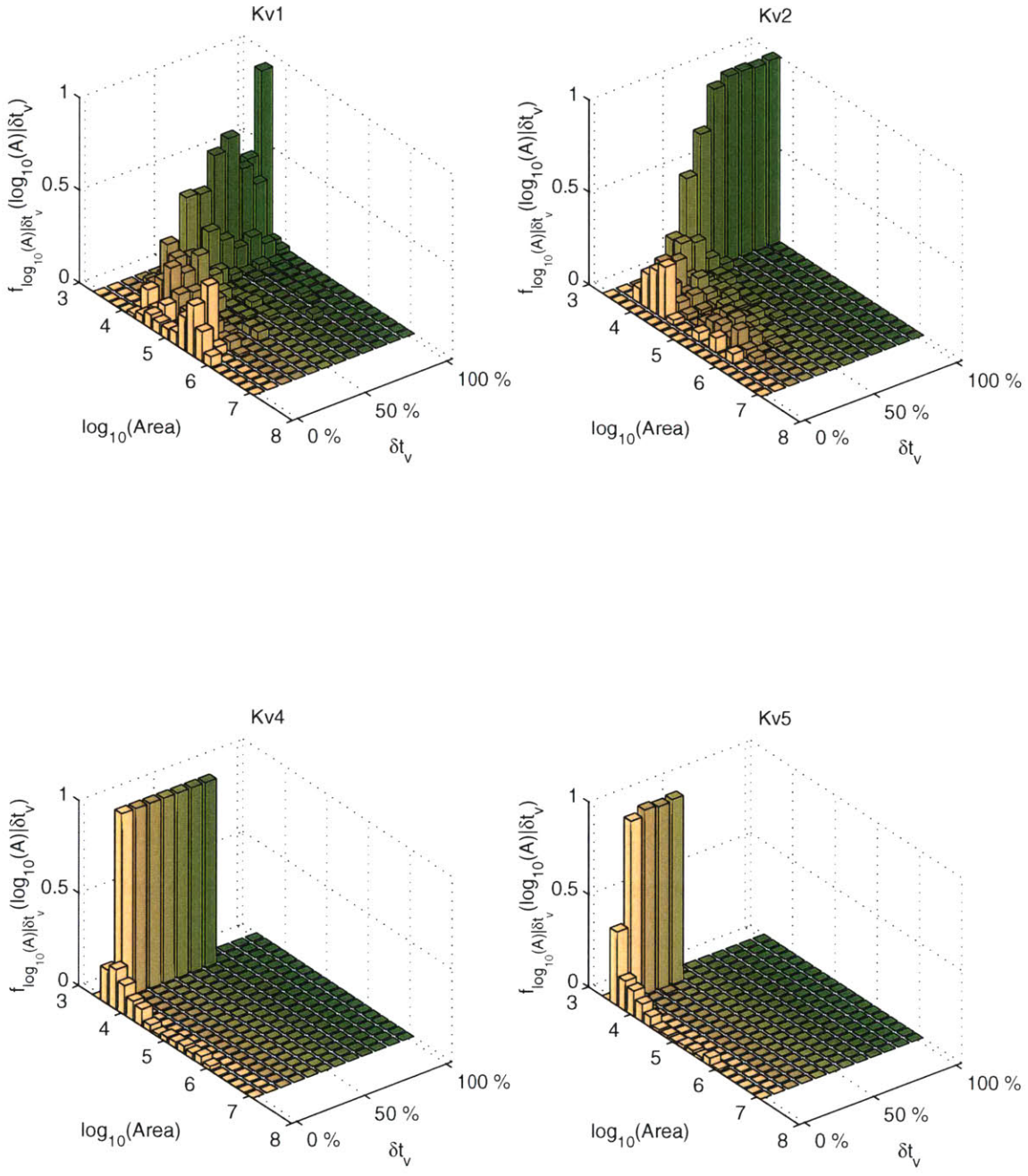

Figure 6-16: Conditional distribution of drainage areas ($log_{10}(A)$) associated with the duration a cell is well-vegetated (δt_V) for the Kv simulations. The probabilities sum to unity along the area-axis.

6.4 Vegetation-Slope-Area Relationship

The variation of node states over 500,000 years covers a wider range of values than a single instant in time. The vegetation-slope-area relationship first raised in chapter 4 is now better clarified, using four simulations as examples (*Mean*, *Tau5*, *Tv1* and *Kv1*). The original trends are preserved, but in addition, identical time-slices are seen as horizontal bands of data points, most apparent for low vegetation density. These bands move vertically in relative synchrony, implying actively eroding regions respond identically, and only, to the prevailing rainfall intensities. This is supported by the similarity between the series of maxima and minima for individual node vegetation series for *Kv4* (raised in Section 6.1). The cause(s) of the V-S-A trends remain the subject of conjecture however, although they are intriguing enough to warrant their inclusion in this thesis. Do low slopes at small drainage areas lead to re-vegetation, which subsequently increases the local slopes? Do individual nodes move about the state space, and if so, do they move in cycles or to and fro along iso-area contours? Is the absence of data in intermediate vegetation densities a result of a hysteretic cusp catastrophe?

Adding the temporal component to the V-S-A relationship highlight an important feature — as cells evolve, iso-area contours move vertically and in synchrony. The degree of variation of V with S for each iso-area contour depends on the vegetation parameters. *Tv1*'s contours are essentially univalued for S, thus V and S are unrelated for a given drainage area. *Mean* shows a wider spread for both states, and the poorly-vegetated states of *Tau5* are less distinct than in other simulations, nor its vegetation density as variable.

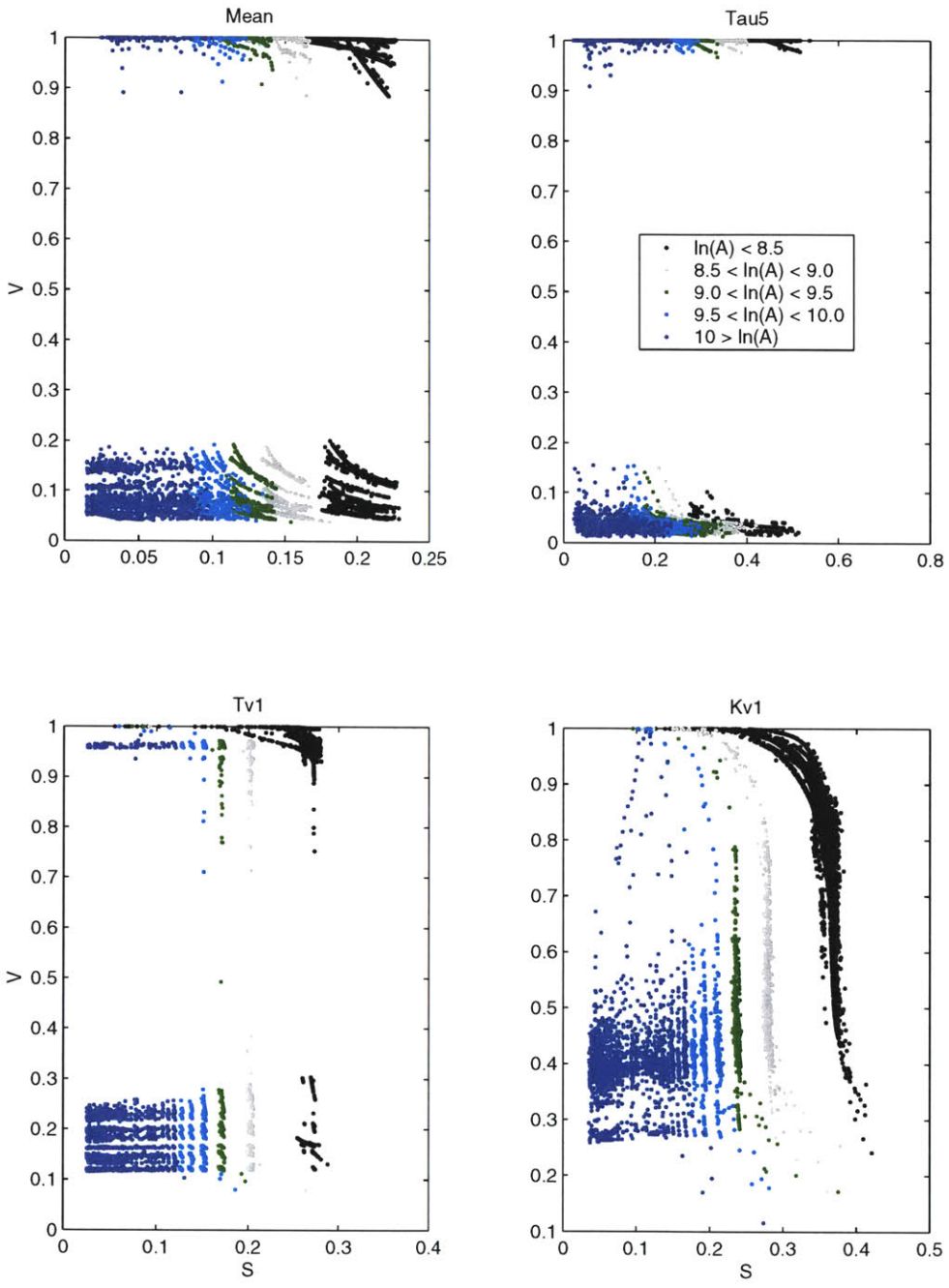

Figure 6-17: V-S-A relationships for four simulations through time. The bands of like area move vertically in synchrony, and possess different profiles depending on the nature of the vegetation.

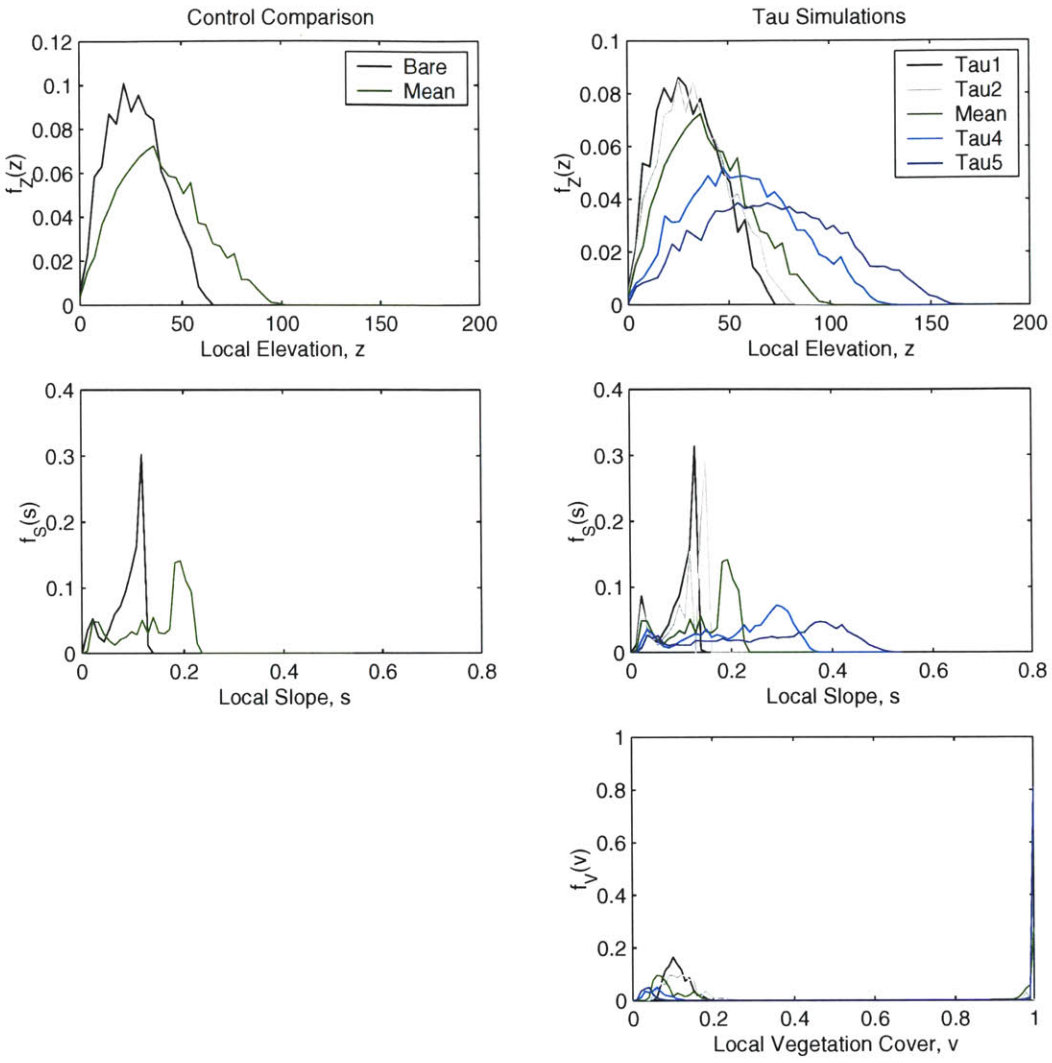

Figure 6-18: PDFs of elevation (z), slope (s) and vegetation density (v) for the control (*Bare* and *Mean*) and *Tau* simulations.

6.5 Complete Statistics

With changing biophysiographic indices, the complete spatial data for each of the 11 time-slices for each simulation are recorded (Figures 6-18 through 6-22). This is done more for completeness' sake than to obtain more insight, as the distributions of z, S and V are to all intents and purposes the same as for purely spatial biophysiography (Figures 4-5 through 4-9).

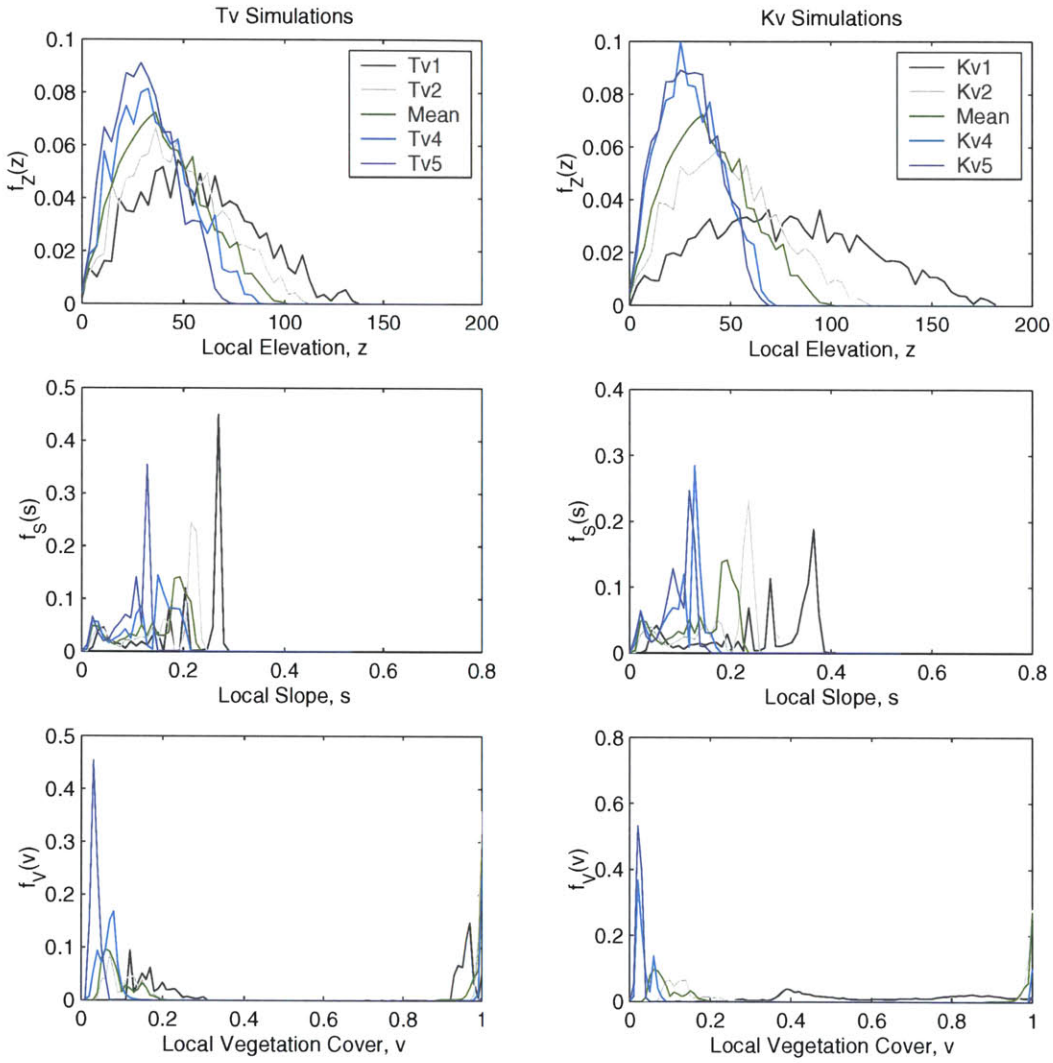

Figure 6-19: PDFs of elevation (z), slope (s) and vegetation density (v) for the Tv and Kv simulations.

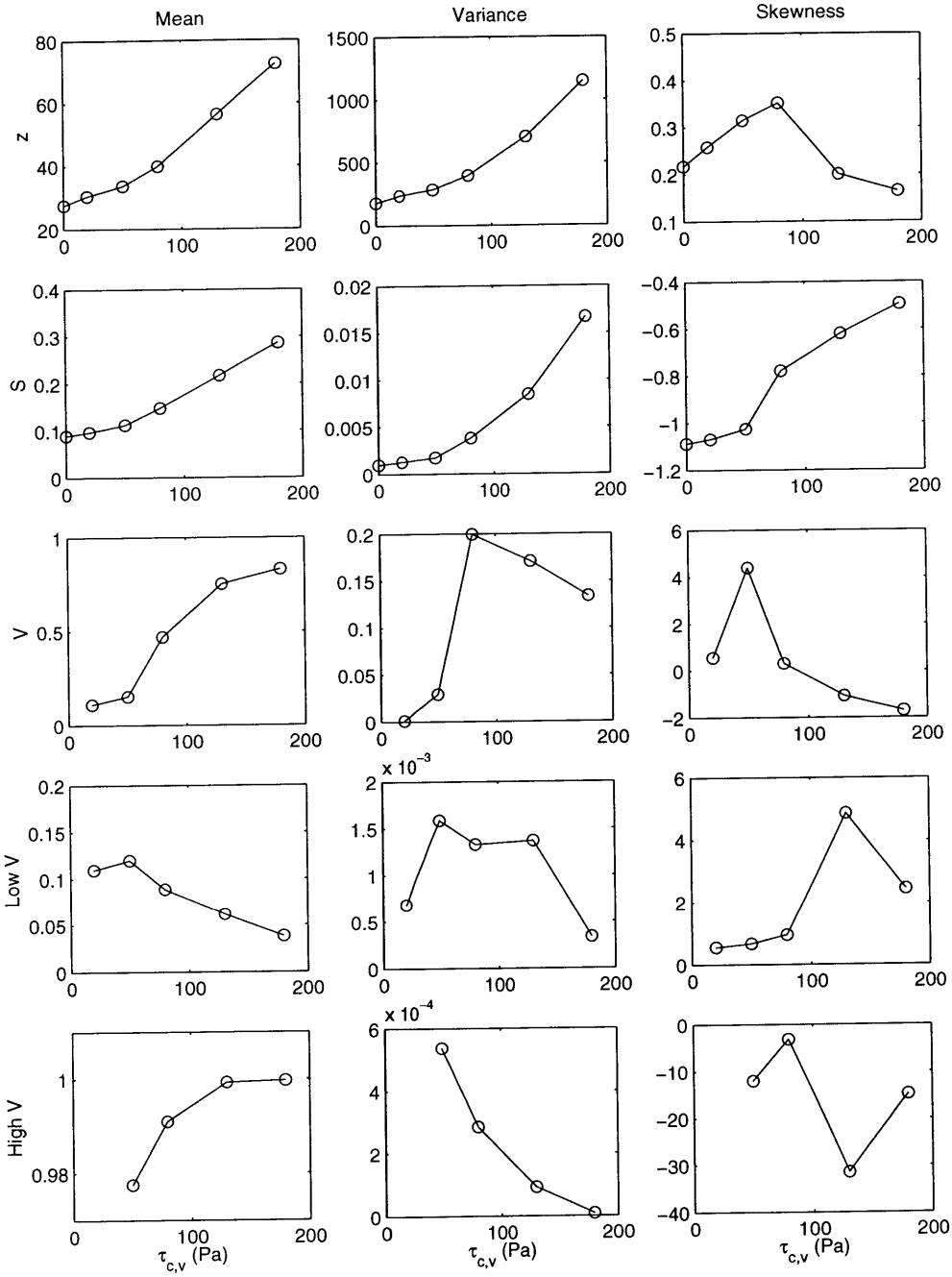

Figure 6-20: Trends in biophysiographic statistics with increasing $\tau_{c,v}$.

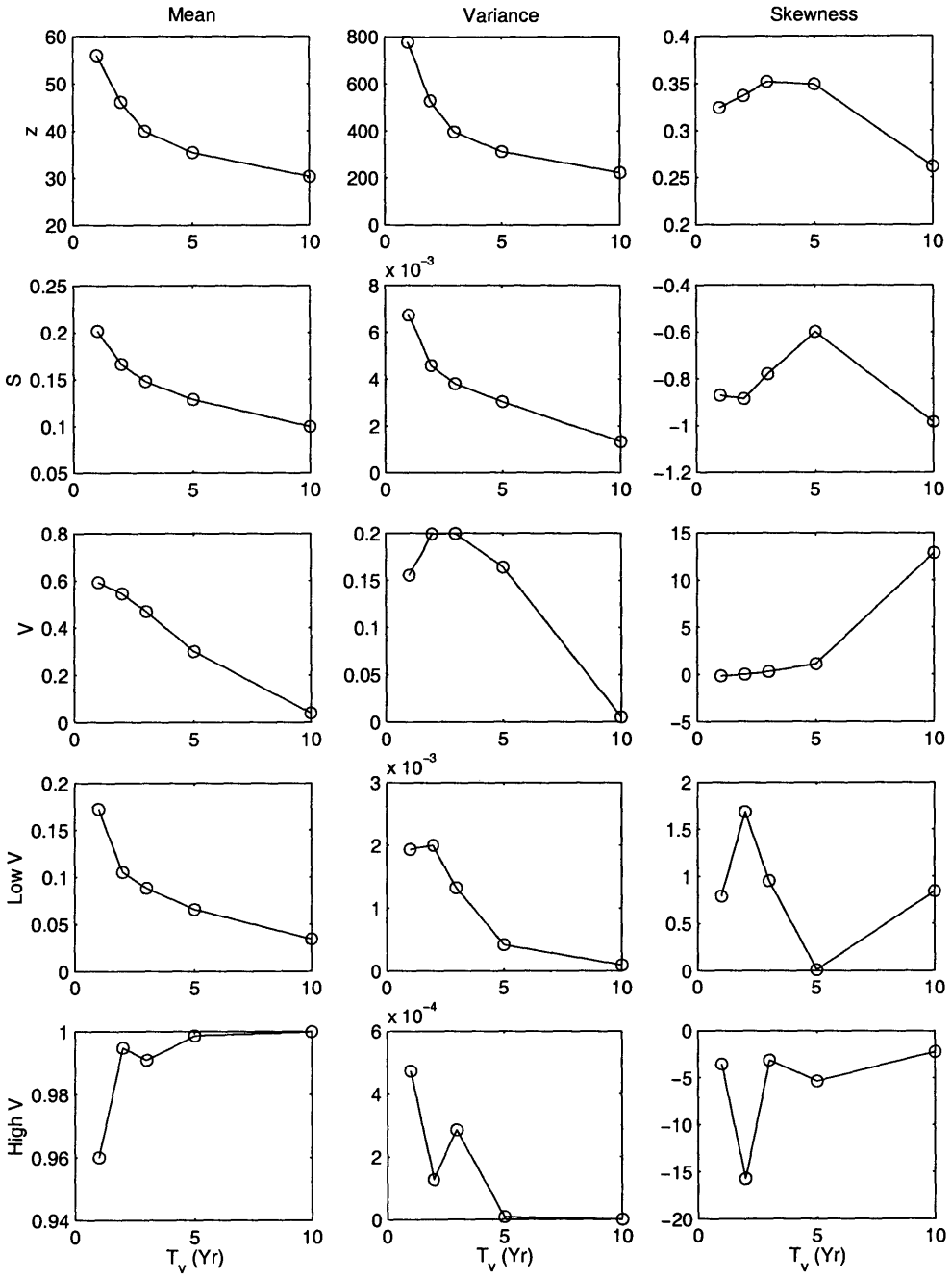

Figure 6-21: Trends in biophysiographic statistics with increasing T_v.

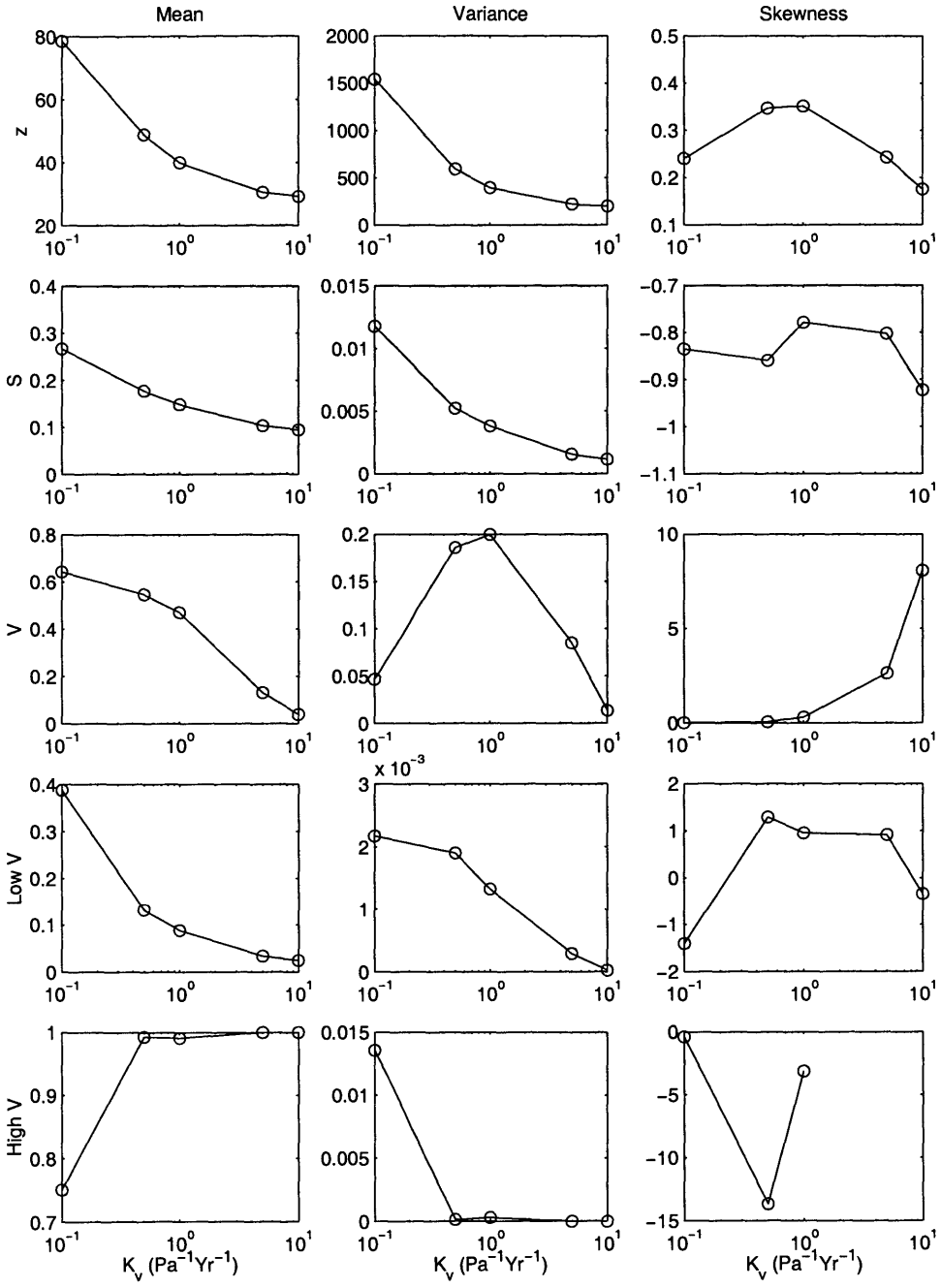

Figure 6-22: Trends in biophysiographic statistics with increasing K_v.

6.6 Summary

1. The drainage networks are not static. Spatially variable critical shear stress leads to spatially variable excess shear stress and erosion rates, allowing first order channels to avulse. This is contingent on a high range of local elevations, which depends on the vegetation properties.

2. Since vegetation states are generally bimodal, the areal extent of active erosion is proportional to the spatial mean vegetation density. Changes between metastable states are therefore changes in the number of eroding cells, indicating that the process that determines the vegetation mode partitioning is responsible for the large-scale fluctuations.

3. As more cells become well-vegetated, fewer are subject to the whims of the stochastic storms, hence vegetation and erosion variability drops as mean vegetation climbs, explaining the observation in Chapter 5.

4. As with avulsions, sites of frequent dense plant cover are the lower order channels, although the distribution is modified by the vegetation properties.

5. Addition of the temporal component to the V-S-A plots shows that poorly-vegetated cells behave synchronously, although the relationship remains unclear.

6. Biophysiographic distributions and statistic trends are essentially identical to those reported for the single, static landscapes in Chapter 4, despite the obvious temporal fluctuations permeating most of the simulations.

Chapter 7

Conclusions

Sensitivity analysis has shown that a landscape's dynamic biophysiography depends on the nature of the vegetation dynamics and coupling, sometimes significantly so. At one extreme of the each parameter's range the landscape resembles a purely abiotic scenario. The other extreme produces distinctly different behavior and morphology. These geomorphically important parameter values are high $\tau_{c,v}$, and low T_v and K_v, although each has its own idiosyncrasies.

Geomorphically important vegetation makes elevations higher, slopes steeper, vegetation more widespread, and may induce large-scale oscillations. These results are innately interwoven. The presence of local vegetation allows slopes to become steeper, which, when they erode, erode faster. This gives more opportunity for vegetation to colonize, as less time is spent eroding in order to maintain equilibrium, thus steeper slopes will support more flourishing flora. This positive feedback relies on cells becoming well-vegetated for at least an instant of time. The calm between the storms, and the production of storms too weak to erode provide the opportunities for the establishment of vegetation. What prevents eternal vegetation cover, and an uneroding landscape, are the highly erosive storms and the non-zero time it takes for disturbed vegetation to recover. Each vegetation parameter has particular mechanisms for achieving these results. High vegetative critical shear stress does so by making regions harder to erode. The time-scale of re-growth changes the recovery time so that more or fewer storms are able to erode. Lastly, vegetation erodibility determines

the extent to which a series of storms may remove plant cover. In this way, low K_v reduces the differential effect storms have on vegetation, smoothing the evolution, and low T_v severs the long-term connection of erosive events. Both of these eliminate long-term persistence, and with it, large-scale oscillations.

The distribution of vegetation states is never uniform, but instead generally bimodal. Regions are either well- or poorly-vegetated, and only the latter are actively eroding. The steeper areas are more often vegetated. This bimodal result may be derived analytically, showing that each region has two locally-stable vegetation states. Transitions from the poor- to the well-vegetated condition requires a sufficiently long period of low intensity storms, while the reverse requires the storms' intensities to be sufficiently high. The global erosion rate is thus dependent on the areal extent of the near-bare ground cover - the partitioning between the two vegetation states. As a result, evolution of landscapes dominated by vegetation proceeds in a punctuated equilibrium fashion. Mean vegetation cover is roughly constant for a time, as is the erosion rate, but as the the number of eroding cells suddenly changes, both vegetation density and erosion rates change. In the long-term, these step changes constitute periodic or aperiodic oscillations, which has implications for pollen-based paleoclimate estimates. Simulations whose net erosion time-scale is shorter than that of net uplift produce aperiodic fluctuations in mean elevation, erosion rate and vegetation density, while a net uplift time-scale less than or equal to that of net erosion produces periodic behavior. The aperiodicity must stem from the stochasticity of the storm events; the periodicity from the steadiness of the uplift, and occur for low-mean values of $\tau_{c,v}$, and mean-high values of both T_v and K_v. Transitions from periodic to aperiodic behavior, or vice versa, are therefore expected with climatic or tectonic changes.

Further analysis of the governing equations leads to an approximate relation between the mean global vegetation density and the centennial erosion rate. This may be extended further to predict the long-term mean vegetation density, although the accuracy is poor for landscape not dominated by vegetation. This has implications for assessing the degree of disequilibrium of these landforms. Also important is that, despite subject to a stationary climate, vegetation cover changes. This may have

bearing on paleoclimate estimates based on pollen counts, although the time-scales considered in this study are likely too long, and may be drowned out by species migration, if not speciation.

On close inspection, the large-scale fluctuations are not mimicked by the entire domain in concert. Different nodes behave differently, and only a small subset of nodes appears to dominate the regional dynamics, although the criterion for this behavior is poorly understood. One consequence, however, is that if neighboring nodes are sufficiently out of harmony, drainage directions will change. This usually occurs for first order channels. The frequency of stream capture depends on the nature of the vegetation properties. Dynamic stream capture is a novel feature of numerical landscape evolution models, arising from the potential for excess critical shear stress to vary spatially.

Not visible in the DEM, but inferable from the vegetation maps, is that during periods of lower erosion rates, incising channels are shorter. As mean erosion increases, so does channel extent. If diffusion were modeled more accurately, and depositional processes considered, these channel changes would look like cut-fill cycles. Instead of climate or land-use change being necessary to induce changes in the erosion regime, it is merely the internal dynamics of the erosion-vegetation coupling which causes these oscillations. This feeds back to the biogeography, more significant if multiple species are considered.

It is thus demonstrated that incorporating even a modest model of vegetation-erosion coupling and dynamics yields a diverse array of biophysiographic behavior. It may be debated whether the model is sufficiently relevant or accurate, specifically the component representing plant death. The model may only apply to humid environments, where water does not dictate plant growth or death. In semi-arid regions, plants tend to accumulate in zones of topographic convergence, attracted by the water, but the results put forward here show repulsion of vegetation from such areas. Nor is the model applicable to steep forested terrain, in which mass wasting drives much of the landscape evolution, as landsliding is not being modeled.

Despite these shortcomings, the proof of concept provides a platform to further

develop regional eco-geomorphic models. Amending the water-independent plant dynamics and mass wasting issues are prime candidates, allowing improved modeling of the geomorphic response to climate change. Also useful is the introduction of multiple species, allowing one to assess the consequences of geomorphic disturbances on biodiversity. Multiple species may also favor cyclic erosional behavior, and would require consideration of resource competition. Extrapolating these principles to the channel scale, the numerous models of vegetation-channel coupling would no doubt benefit from the inclusion of vegetation dynamics.

Chapter 8

References

Abrahams, A.D., Parsons, A.J. and Wainwright, J. 1995. Effects of vegetation change on interrill runoff and erosion, Walnut Gulch, Southern Arizona. Geomorphology, 13: 37-48.

Adams, J.A. and Norton, D.A. 1991. Soil and vegetation characteristics of some tree windthrow features in a South Westland rimu forest. J. Royal Soc. NZ, 21(1): 33-42.

Ahnert, F. 1976. Brief description of a comprehensive three-dimensional process-response model of landform development. Zeit. Geomorph. Suppl., 25: 24-49.

Aldridge, R. and Jackson, R.J. 1968. Interception of rainfall by manuka (*Leptospermum scoparium*) at Taita, New Zealand. N.Z. J. Sci., 11: 301-317.

Anderson, R.S. 1994. Evolution of the Santa Cruz Mountains, California, through tectonic growth and geomorphic decay. J. Geophys. Res., 99: 20,161-20,179.

Angers, D.A. and Caron, J. 1998. Plant-induced changes in soil structure: processes and feedbacks. Biogeochem., 42: 55-72.

Battany, M.C. and Grismer, M.E. 2000. Rainfall runoff and erosion in Napa Valley vineyards: effects of slope, cover and surface roughness. Hydrol. Proc., 14: 1289-1304.

Beatty, S. W. 1984. Influence of microtopography and canopy species on spatial patterns of forest understory plants. Ecology 65: 1406-1419.

Beaumont, C., Fullsack, P. and Hamilton, J. 1992. Erosional control of active compressional orogens. In Thrust Tectonics, K.R. McClay ed. Chapman Hall, New York. pp 1-18.

Beven, K. and Germann, P. 1982. Macropores and water flow in soils. Water Resour. Res., 18(5): 1311-1325.

Beven, K.J. and Kirkby, M.J. 1979. A physically based, variable contributing area model of basin hydrology. Hydrol. Sci. Bull., 24: 43-69.

Biddle, P.G. 1983. Patterns of soil drying and moisture deficit in the vicinity of trees on clay soils. Geotechnique, 33(2): 107-126.

Bormann, B.T., Spaltenstein, H., McClellan, M.H., Ugolini, F.C., Cromack, K., Jr. and Nay, M. 1995. Rapid soil development after windthrow disturbance in pristine forests. J. Ecology, 83: 747-757.

Braun, J., Heimsath, A.M. and Chappell, J. 2001. Sediment transport mechanisms on soil-mantled hillslopes. Geology, 29(8): 683-686.

Brenner, R.P. 1973. A hydrological model study of a forested and a cutover slope. Hydrol. Sci. Bull., 18(26): 124-144.

Bull, W.B. 1979. Threshold of critical power in streams. Geol. Soc. Am. Bull., 90: 453-464.

Burch, G.J., Bath, R.K., Moore, I.D. and O'Loughlin, E.M. 1987. Comparative hydrological behaviour of forested and cleared catchments in Southeastern Australia, J. Hydro., 90: 19-42.

Burnett, M.R., August, P.V., Brown, J.H. and Killingbeck, K.T. 1998. The influence

of geomorphological heterogeneity on biodiversity: 1. a patch-scale perspective. Cons. Bio., 12(2): 363-370.

Chow, V.T. 1959. Open Channel Hydraulics. McGrawHill, New York. pp 680.

Clark, J.J. and Wilcock, P.R. 2000. Effects of land-use change on channel morphology in northeastern Puerto Rico. GAS Bull., 112(12): 1763-1777.

Coppin, N.J. and Richards, I.G. 1990. Use of Vegetation in Civil Engineering. C.I.R.I.A. Burrerworths: London. pp 292.

Cotton, C.A. 1922. Geomorphology of New Zealand, Part 1: Systematic. Wellington, Dominion Museum. pp 462.

Coulthard, T.J., Kirkby, M.J. and Macklin, M.G. 2000. Modelling geomorphic response to environmental change in an upland catchment. Hydrol. Proc., 14: 2031-2045.

Culling, W.E.H. 1960. Analytical theory of erosion. J. Geology, 68: 336-344.

DeRose, R.C., Gomez, B., Marden, M., and Trustrum, N.A. 1998. Gully erosion in Mangatu Forest, New Zealand, estimated from digital elevation models. Earth Surf. Proc. and Land., 23: 1045-1053.

Douglas, I. 1967. Man, vegetation and the sediment yields of rivers. Nature, 215: 925-928.

Dunne, T., Zhang, W. and Aubry, B.F. 1991. Effects of rainfall, vegetation, and microtopography on infiltration and runoff. Water Resour. Res., 27(9): 2271-2285.

Eagleson, P.S. 1978. Climate, soil, and vegetation: 2. the distribution of annual precipitation derived from observed storm sequences. Water Resour. Res., 14: 713-721.

Einstein, H.A. 1950. The bedload function for sediment transportation in open chan-

nel flows. Soil Conservation Service US Department of Agriculture Technical Bulletin, No. 1026, 78pp.

Elliott, W.J., Liebenow, A.M., Laflen, J.M. and Kohl, K.D. 1989. NSERL Report No. 3, USDA-ARS National Soil Erosion Research Lab, West Lafayette, IN.

Evans, K.G. and Willgoose, G.R. 2000. Post-mining landform evolution modelling: 2. effects of vegetation and surface ripping. Earth Surf. Proc. Land., 25: 803-823.

Favis-Mortlock, D.T., Boradman, J., Parsons, A. and Lascelles, B. 2000. Emergence and erosion: a model for rill initiation and development. Hydrol. Proc., 14: 2173-2205.

Federer, C.A. 1973. Forest transpiration greatly speeds streamflow recession. Water Resour. Res., 9(6): 1599-1604.

Fitzpatrick, E.A. 1980. Soils: Their Formation, Classification and Distribution. Longman Group Ltd, London. pp 353.

Fitzpatrick, F.A. and Knox, J.C. 2000. Spatial and temporal sensitivity of hydrogeomorphic response and recovery to deforestation, agriculture, and floods. Phys. Geog., 21(2): 89-108.

Flanagan, D.C. and Nearing, M.A. (eds.) 1995. USDA - Water Erosion Prediction Project (WEPP). National Soil Erosion Research Laboratory Report No. 10.

Geddes, N. and Dunkerley, D. 1999. The influence of organic litter in the erosive effects of raindrops and of gravity drops released from desert shrubs. Catena, 36: 303-313.

Graf, W.L. 1979. The development of montane arroyos and gullies. Earth Surf. Proc., 4: 1-14.

Greenway, D.R. 1987. Vegetation and slope stability. In Slope Stability, M.G. An-

derson and K.S. Richards, eds. John Wiley and Sons Ltd. Wiley, Chichester. pp 187-230.

Gregory, K.J. and Walling, D.E. 1973. Drainage Basin Form and Process, Geomorphological Approach. John Wiley, New York. pp 456.

Hagberg, T.D. 1995. Relationships between hydrology, vegetation and gullies in montane meadows of the Sierra Nevada. MS thesis, Humboldt State University.

Horton, R.E., 1945. Erosional development of streams and their drainage basins; hydrophysical approach to quantitative morphology. Geo. Soc. of Am. Bull., 56: 275- 370.

Howard, A.D. 1994. A detachment-limited model of drainage basin evolution. Water Resour. Res., 30(7): 2261-2285.

Howard, A.D. 1995. Simulation modeling and statistical classification of escarpment planforms. Geomorphology, 12: 187-214.

Howard, A.D. 1997. Badland morphology and evolution: interpretation using a simulation model. Earth Surf. Proc. Land., 22: 211-227.

Howard, A.D. 1999. Simulation of gully erosion and bistable landforms. In Incised River Channels, S. Darby and A. Simon eds. John Wiley and Sons. pp 277-300.

Howard, A.D., Dietrich, W.E. and Seidl, M.A. 1994. Modeling fluvial erosion on regional to continental scales. J. Geophys. Res., 99(B7): 13,971-13,986.

Hupp, C.R. 1986. The headwater extent of fluvial landforms and associated vegetation of Massanutten Mountain, Virginia. Earth SUrf. Proc. and Land., 11: 545-555.

Hupp, C.R. 1999. Relations among riparian vegetation, channel incision processes and forms, and large woody debris. In Incised River Channels: Processes, Forms, Engineering and Management, S. Darby and A. Simon, eds., John Wiley and Sons

Ltd., pp 221-245.

Jakob, M. 2000. The impacts of logging on landslide activity at Clayoquot Sound, British Columbia. Catena, 38: 279-300.

Kelly, EF, Chadwick, OA, and Hilinski, T. 1998. The effect of plants on mineral weathering. Biogeochem., 42: 21-53.

Kirkby, M. 1995. Modelling the links between vegetation and landforms. Geomorphology, 13: 319-335.

Kooi, H. and Beaumont, C. 1994. Escarpment evolution on high-elevation rifted margins: Insights derived from a surface processes model that combines diffusion, advection, and reaction. J. Geophys. Res., 99(B6): 12,191-12,209.

Koons, P.O. 1989. The topographic evolution of collisional mountain belts: a numerical look at the Southern Alps, New Zealand. Am. J. Sci., 289: 1041-1069.

Kosmas, C., Danalatos, N., Cammeraat, L.H., Chabart, M., Diamantopoulos, J., Farand, R., Gutierrez, L., Jacob, A., Marques, H., Martinez-Fernandez, J., Mizara, A., Moustakas, N., Nicolau, J.M. Oliveros, C., Pinna, G., Puddu, R., Puigdefabregas, J., Roxo, M., Simao, A., Stamou, G., Tomasi, N., Usai, D. and Vacca, A. 1997. The effect of land use on runoff and soil erosion rates under Mediterranean conditions. Catena 29: 45-59.

Kulbeth, J. 2000. Personal communication, March 2000.

Laffan, M.D. 1979. Slope stability in the Charleston-Punakaiki region, South Island, New Zealand. 1. Landslide potential. NZ J. Sci., 22: 183-192.

Lancaster, S.T. 1998. A nonlinear river meandering model and its incorporation in a landscape evolution model. PhD Thesis, Massachusetts Institute of Technology.

Lancaster, S.T., Hayes, S.K. and Grant, G.E. 2001. Modeling sediment and wood

storage and dynamics in small mountainous watersheds. In Geomorphic Processes and Riverine Habitat, J.M. Dorava, D.R. Montgomery, B.B. Palcsak and F.A. Fitzpatrick eds. American Geophysical Union, Washington. pp 85-102.

Langbein, W.B. and Schumm, S.A. 1958. Yield of sediment in relation to mean annual precipitation. Trans. Am. Geophys. Union, 39(6): 1076-1084.

Lee, R. 1980. Forest Hydrology. Cambridge University Press, Ney York. pp 349.

Lucas, Y. 2001. The role of plants in controlling rates and products of weathering: importance of biological pumping. Annu. Rev. Earth Planet. Sci., 29: 135-163.

Luo, W. 2001. LANDSAP: a coupled surface and subsurface cellular automata model for landform simulation. Comp. and Geosci., 27: 363-367.

Lyell, C.H. 1834. Principles of Geology: Being an Attempt to Explain the Former Changes of the Earth's Surface by References to Causes Now in Operation. v.3, 3e. John Murray, London.

Melton, M.A. 1958. Correlation structure of morphometric properties of drainage systems and their controlling agents. J. Geology, 66: 442-460.

Mitas, L. and Mitasova, H. 1998. Distributed soil erosion simulation for effective erosion prevention. Water Resour. Res., 34(3): 505-516.

Moglen, G.E. and Bras, R.L. 1995. The effect of spatial heterogeneities on geomorphic expression in a model of basin evolution. Water Resour. Res., 31(10): 2613-2623.

Moglen, G.E., Eltahir, A.B. and Bras, R.L. 1998. On the sensitivity of drainage density to climate change. Water Resour. Res., 34(4): 855-862.

Montgomery, D.R. and Dietrich W.E. 1988. Where do channels begin? Nature, 336: 232-234.

Morgan, R.P.C., Finney, H.J., Lavee, H., Merrit, E. and Noble, C.A. 1986. Plant cover

effects on hillslope runoff and erosion: evidence from two laboratory experiments. In Hillslope Processes, A.D. Abrahams, ed. Allen and Unwin. pp 77-96.

Mosley, M.P. 1982. The effect of a New Zealand beech forest canopy on the kinetic energy of water drops and on surface erosion. Earth Surf. Proc. and Land., 7: 103-107.

Nassif, S.H. and Wilson, E.M. 1975. The influence of slope and rain intensity on runoff and infiltration. Hydrol. Sci. Bull., 20: 539-533.

Newman, B.D., Campbell, A.R., Wilcox, B. 1998. Lateral subsurface flow pathways in a semiarid ponderosa pine hillslope. Water Resour. Res., 34(12): 3485-3496.

Nichols, W.F., Killingbeck, K.T. and August, P.V. 1998. The influence of geomorphological heterogeneity on biodiversity. 1. A landscape perspective. Cons. Bio., 12(2): 371-379.

Norman, S.A., Schaetzl, R.J. and Small, T.W. 1995. Effects of slope angle on mass movement by tree uprooting. Geomorphology, 14: 19-27.

Nortcliff, S., Ross, S.M. and Thornes, J.B. 1990. Soil moisture, runoff and sediment yield from differentially cleared tropical rainforest plots. In Vegetation and Erosion, J.B. Thornes (ed). John Wiley, New York. pp 37-450.

O'Loughlin, C.L. 1974. A study of tree root strength deterioration following clear-felling. Can. J. For. Res., 4: 107-113.

Paola, C., Heller, P.L. and Angevine, C.L. 1991. The l;arge-scale dynamics of grain-size variation in alluvial basins: 1, theory. Basin Res., 4:73-90.

Patton, P.C. and Schumm, S.A. 1975. Gully erosion, Northwestern Colorado: a threshold phenomenon. Geology, 3: 88-90.

Preston, N.J. and Crozier, M.J. 1999. Resistance to shallow landslide failure through

root-derived cohesion in East Coast hill country soils, North Island, New Zealand. Earth Surf. Proc. and Land., 24(8): 665-675.

Prosser, I.P. and Dietrich, W.E. 1995. Field experiments on erosion by overland flow and their implications for a digital terrain model of channel initiation. Water Resour. Res., 31(11): 2867-2876.

Prosser, I.P. and Slade, C.J. 1994. Gully formation and the role of valley-floor vegetation, southeastern Australia. Geology, 22: 1127-1130

Prosser, I.P., Dietrich, W.E. and Stevenson, J. 1995. Flow resistance and sediment transport by concentrated overland flow in a grassland valley. Geomorphology, 13: 71-86.

Putz, F.E. 1983. Treefall pits and mounds, buried seeds, and the importance of soil disturbance to pioneer trees on Barro Colorado Island, Panama. Ecology, 64(5): 1069-1074

Ragab, R. and Cooper, J.D. 1993. Variability of unsaturated zone water transport parameters: implications for hydrological modelling. 1. In situ measurements. J. Hydrol., 148: 109-131.

Rawlins, B.G., Baird, A.J., Trudgill, S.T., Hornung, M. 1997. Absence of preferential flow in the percolating waters of a coniferous forest soil. Hydrol. Proc., 11(6): 575-585.

Reid, L.M. 1989. Channel incision by surface runoff in grassland catchments. PhD thesis, University of Washington.

Robertson K.M. and Augspurger, C.K. 1999. Geomorphic processes and spatial patterns of primary succession on the Bogue Chitto River, USA. J. Ecology, 87: 1052-1063.

Robinson, R.A.J. and Slingerland, R.L. 1998. Origin of fluvial grain-size trends in

a forel;and basin: the Pocono Formation on the Central Applachian Basin. J. Sed. Res., 68(3): 473-486.

Roe, G.H., Montgomery, D.R. and Hallet, B. 2002. Effects of orographic precipitation variations on the concavity of steady-state river profiles. Geology, 30(2): 143-146.

Rogers, R.D. and Schumm, S.A. 1991. The effect of sparse vegetative cover on erosion and sediment yield. J. Hydrol., 123: 19-24.

Sala, M. and Calvo, A. 1990. Response of four different Mediterranean vegetation types to runoff and erosion. In Vegetation and Erosion, J.B. Thornes, ed. John Wiley and Sons Ltd. pp 347-362.

Scheidegger, A.E. 1961. Mathematical models of slope development. Geol. Soc. Am. Bull., 72: 37-50.

Schmidt, K.M., Roering, J.J., Stock, J.D., Dietrich, W.E., Montgomery, D.R. and Schaub, T. 2001. The variability of root cohesion as an influence on shallow susceptibility in the Oregon Coast Range. Can. Geotech. J., 38: 995-1024.

Seidl, M.A., and Dietrich, W.E. 1992. The problem of channel erosion into bedrock. Catena Suppl., 23, 101-124.

Selby, M.J. 1993. Hillslope Materials and Processes, 2e. Oxford Unifversity Press, New York. pp 451.

Shugart, H.H. 1998. Terrestrial Ecosystems in Changing Environments. Cambridge University Press. pp 537.

Sidle, R.C. 1991. A conceptual model of changes in root cohesion in response to vegetation management. J. Environ. Qual., 20: 43-52.

Sidle, R.C. 1992. A theoretical model of the effects of timber harvesting on slope stability. Water Resour. Res., 28(7): 1897-1910.

Siepel, A.C., Steenhuis, T.S., Rose, C.W., Parlange, J.-Y. and McIssac, G.F. 2002. A simplified hillslope erosion model with vegetation elements for practical applications. J. Hydrology, 258: 111-121.

Simon, A., Curini, A., Darby, S.E., and Langendoen, E.J. 1999. Streambank mechanics and the role of bank and near-bank processes in incised channels. In Incised River Channels, S. Darby and A. Simon (eds). pp 123-152.

Small, T.W. 1997. The Goodlett-Denny mound: a glimse at 45 years of Pennsylvania treethrow mound evolution with implications for mass wasting. Geomorphology, 18: 305-313.

Smock, L.A., Metzler, G.M. and Gladden, J.E. 1989. Role of debris dams in the structure and functioning of low-gradient headwater streams. Ecology, 70(3): 764-775.

Snow, R.S. and Slingerland, R.L. 1986. Mathematical modeling of graded river profiles. J. Geology, 95: 15-33.

Terwilliger, V.J. 1990. Effects of vegetation on soil slippage by pore pressure modification. Earth Surf. Proc. and Land., 15: 553-570.

Thom, B.G. 1967. Mangrove ecology and deltaic geomorphology: Tabasco, Mexico. J. Ecology, 55: 301-343.

Tucker, G.E. and Bras, R.L. 2000. A stochastic approach to modeling the role of rainfall variabilty in drainage basin evolution. Water Resour. Res., 36(7): 1953-1964.

Tucker, G.E. and Slingerland, R.L. 1994. Erosional dynamics, flexural isostasy , and long-lived escarpments: a numerical modeling study. J. Geophys. Res., 99: 12,229-12,243.

Tucker, G.E. and Slingerland, R. 1996. Predicting sediment flux from fold and thurst belts. Basin Res., 8: 329-349.

Tucker, G.E. and Slingerland, R.L. 1997. Drainage basin response to climate change. Water Resour. Res., 33(8): 2031-2047.

Tucker, G.E., Lancaster, S.T., Gasparini, N.M., Bras, R.L. and Rybarczyk, S.M. 2001a. An object-oriented framework for distributed hydrologic and geomorphic modeling using triangular irregular networks. Comp. and Geosci., 27: 959-973.

Tucker, G., Lancaster, S., Gasparini, N. and Bras, R. 2001b. The Channel-Hillslope Inegrated Landscape Development Model (*CHILD*). In Landscape Erosion and Evolution Modeling, R.S. Harmon and W.W. Dow III (eds). Kluwer Academic/Plenum Puiblishers, Ney Work. pp 349-384.

Turton, D.J., Barnes, D.R. and Návar J. de J. 1995. Old and new water in subsurface flow from a forest soil block. J. Environ. Qual., 24: 139-146.

Vis, M. 1986. Interception, drop size distributions and rainfall kinetic energy in four Colombian forest ecosystems. Earth Surf. Proc. and Land., 11: 591-603.

Wainwright, J., Parsons, A.J. and Abrahams A.D. 2000. Plot-scale studies of vegetation, overland flow and erosion interactions: case studies from Arizona and New Mexico. Hydrol. Proc., 14:2921-2943.

Webb, E.K. 1995. Simulation of braided channel topology and topography. Water Resour. Res., 31(10): 2603-2611.

Whipkey, R.Z. 1966. Subsurface stormflow from forested slopes. Bull. Int. Assoc. Sci. Hydrol., 10(2): 74-85.

Whipple, K.X. and Tucker, G.E. 1999. Dynamics of the stream-power river incision model: Implications for height limits of mountain ranges, landscape response timescales, and research needs. J. Geophys. Res., 104(B8): 17,661-17,674.

Wilcox, B.P., Pitlick, J., Allen, C.D. and Davenport, D.W. 1996. Runoff and erosion from a rapidly eroding pinyon-juniper hillslope. In Advances in Hillslope Processes,

v.1, M.G. Anderson and S.M. Brooks, eds. John Wiley and Sons Ltd., pp 51-77.

Willgoose, G., Bras, R.L. and Rodriguez-Iturbe, I. 1991. A coupled channel network growth and hillslope evolution model. 1. theory. Water Resour. Res., 27(7): 1671-1684.

Woo, M.K., Fang, G. and diCenzo, P.D. 1997. The role of vegetation in the retardatin of rill erosion. Catena, 29: 145-159.

Ziemer, R.R. 1981. Roots and the stability of forested slopes. In proceedings: Symposium on Erosion and Sediment Transport in Pacific Rim Steeplands. Christchurch, New Zealand. pp 343-361.